Advanced Impingement/Film-Cooling Schemes for High-Temperature Gas Turbines – Numerical Study

By

Ariane Aimée Immarigeon

A Thesis

in the Department of

Mechanical and Industrial Engineering

Presented in Partial Fulfillment of the Requirements

for the Degree of Master of Applied Science at

Concordia University

Montréal, Québec, Canada

December 2003

Your file Votre référence
ISBN: 0-612-91047-4
Our file Notre référence
ISBN: 0-612-91047-4

ABSTRACT

Advanced Impingement/Film-Cooling Schemes for

High-Temperature Gas Turbines – Numerical Study

Ariane Aimée Immarigeon

Ongoing research strives to optimize gas turbine blade film cooling so that it achieves maximum performance while using a minimum amount of coolant. It was found that film cooling performance is mainly affected by the blowing ratio, the injection and orientation angles, the relative spacing between film holes, the coolant-to-mainstream density ratio, the hole geometry and the turbulence intensity in the mainstream flow.

The feasibility of an advanced impingement/film cooling scheme will be numerically investigated in this thesis. This scheme combines both the advantages of traditional film cooling with those of impingement cooling. The hole that transports the coolant fluid from the inside to the outside of the blade in this scheme is designed in such a way that the coolant must go through a bend before exiting into the mainstream, thus impinging onto the blade material. Furthermore, flow turbulators, or pedestals, are located on the path of the coolant before it exits from the hole, minimizing aerodynamic losses. Turbulence was modeled using the standard k-ε turbulence model and two of its variants, namely the realizable and Renormalization Group k-ε turbulence models with enhanced wall treatment. The shape of the impingement nozzle (hole inlet) as well as the configuration of the pedestals inside the hole were varied in order to determine the effect of hole geometry on the adiabatic film cooling effectiveness. Based on the hole inlet

conditions, the blowing rates were varied between 0.87 and 5.22, while mainstream turbulence intensities were either 3% or 10%. The flowfield, the temperature field, as well as the turbulence field were studied in great detail. The results showed that the film cooling effectiveness was affected by the shape of the nozzle, the pedestal configuration and the choice of turbulence model. Furthermore, the cooling jet remains attached to the surface at much higher blowing rates than for standard circular holes, indicating a superior performance for the proposed cooling schemes.

This work is dedicated with all my heart
to my dear parents, Marie and Jean-Pierre.

ACKNOWLEDGEMENTS

This work could not have been completed without the help of many individuals. Although it is not possible to name them all here, I would like to mention a few who deserve my deepest appreciation.

I wish to express my sincere gratitude to my thesis supervisors, Dr. Ibrahim Hassan and Dr. Hany Moustapha, for their guidance, support and advice throughout my graduate program.

I would also like to thank my loving family; my parents Marie and Jean-Pierre for inspiring and encouraging me to pursue graduate studies, and my sister Gabrielle for her invaluable friendship.

I am very grateful to Martin St-Jean, who gave me love, support and encouragement, and who kindly spent many hours reviewing my work. As well, I wish to thank Wajih Atallah for his moral support and his helping me in many ways. Many thanks to my friends Korhan Pehlivan, Mohamed Abdelgawad, Roland Muwanga and Ali Farjam-Andaleeb for the good times and helping me discover new ways of thinking.

The financial assistance provided by Concordia University and Pratt & Whitney Canada in support of this project is also gratefully acknowledged.

Table of Contents

List of Figures

List of Tables

Nomenclature

a_C, a_{nb}	Constants in the general conservation equation
b	Constant in the general conservation equation; also constant in the turbulence transport equations
C	Denotes a general element in the computational domain
C_p	Specific heat at constant pressure, (kJ/kg·K)
C_μ	Empirical constant or variable in the turbulence equations
D	Circular hole diameter; also scaling parameter, (m)
D_h	Hydraulic diameter of hole at exit plane, (m)
DR	Density ratio, $(DR = \frac{\rho_j}{\rho_\infty})$
G_k, G_b	Generation terms in the turbulence transport equations
h	Local heat transfer coefficient, $(\frac{W}{m^2 \cdot K})$
I	Momentum flux ratio, $(I = \frac{\rho_j U_j^2}{\rho_\infty U_\infty^2})$
K	Thermal conductivity, (W/m·K)
k	Turbulent kinetic energy, (m^2/s^2)
L	Length of injection hole (for cylindrical holes), (m)
M	Blowing ratio (or rate), $(M = \frac{\rho_j U_j}{\rho_\infty U_\infty})$
m	Number of iterations for which residuals are greatest
n	Number of iterations

Nu	Nusselt number, ($Nu = \frac{hx}{k}$)
P	Pressure, (N/m^2); also refers to first element off the wall
p	Spanwise distance (or pitch) between hole centerlines, (m)
Pr	Molecular Prandtl number in the energy equation
Pr_T	Turbulent Prandtl number in turbulent heat flux equation
q"	Local heat flux at the wall, ($\frac{W}{m^2}$)
R	Residual in one element
R^{Φ}	Total residual in domain for the variable Φ
Re	Reynolds number, ($Re = \frac{\rho UD}{\mu}$)
S	Modulus of the mean rate-of-strain tensor in the turbulence transport equations
St	Stanton number, ($St = \frac{h}{\rho C_p U_\infty}$)
S_ε, S_k	Source terms in the turbulence transport equations
S_{ij}	Rate of strain tensor in the Reynolds-stress tensor
T	Temperature, (K)
T_{aw}	Adiabatic wall temperature, (K)
$\overline{T}_{aw}$	Spanwise averaged adiabatic wall temperature, (K)
Ti	Turbulence intensity
U, u_j	Averaged velocity components, (m/s)
u_j'	Fluctuating velocity components, (m/s)

$\overline{u_i' u_j'}$ Reynolds-stress tensor, $(\overline{u_i' u_j'} = \frac{1}{\rho}\left(\frac{2}{3}\delta_{ij}\rho k - 2\mu_T S_{ij}\right))$

$\overline{\theta u_j'}$ Turbulent heat flux in the energy equation, $(\overline{\theta u_j'} = \frac{1}{\rho}\left(-\frac{\mu_T}{Pr_T}\frac{\partial T}{\partial x_j}\right))$

u_τ Frictional velocity, $(u_\tau = \sqrt{\frac{\tau_w}{\rho_w}})$

x Streamwise distance measured from hole center, (m)

y Vertical distance measured from the test surface, (m)

Y_M Contribution term to the overall dissipation rate in the turbulence transport equations

y^+ Non-dimensional wall distance, $(y^+ = \frac{\rho u_\tau y_p}{\mu})$

y_p Height of the first node P off the wall, (m)

z Vertical distance measured from the hole centerline plane, (m)

GREEK SYMBOLS

α Injection (or inclination) angle for cylindrical holes

$\alpha_k, \alpha_\varepsilon$ Inverse effective Prandtl numbers for k and ε in the turbulence transport equations

β Orientation angle for cylindrical holes

δ_{ij} Kronecker delta in the Reynolds-stress tensor

ε Dissipation rate of turbulent kinetic energy, (m^2/s^3)

θ Fluctuating temperature (K)

θ_e	Angle of an equilateral face of an element, ($\theta_e = 60°$)
θ_{max}, θ_{min}	Largest and smallest angle in an element face
η	Local adiabatic film cooling effectiveness, ($\eta = \frac{T_{aw} - T_\infty}{T_j - T_\infty}$)
$\bar{\eta}$	Spanwise averaged film cooling effectiveness, ($\bar{\eta} = \frac{\overline{T}_{aw} - T_\infty}{T_j - T_\infty}$)
μ	Laminar dynamic viscosity, (kg/m·s)
μ_T	Turbulent dynamic viscosity, (kg/m·s)
ν	Laminar kinematic viscosity, (s/m^2)
ρ	Density, (kg/m^3)
$\sigma_k, \sigma_\varepsilon$	Turbulent Prandtl numbers for k and ε in the turbulence transport equations
τ	Shear stress, (N/m^2)
Φ	General variable in the conservation equation
ω	Specific dissipation rate, (s^{-1})

SUBSCRIPTS AND SUPERSCRIPTS

aw	Adiabatic wall
e	Exit conditions
i	Inlet conditions
j	Refers to the jet
nb	Neighbor element

ref	Reference value at $x/D_h = -10$, $y/D_h = 10$, $z/D_h = 0$
w	Wall conditions
Φ	Refers to the general variable Φ
∞	Mainstream conditions at inlet plane and in freestream

ABREVIATIONS

CFD	Computational fluid dynamics
Imb	Imbalance in mass flow rate
NOVi-jp	Hole configuration nomenclature, where i designates the nozzle geometry and j designates the number of pedestals (Table 3-1)
RANS	Reynolds-averaged Navier-Stokes
RKE	Realizable k-ε turbulence model
RNG	Renormalization Group; also refers to the RNG k-ε turbulence model
RSM	Reynolds Stress Model
SKE	Standard k-ε turbulence model

Chapter I

Introduction

Thermal protection of a surface by means of a film of fluid is used in many applications, notably to protect gas turbine blades and combustor walls from hot combustion gases. This process is referred to as film and effusion cooling, respectively. A similar thermal protection technique is also used to prevent the accumulation of ice on gas turbine engine components near the intake; in this case the injected fluid is hotter than the surrounding fluid, and the process is thus termed film heating.

When gas turbine engines first appeared in the 1930s, their thermal efficiencies were greatly limited by poor compressor performance and low turbine inlet temperature. This led to very low thrust-to-weight ratios for these engines. In gas turbine engines, the specific work output and engine efficiency increase with increasing the turbine inlet temperature. This can be seen on Figure 1-1. One therefore sees the necessity to operate the engine with as high a turbine entry temperature as possible. The blades, already subject to high structural stresses due to the centripetal acceleration they undergo, can become prone to failure if the thermal stresses and oxidation of the blade material, generated by high temperatures an temperature gradients, become too important. While advances in the field of materials (such as the development of effective thermal barrier coatings) combined with effective cooling can help reduce the thermal and structural stresses experienced by the blade, effective cooling can allow the blade to withstand turbine inlet temperatures that exceed the blade material limits. Therefore one of the

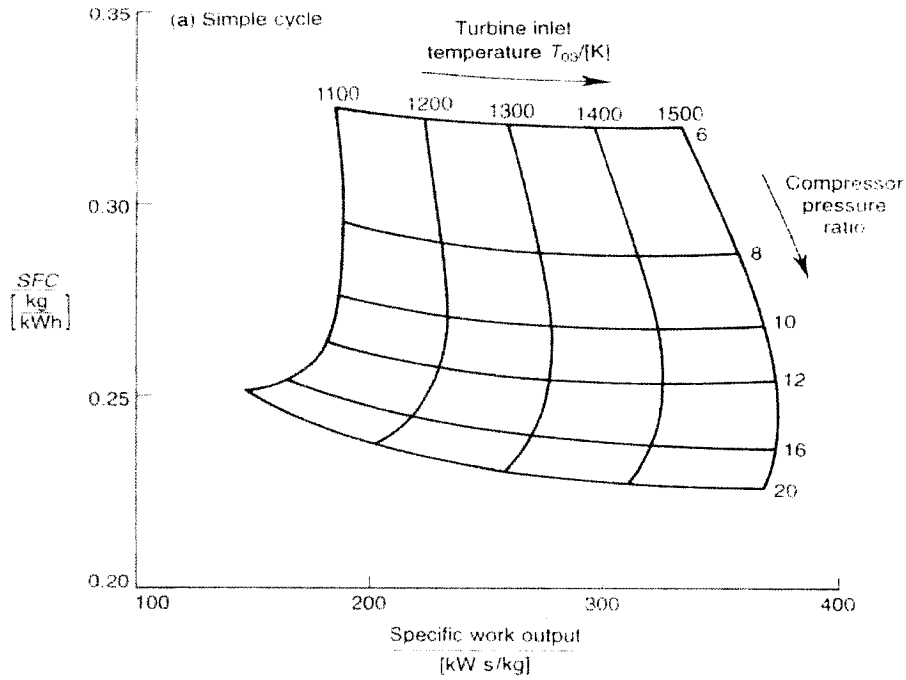

Figure 1-1. Effect of turbine inlet temperature on specific work (Cohen et al., 1996).

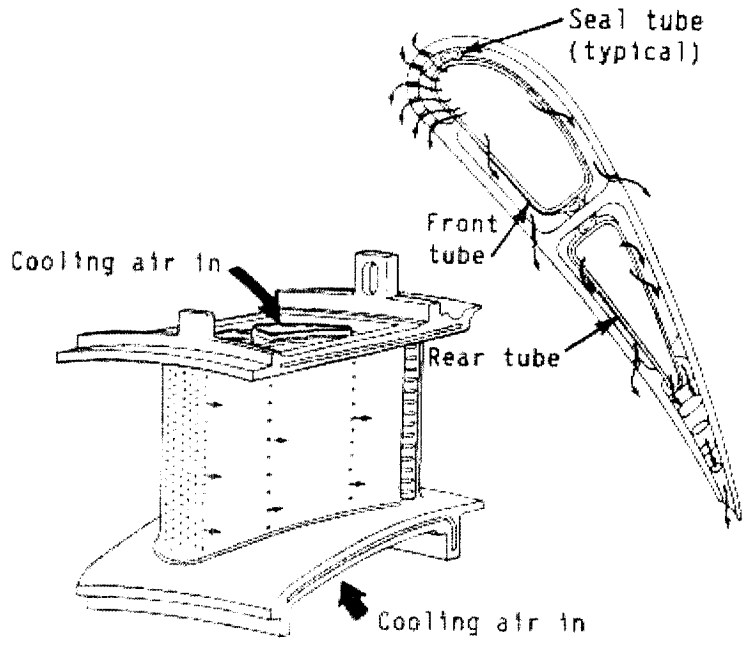

Figure 1-2. Typical film-cooled airfoil (Nirmalan and Hylton, 1990).

goals of a cooling scheme designer is to minimize the temperature as well as the temperature gradients on the turbine blade surface.

Film cooling involves bleeding air from the compressor stage and redirecting it towards the hollow and intricate interior of the blades, where it finally exits back into the relatively hot mainstream through holes in the blade surface. Figure 1-2 shows a typical film-cooled airfoil. Cooling takes a toll on the overall engine efficiency, as the diverted compressed air does not do any significant work on the turbine and introduces aerodynamic penalties once it is re-injected into the mainstream. However, this loss should be more than compensated by the larger gain in efficiency due to the increased turbine inlet temperature. One of the challenges in designing cooling schemes lies in achieving high film cooling performance with a minimum amount of coolant, i.e., high engine performance at low costs.

It was found that film cooling performance is mainly affected by the blowing ratio, the injection and orientation angles, the relative spacing between film holes, the coolant-to-mainstream density ratio, the hole geometry and the mainstream turbulence. Recent work has shown that hole geometry as well as internal features (such as plenum geometry) have an important impact on film cooling performance. Papell (1984), Makki and Jakubowski (1986) were among the first to experiment with new film cooling hole shapes. Gritsch et al. (1998a, 1998b), Thole et al. (1998), Saumweber at al. (2003) investigated other hole geometries and their effect on film cooling performance, while Gillespie et al. (1996), Burd and Simon (1997), Hale et al. (2000), Wilfert and Wolff

(2000) are among the researchers who explored various aspects of internal flow and geometries, and what impact these parameters have on the external flow. This study proposes to investigate such a novel film cooling scheme, designed in such a way that the coolant must go through a bend before exiting into the mainstream, thus impinging on the blade material (Figure 1-3). A diffused exit and pedestals located inside the hole on the path of the coolant are among other features which make this design unique. This study aims at providing, through computational fluid dynamics (CFD), an understanding of how various flow and geometrical parameters affect the adiabatic film cooling effectiveness delivered by this scheme. It is believed that the present work will provide a good contribution for the design of cooling schemes for future generations of commercial gas turbine engines.

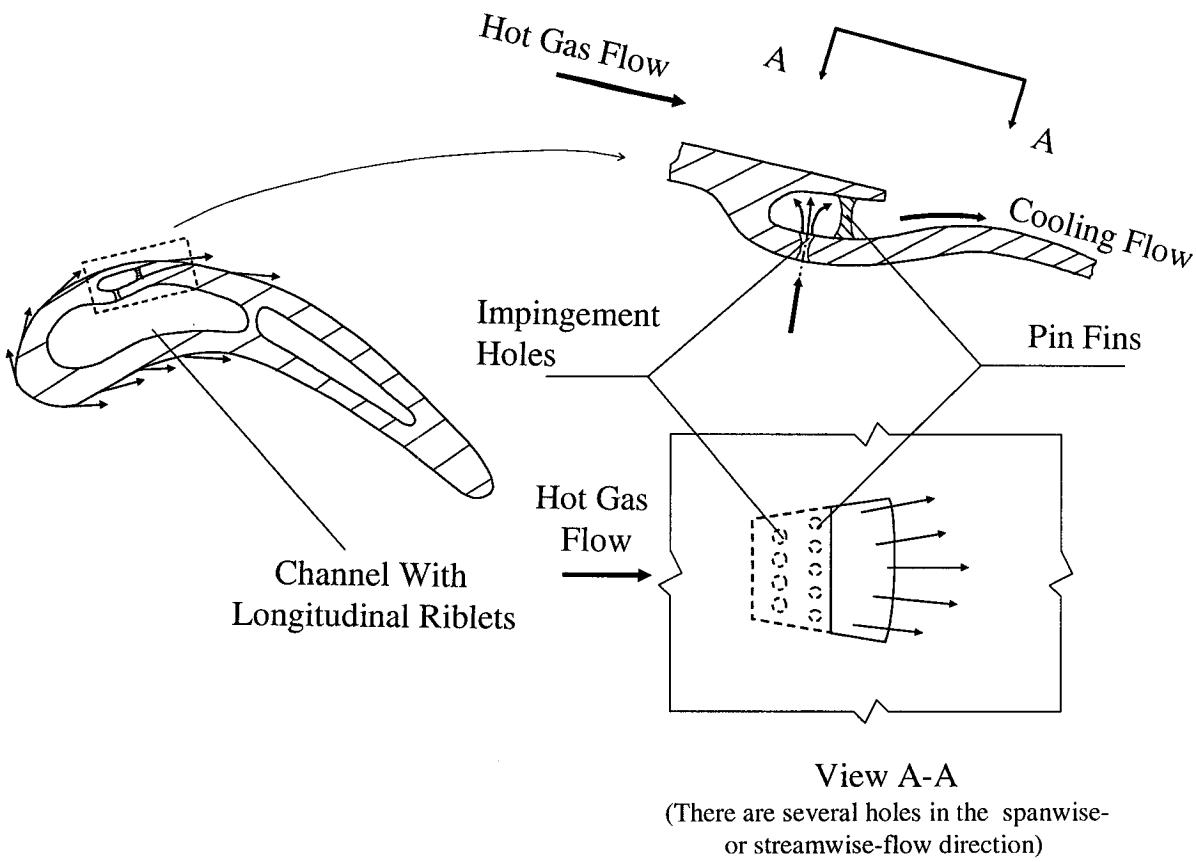

Figure 1-3. Proposed cooling scheme.

Chapter II

Literature Review

2.1 Heat Transfer and Film Cooling Fundamentals

A simplified film cooling configuration is shown in Figure 2-1. The relatively cool fluid is ejected from the hole with a velocity U_j into the mainstream fluid which is moving at a velocity U_∞. The performance of such a film cooling process is evaluated with two parameters, namely the adiabatic film cooling effectiveness and the heat transfer coefficient.

The adiabatic film cooling effectiveness describes the ability of the film to cool the surface. It is defined as:

$$\eta = \frac{T_{aw} - T_\infty}{T_j - T_\infty} \tag{2.1}$$

where T_j is the coolant temperature, T_∞ is the mainstream temperature and T_{aw} is the adiabatic wall temperature, i.e. the temperature the wall attains if there is no heat transfer through it.

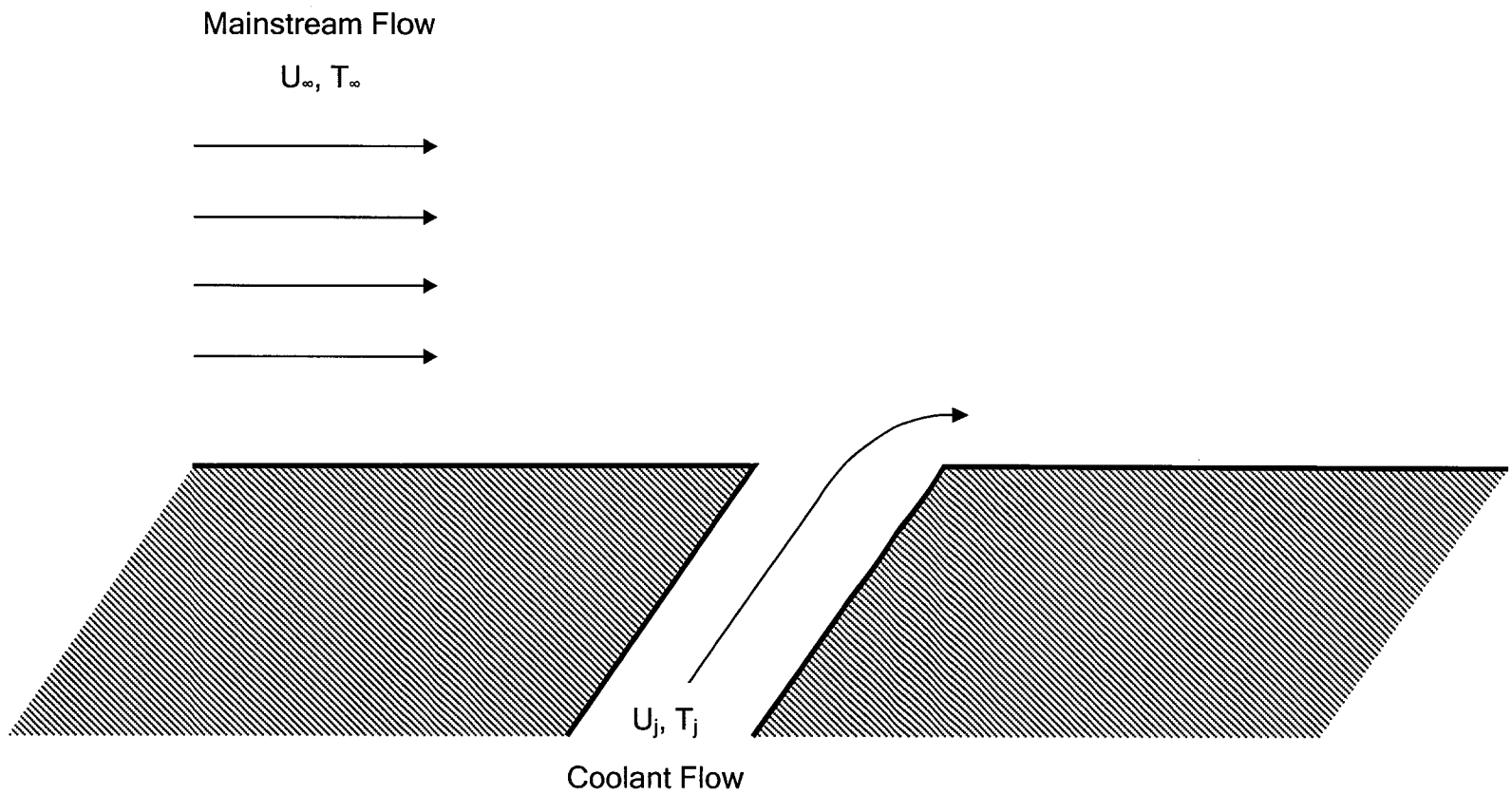

Figure 2-1. Schematic of a film cooling arrangement.

The local heat transfer coefficient is defined as:

$$h = \frac{q''}{(T_{aw} - T_w)} \tag{2.2}$$

where q" is the local heat flux to the surface.

The cooling performance of the film increases as the adiabatic film cooling effectiveness approaches unity and the heat transfer coefficient decreases. It was shown by Licu et al. (2000) that regions of highest effectiveness don't necessarily correspond to regions of lowest heat transfer coefficient, and vice versa. This shows that it is essential to measure and analyze both these parameters in order to get a good understanding of the underlying mechanisms of film cooling.

Several methods have been developed to experimentally measure both the heat transfer coefficient and the adiabatic film cooling effectiveness locally on a film-cooled surface. One popular non-intrusive measurement technique uses thermochromic liquid crystals to obtain accurate, full-surface temperature resolution of the region downstream of injection and extract from these temperature maps the heat transfer coefficient and adiabatic film effectiveness (Ekkad and Han, 2000). Computational research is a useful predictive tool which complements experimental research. It allows for a faster turnover rate than experiments, thus ensuring lower overall costs.

Typically, film cooling holes are characterized, as shown in Figure 2-2, by their length-to-diameter (L/D) ratio, inclination (or injection) angle α, orientation angle β as well as their pitch-to-diameter (p/D) ratio, in the case of a row of holes. The flow conditions are described using the coolant-to-mainstream density ratio DR, the blowing ratio M, the momentum flux ratio I, as well as the mainstream turbulence intensity Ti. These parameters are defined as follows:

Blowing ratio (or rate) M

$$M = \frac{\rho_j U_j}{\rho_\infty U_\infty} \tag{2.3}$$

Momentum flux ratio I

$$I = \frac{\rho_j (U_j)^2}{\rho_\infty (U_\infty)^2} \tag{2.4}$$

Coolant-to-mainstream density ratio DR

$$DR = \frac{\rho_j}{\rho_\infty} \tag{2.5}$$

Mainstream turbulence intensity Ti

$$Ti = \frac{\sqrt{k/1.5}}{U_\infty} \tag{2.6}$$

where k is the turbulent kinetic energy and U_∞ is the mainstream velocity.

The goal of film cooling is to offer thermal protection to a surface. Ideally, the ejected film spreads widely onto the surface and remains attached to it with minimal mixing, while its cooling influence continues far downstream of injection. More coolant mass flow rate should ensure a better coverage. In reality two major problems arise from film cooling methods. First, the cooling jets associated with large blowing ratios tend to detach from the surface and penetrate the mainstream. As a consequence, the adiabatic film cooling effectiveness is reduced in regions where the surface is not as well protected from the mainstream. Many studies have assessed this phenomenon to determine how the onset of detachment is affected by parameters such as the coolant-to-mainstream density ratio (Sinha et al., 1991), the mainstream turbulence intensity (Schmidt and Bogard, 1996), and the hole geometry (Gritsch et al., 1998a). Second, the blade surface is not at a uniform temperature, because the jets originate from discreet holes and do not cover evenly the whole surface. This causes variations in the blade temperature in the lateral direction which leads to thermal stresses in the blade. This is definitely a design problem, which has led researchers to investigate compound injection and other hole configurations (Ahn et al., 2000).

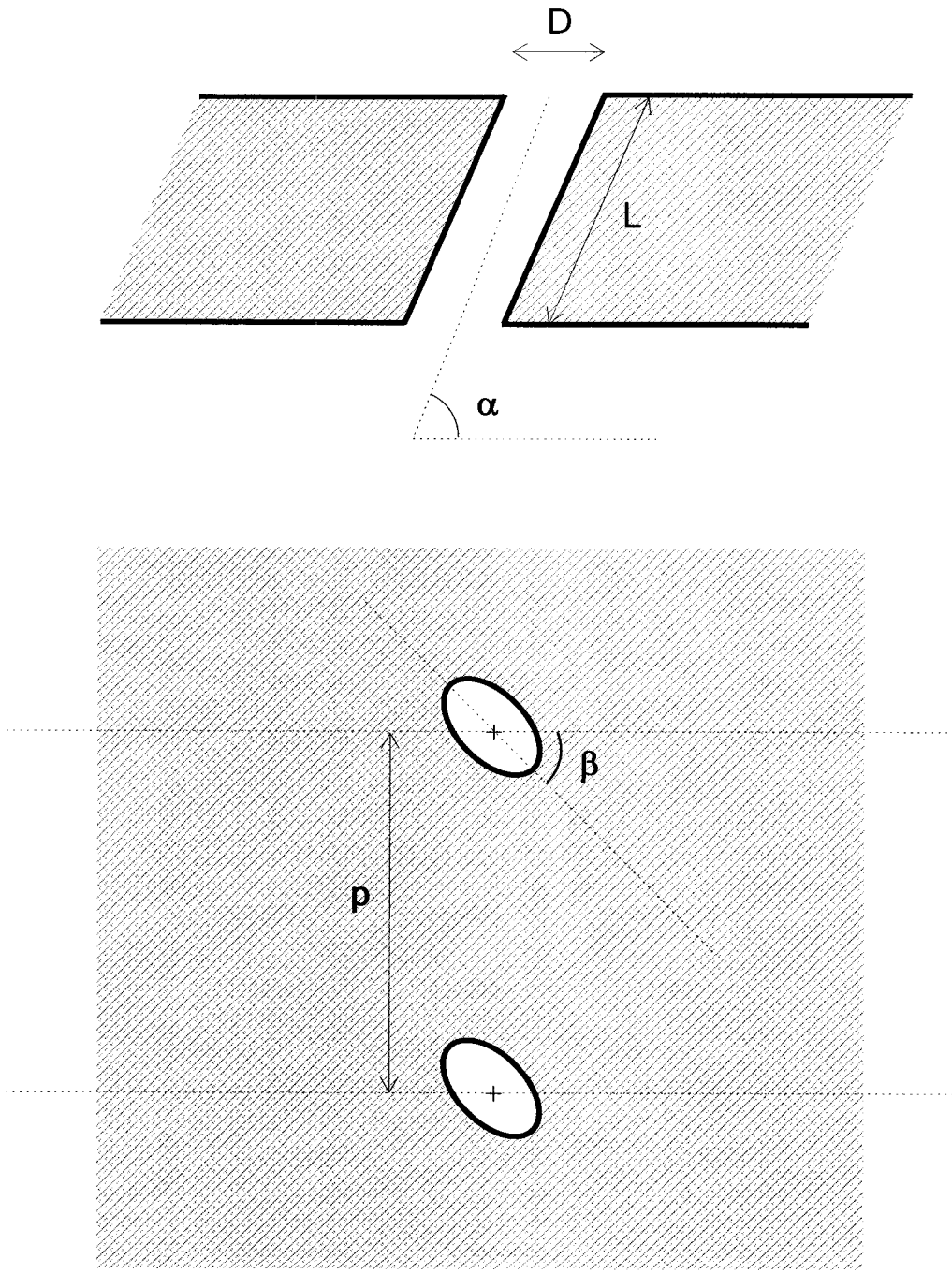

Figure 2-2. Standard circular film cooling hole nomenclature.

2.2 Advances in Experimental Research

2.2.1 Film Hole Geometry and Orientation

Hole shape

Goldstein et al. (1968) were some of the first researchers to study the adiabatic film cooling effectiveness originating from a single circular hole in a flat plate. They did so in 1968, when most previous studies had been concerned with slot film cooling. In this study, the authors used an injection hole inclined at 35 and 90 degrees to the mainstream and they varied the blowing rates from 0.1 to 2.0. Goldstein et al. (1970) extended this work by producing a study on the adiabatic film cooling effectiveness originated from a row of circular film cooling holes. The hole spacing was set to p/D = 3, and the inclination angle was set at 35 degrees to the mainstream. They also examined the film effectiveness downstream of a single circular hole inclined at 35 degrees and oriented at 15 and 35 degrees. From this study they understood that film cooling which involved several holes led to considerably higher effectiveness values than cooling configuration involving only of one, especially at high blowing rates.

Eriksen and Goldstein (1974) included measurements of the heat transfer coefficient as well as effectiveness in a study of inclined circular film cooling holes. They showed that 35-degree injection leads to smaller heat transfer coefficients than normal injection due to reduced coolant-to-mainstream interaction. The film cooling configurations that they studied (a single circular hole and a row of five circular holes, all inclined at 35 degrees streamwise) injected heated as well as unheated air into the main stream, at blowing rates

between 0.1 and 1.95. They found that for blowing rates higher than 0.5, jet penetration became important, and the increase in heat transfer coefficients with increasing blowing ratio became noticeable. For blowing rates below 0.5, there was no significant difference between the heat transfer coefficient distributions obtained from the single hole configuration or the row configuration; however above 0.5, the row configuration produced higher values of heat transfer coefficients than the single hole, showing peaks between holes.

The same year, Goldstein et al. (1974) tested circular holes with exits expanding laterally by 10 degrees. They were among the first to show that laterally expanding holes were advantageous over simple circular holes, as they offer improved adiabatic effectiveness of the film over a wider range of blowing ratios. Indeed, through their experiments, the authors show that the centerline effectiveness for both the round holes and the shaped holes is essentially the same up to a blowing rate of 0.3, a value that causes the jet to detach. At blowing rates larger than 0.3, the centerline effectiveness drops dramatically for the round hole. However for shaped holes, the centerline effectiveness keeps on increasing steadily up until a blowing rate of 0.8, after which it remains more or less constant (with a slight declining tendency) up until a blowing rate of 2.2. The authors attributed these results to the reduced momentum of the jet caused by the increase in area at the exit of the shaped hole. In these experiments, the holes were placed in rows of eleven, and were inclined streamwise at 35 degrees.

Papell (1984) also showed that the shape of a film-cooling hole has an effect on the cooling performance of the film. For this study he tested cusp-shaped holes which influence the direction of rotation of the counter-rotating vortex pair within the coolant flow. The holes were oriented in two different manners, so that the vortex structure within the jet either cancelled with or amplified the vortex structure caused by the crossflow. His results showed that vortex cancellation leads to reduced jet separation.

Makki and Jakubowski (1986) then demonstrated the superiority of forward-and laterally-expanded holes (trapezoidal shaped exit) over circular holes in terms of cooling performance. Both configurations tested consisted of 51 holes, inclined at 35 degrees to the mainstream and with a pitch-to-effective diameter ratio of 3. They found that trapezoidal shaped holes led to higher effectiveness levels and lower heat transfer coefficient levels than round holes in the immediate downstream area ($x/D < 50$), and particularly at low or moderate blowing ratios. They observed that when the coolant-to-mainstream temperature ratio was increased, the coolant-to-mainstream density ratio decreased and the coolant-to-mainstream velocity ratio and momentum flux ratio both increased, hence causing a decrease in the effectiveness.

Haven and Kurosaka (1997) studied the vortices produce by the film cooling jet exiting from holes of various shapes in a flat plate. In particular they discovered within each jet a double-decked structure consisting of two pairs of kidney vortices. The authors found that for high aspect ratio rectangular holes each kidney pair rotates in opposite direction, whereas for low aspect ratio rectangular holes they rotate in the same direction. Kidney

pairs rotating in the same direction were found to promote jet liftoff more than those rotating in opposite directions. By studying rectangular holes rather than round ones, the authors were able to get a very detailed understanding of the flowfield in the vicinity of the hole.

Thole et al. (1998) showed that a hole with a forward and/or laterally expanded exit causes less jet penetration into the mainstream and generates less velocity gradients in the mixing region of the jet than a round hole. However the study indicates that the laterally-and-forward-expanding hole exhibits a disadvantage compared to the laterally expanding hole, due to its geometry. Because the coolant exits this type of hole mainly through the downstream part of the hole, the hot mainstream gas is allowed to penetrate into the upstream portion of the hole. This reduces the overall performance of the resulting cooling jet. The blowing ratio and a density ratio were set to one, while the mainstream Mach number (of 0.25) was almost equal to that of the coolant (0.3).

Berger and Liburdy (1998) analyzed the flowfield around a circular hole, a 12-degree laterally expanding hole, and a 15-degree forward expanding hole, all with an inclination angle of 35 degrees and orientation angles of 0, 45, 60 and 90 degrees in turn. The jet exiting from the laterally expanding hole was seen to not penetrate as far in the mainstream as with other holes tested, and to remain close to the test surface.

Gritsch et al. wrote two articles in 1998. One of them, by Gritsch et al. (1998a), presents the adiabatic wall effectiveness as measured on a flat wall downstream of a laterally-

expanding hole as well as a laterally-and-forward-expanding hole, and compares these values with those obtained downstream of a cylindrical hole. While many previous papers implement mainstream Mach numbers less than 0.1, this study employs mainstream Mach number of 0.3, 0.6 and 1.2. The film holes were inclined at 30 degrees with the mainstream, all possess a length-to-diameter ratio of 6 and delivered coolant into the mainstream at a coolant-to-mainstream density ratio of 1.85. Blowing rates were varied from 0.25 to 2. The study concludes that both shaped holes offer better thermal protection of the surface (due to a wider spreading and better adherence of the coolant on the surface) than circular holes, especially at high blowing rates, and that the laterally-and-forward-expanding hole provides the highest laterally-averaged film-cooling effectiveness. The other paper written by Gritsch et al. (1998b) examines the heat transfer coefficient distributions obtained by the same holes as in Gritsch et al. (1998a), with the same density ratio but with blowing rates of 0.25 to 1.75 and mainstream Mach number of 0.6. This paper confirms the superiority of the laterally-and-forward-expanding hole, which provides better lateral distribution of the coolant than the laterally-expanding hole, and also generates lower laterally averaged heat transfer coefficients.

The performance of holes with conically expanding exits and compound injection angle was evaluated by Cho et al. (2001). The authors compared the local film cooling effectiveness and heat/mass transfer characteristics obtained from a round hole with those obtained from holes expanding conically by 4 degrees in every direction, with and without forward expansion. Various tests were performed with the following parameters: inclination angle of 30 degrees, compound angles alternatively set to 0, 45 and 90

degrees, and blowing rate varying between 0.5 and 2.0. All conical holes were found to promote lower heat/mass transfer coefficient than the round hole. Even though at low blowing rates all holes perform the same, the conical hole with no forward expansion shows superiority in performance over other holes when blowing rates are high.

Hole inclination and orientation

Foster and Lampard (1980) studied the effect of hole inclination on adiabatic film cooling effectiveness and on the general flow behavior. They tested a row of 15 circular holes with inclination of 35 and 55 degrees and found that at low blowing rates the 35 degree inclined holes lead to higher laterally averaged effectiveness than the 55 degree inclined ones, but this behavior is reversed at high blowing rates. The authors also noticed that at a far enough distance downstream of injection, the spanwise averaged effectiveness values become independent of inclination angle; the distance for which this applies is shorter when blowing rates are low.

Ligrani et al. (1992) investigated more film cooling geometrical parameters. They focused their efforts on collecting and analyzing distributions of Stanton numbers and adiabatic film cooling effectiveness downstream of one row and two staggered rows of film holes. The holes had an injection angle of 35 degrees and a compound angle of 30 degrees, with p/D = 7.8, or 3.9 for the staggered configuration. Through their study, the authors report that smaller hole spacing in the staggered hole arrangement leads to higher downstream spanwise-averaged effectiveness values than for in-line holes. They also

conclude that in the vicinity of the hole, the values of spanwise-averaged effectiveness are highest at a blowing rate of 0.5, and they decrease with a further increase in blowing rate; far downstream of the hole the trend is reversed and the spanwise-averaged effectiveness increases for increasing blowing rates higher than 0.5, up to 1.5.

In 1996 two articles reported the film cooling effectiveness and heat transfer coefficient distributions originating from compound shaped holes. Schmidt et al. (1996) compared the cooling effectiveness of round holes with that of holes with forward-expanding exits. The cooling configuration involved a single row of holes inclined at 35 degrees in the streamwise direction, with compound angle of 60 degrees, L/D of 4 and momentum flux ratios varying from 0.16 to 3.90. It was found that both compound circular holes and compound forward expanding holes generate better lateral spreading of the cooling flow (the latter one performing better than the former one), and thus greater areas of high effectiveness than standard round holes, for all momentum fluxes tested. Sen et al. (1996) demonstrated that in order to evaluate the cooling performance of the film, both the heat transfer coefficients as well as the adiabatic film effectiveness must be known. Using the heat-mass transfer analogy and the same hole configurations as in Schmidt et al. (1996), they found that compound angle injection at high momentum flux ratios lowers the overall cooling performance due to higher heat transfer coefficients than simple angle injection, even though it demonstrates greater effectiveness.

This led Kohli and Bogard (1999) to examine the effect that laterally-and-forward expanding holes have on film cooling performance, when a large injection angle is used.

They conducted their experiments with a single row of holes inclined at 55 degrees; they compared standard circular holes with two types of laterally-and-forward expanding holes (forward expansion of 15 or 25 degrees). Coolant-to-mainstream density ratio was set to 1.6. The authors established that the shaped holes perform better than the round holes even when the injection angle is large, as they produce higher spatially averaged adiabatic effectiveness. However they state that the holes with 15 degree forward expansion perform better at a high inclination angle than the holes with 25 degree forward expansion. This is attributed to the fact that the advantages of the forward expansion (i.e. increased adherence of the jet to the surface at higher momentum flux ratios) are outweighed by the disadvantages of the increased injection angle (separation occurring within the hole and ingestion of hot gas, which cause higher film temperature and jet trajectory).

Jung and Lee (2000) investigated the effect of orientation angle on the film performance, by measuring the adiabatic film cooling effectiveness downstream of a row of five film holes on a flat test surface with velocity ratios of 0.5, 1.0 and 2.0. The holes had an injection angle of 35 degrees and orientation angles of 0, 30, 60 and 90 degrees. The jet was heated to 40 °C while the mainstream was maintained at a temperature of 20 °C. Jung and Lee found that compound angles promote the mixing between the jet and the mainstream, which dilutes and cools down the jet. However, they also observed that compound angles cause the jet to spread more in the lateral direction and coalesce with neighboring jets, which has the effect of supplying a more uniform and higher film effectiveness on the surface. They also noticed that medium and high velocity ratios (1.0

and 2.0) promote the appearance of stronger vortices that push the jet towards the test surface, which results in a high fluid temperature near the surface. This tendency is amplified as the compound angle increases.

Ahn et al. (2000) tested two rows of circular film cooling holes with opposite orientation angles, positioned in different staggered and in-line configurations on a flat test surface. Their goal was to see how the different configurations influenced the heat transfer coefficient ratio distributions. Each row was composed of four holes inclined at 35 degrees to the mainstream, with orientation angles of – 45 and 45 degrees spanwise for the holes in the first row and second row respectively. Tests were conducted at blowing rates of 0.5, 1.0 and 2.0, successively. It was concluded from these experiments that even though all staggered-hole configurations produce lower heat transfer coefficient distributions than the in-line hole configuration at blowing rates of 1.0 and 2.0, the in-line hole configuration delivers an overall better film cooling performance, as it leads to enhanced adiabatic film cooling effectiveness downstream of the holes.

The study by Goldstein and Jin (2001) mentions the presence of the asymmetric vortex motion related to the lateral component of coolant momentum associated with compound angle injection at high blowing rates. The authors explain that even though the compound injection has the advantage of promoting adherence of the laterally shifted jet on one side of the hole, the strong vortex motion on the other side tends to strip the surface of its protective film. The study was done on a flat surface with one row of twelve holes

inclined at 35 degrees streamwise and oriented at 45 degrees, with p/D spacing of 3. Blowing rates were varied from 0.5 to 2.0, with a density ratio of unity.

Lee et al. (2002) focused their attention on the flow behavior in and around compound oriented holes with a 15-degree forward expansion and a 35-degree inclination. They used a single row of seven of those shaped holes, setting the orientation angle to 0, 30, and 60 degrees alternatively. Experiments were done at blowing rates of 0.5, 1.0 and 2.0. The authors observed that holes that have a large orientation angle tend to allow the hot mainstream to penetrate into the hole through the leeward side. They attributed this reversal of the mainstream flow to the reduced momentum of the coolant as it exits the leeward expanded portion of the hole exit. Nevertheless the results showed that shaped holes with a compound angle show better performance than their cylindrical counterparts, even at high blowing rates.

2.2.2 Flow and Mainstream Parameters

Density ratio

Pedersen et al. (1977) examined the effect of varying the ratio of the density of the coolant flow and that of the mainstream. They mixed helium, CO_2 or refrigerant F-12 to the coolant stream in order to achieve density ratios varying from 0.75 to 4.17, and measured the adiabatic film-cooling effectiveness downstream of a row of 15 circular

holes with p/D spacing of 3, using the mass transfer analogy. The authors found that as expected, the density ratio does indeed influence the film cooling effectiveness.

This study led Teekaram et al. (1989) to investigate two methods of recreating the coolant-to-mainstream density ratio in film cooling experiments. One method is to use foreign gases as coolant; the other method is to vary the coolant-to-mainstream temperature ratio. In both cases they used density ratios of 1.25 and 1.67, and they varied the blowing rates from 0.1 to 1.2. Experiments were conducted on a row of film holes inclined at 30 degrees to the mainstream, with 2.5-diameter spacings. They found that both methods indeed are equivalently suitable for this purpose. Unlike the method used by Pedersen et al., the method used in this study allowed the authors to use isothermal wall boundary conditions (which simulate real-engine situations better than adiabatic), and to obtain the film cooling parameters in a smaller number of experiments.

Ammari et al. (1990) reported the heat transfer coefficient data downstream of a row of holes with p/D of 3 and either 35 degree or 90 degree inclination to the mainstream. They observed that the heat transfer coefficient at a fixed blowing rate increases when the density ratio decreases. This dependence was noticed only for the 35-degree injection. The authors conducted the experiments for density ratios of 1, 1.38 and 1.52, while varying the blowing rate between 0.5 and 2.0.

Sinha et al. (1991) attempted to correlate the effect of density ratio on the centerline adiabatic film cooling effectiveness and laterally averaged adiabatic film cooling

effectiveness, with the blowing rate, the velocity ratio and the momentum flux ratio. They found that in general it could not be correlated, except for particular cases. They noticed that when the cooling jet remains attached to the test surface (at low blowing rates), the adiabatic centerline film cooling effectiveness correlates best with the blowing ratio. However when the jet detaches and reattaches (at high blowing rates), the effectiveness correlates best with the momentum flux ratio. They also noted that decreasing the density ratio and increasing the momentum flux have the same effect on the coolant jet, which is to reduce its lateral spreading and consequently the laterally averaged adiabatic film cooling effectiveness. Tests involved a single row of short holes (L/D = 1.75) inclined at 35 degrees streamwise, in a flat surface.

More tests were done by Salcudean et al. (1994), to study the effect of density ratio on film cooling effectiveness. Rather than using a flat plate, they used a semi-circular blade leading edge, with different configurations of cooling holes, tested at density ratios of 1 and 1.53. Their results showed that higher density coolant is more effective at high blowing rates in comparison with a lower density coolant, especially far downstream of the film holes.

Ekkad et al. (1998) studied the effect of coolant density on film cooling on a cylindrical leading edge model. They reported the Nusselt number as well as the adiabatic film cooling effectiveness distributions on the surface of the model for blowing rates of 0.4, 0.8 and 1.2. This study showed that as the coolant density is increased, the Nusselt numbers (proportional to the heat transfer coefficient) decrease, at all blowing rates. It

also shows that the lower-density coolant (air) is most effective at a blowing rate of 0.4, whereas the higher-density coolant (CO_2) is most effective at a blowing rate of 0.8. The holes, located at ±15 degrees from the stagnation point on the model, were inclined and oriented at 30 and 90 degrees, respectively.

Blowing ratio

Bergeles et al. (1977) noticed two regimes of injection for standard circular film cooling holes. They observed that the flow remains attached to the test surface for blowing rates of 0.3 or less, and lifts off the surface for blowing rates greater than 0.5. Tests were done using a single circular hole inclined at 30 degrees to the flat test surface, with blowing rates varying between 0.1 and 1.5. The rise in effectiveness observed on the test surface in the case of the attached jet as the blowing ratio increases, is attributed to the strong pressure and velocity disturbances on the surface. Effectiveness was seen to be optimal for a blowing rate of 0.5. The decrease of effectiveness observed at blowing rates higher than 0.5 is attributed to the lack of coverage caused by the jet lift-off. The study by Forth and Jones (1988) also described the two regimes and described them as weak injection (film remains attached to the surface) and strong injection (flow detaches and lifts off from surface). Three film cooling configurations were tested for this study, namely a 30-degree inclined slot of width ratio 5, a single row and double row (staggered) circular holes inclined at 30 degrees.

Vedula and Metzger (1991) developed an experimental method based on transient liquid crystal thermography to measure local heat transfer coefficients and film cooling effectiveness. They tested a single row of five circular film-holes with injection angle of 35 degrees. Tests were done using blowing ratios of 0.5 and 0.6. Results showed that for a given blowing ratio, the effectiveness is highest near the hole, and drops off downstream in the streamwise direction. At x/D = 8, the spreading of the flow has increased the values of effectiveness at lateral locations. As the blowing ratio increases from 0.5 to 0.6, the centelrine effectiveness near the hole decreases due to the high jet momentum that causes lift-off of the film. However very far downstream the jet associated with the higher blowing rate produces best coverage, ensuring higher values of film effectiveness there.

Ekkad et al. (1997) varied many parameters related to film cooling to understand how these factors affect each other and the cooling performance of a film generated by a single row of holes over a flat surface. The holes were oriented at 0, 45 and 90 degrees and inclined at 35 degrees to the mainstream. Two density ratios (0.98 and 1.46) and three blowing rates (0.5, 1.0 and 2.0) were used. This study revealed that compound angle holes lead to higher heat transfer coefficients on the test surface than simple angle holes, and that this trend is amplified at high blowing rates. They also state that compound holes produce higher film effectiveness than simple holes for both density ratios, and that the highest effectiveness for compound angle injection is obtained at a blowing ratio of 1.0. Finally, they discovered that decreasing the density ratio has no

noteworthy effect on the heat transfer coefficient values in the case of holes with simple holes, but it does lead to an increase in the heat transfer coefficient for compound holes.

Mainstream Turbulence

Jumper et al. (1991) concluded that high mainstream turbulence (14 to 17%) causes a faster streamwise decay in effectiveness downstream of the film hole than low mainstream turbulence intensities (0.5%). This was done by testing a row of circular holes inclined at 30 degrees in a flat plate. As was demonstrated by Schmidt and Bogard (1996), film cooling behaves differently whether the mainstream turbulence level is low or high. While it was shown in other studies that for low mainstream turbulence the optimum momentum flux ratio is low to moderate, Schmidt and Bogard (1996) reported that this range is not optimum anymore for high mainstream turbulence, and the trend in spanwise averaged adiabatic film cooling effectiveness is reversed to what it is for low mainstream turbulence. Whereas the spanwise averaged adiabatic film cooling effectiveness decreases for $x/D > 25$ with increasing momentum flux ratio (greater than 1.0) for a mainstream turbulence of 0.3%, it actually increases with increasing momentum flux ratio for a mainstream turbulence of 17%.

Menhendal and Han (1992) studied the effects of freestream turbulence (0.75% to 12.9%) on leading edge film effectiveness and heat transfer coefficient with holes inclined at 30 degrees and oriented at 90 degrees. They concluded that an increase in freestream turbulence from 0.75% to 12.9 % at low blowing rates causes the spanwise averaged

adiabatic film cooling effectiveness to decrease and the heat transfer coefficient to increase.

Drost et al. (1997) related the mainstream turbulence to the adiabatic film cooling effectiveness measured on a flat plate downstream of a single row of fourteen cooling holes inclined at 35 degrees to the mainstream, with p/D spacing of 3 and length-to-diameter ratio of 3.5. They found that for blowing rates below 1.5, the spanwise averaged effectiveness is higher far downstream for low mainstream turbulence intensities than for high ones. However, for blowing rates of 1.5, this trend is reversed and the spanwise averaged effectiveness is higher for high mainstream turbulence intensities than for low ones.

However about year later, Drost and Bölcs (1998) showed that this statement is in fact only valid for film cooling on the pressure side of a turbine vane, as the mainstream turbulence was observed to have merely a weak influence on suction side cooling effectiveness. This conclusion was obtained as the authors carried out a study complimentary to that of Drost et al. (1997); they further analyzed the film cooling effectiveness and heat transfer characteristics on a gas turbine airfoil in a linear cascade, at two mainstream turbulence intensities (5.5% and 10%), three exit Reynolds numbers of 0.52×10^6, 1.02×10^6 and 1.45×10^6, Mach numbers of 0.33, 0.62 and 0.8, density ratios of 1 and 1.65, and blowing rates varying between 0.25 to 7.3 (with pressure side cooling using higher blowing rates than the suction side). The authors were thus better able to understand the physics of turbine blade cooling; from this study it became apparent that

the cooling film performed differently whether it was generated on the pressure surface or on the suction surface. In particular it was seen that the adiabatic film cooling effectiveness on the suction surface in the near-hole region was higher when the film was released into a laminar boundary layer.

Ekkad et al. (1998) conducted several tests on a cylindrical leading edge model to evaluate the extent of the influence of free-stream turbulence on film cooling performance. When they compared results obtained from tests using blowing rates of 0.4, 0.8 and 1.2 with air and CO_2, they found that spanwise averaged adiabatic film cooling effectiveness decreases when free stream turbulence is increased from 1% to 7.1% at the blowing rate of 0.4, but that it is not significantly dependent on turbulence intensity at a blowing rate of 1.2. In parallel, tests done with free stream turbulence of 1%, 4.1% and 7.1% revealed that the turbulence does not have a big influence on heat transfer coefficients for both types of coolant used. However similar tests done without any film injection show that an increase in free stream turbulence causes an increase in heat transfer coefficient on the test surface of up to 30% for turbulence of 4.1% and up to 50% for turbulence of 7.1%, compared to heat transfer coefficients obtained with turbulence of 1%.

Saumweber et al. (2003) also examined the combined influences of blowing rate and freestream turbulence intensity on effectiveness distributions downstream of cylindrical, laterally-expanding and laterally-and-forward expanding holes. As proven by Jumper et al. (1991), centerline effectiveness downstream of circular holes indeed decreases with

increasing mainstream Ti, but only at low blowing rates. Saumweber et al. showed that for cylindrical holes, there is a critical mass flow rate below which increasing the Ti at constant M causes a reduction in spatially averaged effectiveness, and above which increasing Ti at constant M causes an increase in effectiveness.

2.2.3 Plenum and Other Internal Factors

Obot et al. (1979) realized that the heat transfer obtained from a round turbulent jet impinging on a target surface depended on the geometry of the nozzle. They conducted experiments with sharp-edged and quarter ellipse contoured nozzles of different length-to-diameter ratios (1, 10, 20, 40 and 50) to measure, in terms of turbulence and velocity profiles, the extent of the effect. The effect of the nozzle-to-target plate distance-to-diameter ratio (varied between 2 and 12) was also investigated. The authors concluded that the nozzle inlet shape did have an impact on the turbulence and velocity profiles when the nozzle length-to-diameter ratio was equal to unity, but this influence lessened as this ratio increased, to disappear completely for length-to-diameter ratios greater than 40. Furthermore, for length-to-diameter ratios of 1, 10 and 20, the largest influence of the nozzle inlet geometry is felt when the nozzle-to-target plate distance-to-diameter ratio is less than 6.

Pietrzyk et al. (1989) observed that a separation region appears at the leeward entrance of circular holes. This was found after studying a row of 35 degree inclined circular holes. By investigating the hydrodynamics of the flow, they notice that the presence of

separation regions within the holes have an effect on the outcoming coolant jet, causing it to undergo more turbulent mixing and dilution. Thole et al. (1998) observed that the separation region inside a round hole is larger when the coolant is supplied through a stagnant plenum, than when it is supplied through a crossflow channel. This separation region causes high levels of turbulence at the exit of the hole, which brings about coolant dilution. The authors examined the flowfield around a single circular hole and single laterally-expanded and laterally-and-forward-expanded holes for a blowing ratio and density ratio of unity.

Gillespie et al. (1996) investigated a cooling scheme that combine film cooling with impingement cooling; they specified that as the impingement jet got closer to the entrance of the film cooling hole, it tended to get sucked into the film cooling hole more, thus decreasing the heat transfer and the effectiveness on the impingement target. In the cooling schemes tested, coolant was directed onto a target surface by means of seven tapered impingement holes with spanwise pitch of 4 diameters, after which it was ejected through a row of five film cooling holes. These film holes were inclined at 30 degrees with respect to the surface, and had a diameter of 1.08 times that of the impingement holes, and a spanwise pitch of 5.475 times that same diameter.

Burd and Simon (1997) focused their efforts on understanding how the coolant supply plenum geometry and hole length-to-diameter ratio (L/D) affect the injected cooling flow properties. Those effects were measured in terms of hole exit velocity and turbulence intensity distributions, as well as adiabatic film cooling effectiveness. Experiments

involved a row of film cooling holes inclined at 35 degrees with respect to the mainstream, with length-to-diameter ratios equal to 2.3 and 7.0. The authors varied the density ratios from 0.96 to 1.0, and used two coolant-to-mainstream velocity ratios (VR) of 0.5 and 1.0, as well as three plenum geometries (unrestricted plenum, co-flow plenum, and counter-flow plenum). It was found that the highest centerline effectiveness in the vicinity of the hole (x/D = 1.25) is achieved with the counter-flow plenum, for both velocity ratios, but that this superiority vanishes quickly downstream. Co-flow plenum is only superior to the counter-flow and unrestricted configurations – in terms of centerline effectiveness - when VR=1 and when considering areas far downstream of injection (x/D > 3.5). The authors attribute this to a possible detachment and reattachment of the jet near the hole exit. As for the L/D factor, it was found that at VR = 0.5, shorter and longer holes perform similarly in terms of centerline effectiveness, except in the vicinity of the hole (x/D <3) where short holes are slightly better. However for VR= 1.0, shorter holes are superior to longer ones for $x/D \leq 2$, but this situation is reversed in the region of $2 \leq x/D \leq 10$.

In their study mentioned previously, Gritsch et al. (1998a) investigated the effect of varying the internal crossflow orientation and Mach numbers (0, 0.3 and 0.6). According to their study, the adiabatic film cooling effectiveness downstream of the film holes strongly depends on the conditions of the flow inside the plenum. Tests were done with external Mach numbers of 0.3, 0.6 and 1.2.

Because hole length-to-diameter ratio seemed to have an important influence on the film cooling characteristics, Lutum and Johnson (1999) devoted themselves to collect film cooling effectiveness data on a flat surface downstream of a row of seven cylindrical film holes with variable length-to-diameter ratio. Experiments were done using a hole inclination of 35 degree in the streamwise direction and hole length-to-diameter (L/D) ratios of 1.75, 3.5, 5, 7 and 18, with blowing rates varying from 0.52 to 1.56. They found out that L/D ratios of 5, 7 and 18 did not have significant effects on the adiabatic film-cooling effectiveness downstream of the hole. For smaller L/D ratios, the adiabatic film cooling effectiveness was found to decrease with decreasing L/D ratio.

Hale et al. (2000) obtained, compared and studied the film cooling effectiveness distributions associated with short film cooling holes of length-to-diameter ratio varying from 0.66 to 3.0, fed by a narrow plenum of height-to-diameter ratio h/D = 1. Tests were conducted for blowing ratios of 0.5, 1.0 and 1.5 and for two plenum configurations (co-flow plenum and counter-flow plenum), with density ratios varying from 0.9 to 0.94. Two injection angles were investigated for this study, namely 35 and 90 degrees. Their results pointed to the conclusion that long 35-degree holes produce better coverage than short 35-degree holes for all plenum cases, but long 90-degree holes only produce better coverage than the short 90-degree holes when tested with the co-flow plenum configuration. Plenum flow direction was observed to have little effect on the film cooling effectiveness for long 90-degree holes and short 35-degree holes.

Building on these findings, Wilfert and Wolff (2000) systematically studied and compared five different plenum configurations to understand how internal flow and plenum geometry affect the film cooling effectiveness. Tests were done using a single row of cylindrical film holes with a 30° streamwise injection angle with pitch-to-diameter ratio p/D of 4, and length-to-diameter L/D ratio of 4 and 8, discharging air over a flat plate at blowing ratios between 0.5 and 1.25 and constant density ratio of 1.15. They compared results obtained from a reference unrestricted plenum and those obtained with plenum configurations fed by a channel running parallel to the mainstream and involving combinations of internal crossflow and/or impingement and/or ribs, or none. The authors also developed and tested a vortex generator, placed at the inlet of the film hole to intensify counter-rotating vortices, as a possible alternative to ribs. From this study it was clear that all the plenums tested are more effective than the reference stagnant plenum, and that these plenums lead to an improvement of 30% in the lateral averaged adiabatic film cooling effectiveness when L/D = 4, compared to that displayed when L/D = 8. It was also found that plenums equipped with vortex generators lead to better lateral spreading of the coolant jet and higher effectiveness downstream of the hole than with any plenums equipped with ribs.

2.3 Advances in Computational Research

Computational fluid dynamics (CFD) is an analytical tool used to predict the flow physics in various systems. In particular the use of CFD to predict the performance of gas turbine blade film cooling schemes has become increasingly widespread. Its advantages lie in faster results at lower costs than with experimental studies. Many parameters used in CFD have an influence on predicted film cooling results, which is the cause of much active research in this field.

Launder and Spalding (1974) proposed a semi-empirical model for predicting turbulence, which predicts the turbulence kinetic energy k and the dissipation rate ε by solving transport and governing equations simultaneously. This model is known today as the standard k-ε model. It is considered a high-Reynolds model, i.e. it is valid only in fully turbulent regions, far enough from walls or other physical boundaries. Two variants of this model, the RNG (renormalization group) k-ε model and the realizable k-ε model, were introduced by Yakhot and Orszag (1986) and Shih et al. (1995), respectively. Both offer many refinements compared to their precursor, and lead to more accurate predictions for certain types of flow.

Amer et al. (1992) compared four different turbulence models (standard k-ε and k-ω, as well as two modified versions of each of these models) applied to a simulation involving two rows of film cooling holes in a flat plate, inclined at 30 degrees with respect to the flow direction, with M from 0.2 to 1.0. They measured the performance of the turbulence

models to predict the adiabatic film cooling effectiveness distributions on the film-cooled surface. The study shows that the performance of those models is highly dependent on the blowing rate used and on the distance downstream of injection.

Kim and Benson (1991) simulated a circular film-cooling hole with normal injection on a flat surface using a structured hexahedral grid approach. This study provided two important insights. First, it demonstrated the importance of including the near upstream region in the computational domain. The flow and turbulence fields in the upstream region of the domain are influenced by the strong interactions between the crossflow and the jet at the film-hole exit. Secondly, the authors showed that the use of a fixed boundary condition at the jet exit (such as constant vertical velocity or total pressure conditions) could possibly compromise the accuracy of the results. This came from the observation that the jet velocity, static pressure, and total pressure vary widely over the cross-section of the jet. For this study, the computational grid included the mainstream as well as the hole (of length L/D = 1), and was composed of 148, 61 and 94 mesh points in the streamwise, spanwise and heightwise directions respectively.

Leylek and Zerkle (1993) obtained numerical results for a row of short circular film-holes (L/D = 1.75 and 3.5) inclined at 35° to the mainstream on a flat plate, which they compared to previously obtained experimental results. Simulations were conducted using a structured hexahedral grid, and turbulence was modeled with the standard k-ε model with standard wall functions. The authors stress the importance of modeling the plenum, even more so as L/D decreases and M increases, because the conditions at the hole exit

are dependent on those at the plenum and hole inlets. The computational domain used included the mainstream, film-hole region as well as the plenum. The simulations showed that the coolant flow does not interact in the same manner with the crossflow at the film hole exit for short and long holes. Specifically, computations showed that the jetting effect on the upstream wall of the film hole is more pronounced in the case of short holes than in the case of long holes. Furthermore, the authors isolate three phenomena which compete to dictate the flow characteristics at the jet exit, namely the counter-rotating vortex structure, the local jetting effect within the film hole, and the mainstream blockage determined by the blowing ratio.

The numerical study by Zhou et al. (1993) simulated flow behavior for one and two rows of square holes of pitch 4D inclined and oriented at various angles on a flat surface for blowing rates of 0.2, 0.4 and 0.8. A mesh of hexahedral structured elements was used for this purpose. They predicted that laterally oriented jets are less sensitive to fluctuations in the mass flow rate than other jets. Additionally, these types of holes, whether in a single row or a double row configuration, offer better coverage in the near-hole area. This conclusion comes from the fact that the flow structure dictated by the laterally oriented jets pushes the coolant onto the surface and promotes higher levels of effectiveness near the hole (compared to streamwise oriented jets, in which the symmetrical counter-rotating vortices tend to lift the coolant jet from the surface). However the simulations show that laterally oriented holes lose their superiority compared to streamwise oriented holes when effectiveness contours are compared further downstream of injection. Double row film cooling using row spacing of 3D was found to promote higher spanwise averaged film

cooling effectiveness than single row film cooling, no matter what the inclination and orientation of the jet were simulated. The turbulence model used in this study is the standard k-ε model with standard wall functions, except in regions close to the wall, where a low-Re number model was used.

Sarkar and Bose (1995) compared various turbulence models, including low-Reynolds-number k-ε models and k-ω models. The models were implemented in simulations of a slot in a flat plate at blowing rates of 1.0 and 1.8, using a structured quadrilateral non-uniform mesh with 60 x 50 nodes in the streamwise and heightwise directions, respectively. The boundary condition at the slot exit was set as a uniform velocity profile, an approximation that the authors considered reasonable considering that the slot is short enough compared to its width. The predictions were compared in terms of computed adiabatic effectiveness, flow and temperature fields, and turbulence parameters. Results show that all models tested tend to underpredict effectiveness at far-downstream locations ($x/d > 35$), and this trend is more pronounced at $M = 1.0$ than at $M = 1.8$. Both versions of the low Reynolds number k-ε models were found to best predict the adiabatic effectiveness distributions for this film cooling geometry.

Garg and Gaugler (1995) showed that jet exit plane conditions have a significant impact on downstream film cooling results. They predicted the effect of coolant velocity and temperature distribution at the film-hole exit on the heat transfer coefficient for three different types of film-cooled turbine blades. Their study suggests that the heat transfer

coefficient is more sensitive to these effects when the film hole is located on the suction rather than on the pressure surface of the blade.

Analysis of the numerical and experimental flowfield around one row of six rectangular jets of normal injection, with pitch to diameter ratio of 3 and length to diameter ratio of 5, was carried out by Ajersch et al. (1995). The blowing rates investigated were 0.5, 1.0 and 1.5. The 3-D computational domain, which contains a non-uniform structured mesh composed of 200 000 hexahedral cells, encloses the mainstream (of height 25D) and the film-hole itself, the hole being located 10D downstream of the mainstream inlet boundary. The authors imposed a uniform-velocity and kinetic energy boundary condition at the jet inlet. The authors found that the streamwise velocity downstream of injection is overpredicted, whereas the turbulence kinetic energy is found to be in general underpredicted, especially inside the hole near the exit plane.

Walters et al. (1995) introduced a systematical approach applied to numerical simulations involving film cooling experiments, in an attempt to yield consistently more accurate results. Simulation of a 2D slot with normal injection was conducted (the momentum flux ratio was varied between 2.0 and 7.3, while keeping the density ratio constant at a value of 1.0), using an unstructured/adaptive mesh with two variations of the k-ε turbulence model (standard and RNG k-ε models); the wall y^+ varies between 30 and 80 inside the slot, and assumes a value of 50 for the bottom wall of the mainstream and 100 for the top wall. The study states that in order to obtain more accurate solutions, the mesh must be of high refinement and high quality in terms of skewness, and realistic

modeling and boundary conditions must be implemented. In addition, a higher-order discretization scheme must be used in the computations. Comparison of results obtained with the two turbulence models indicates that performance of turbulence models should only be compared if the these criteria are met. In particular, the authors state that the greater the number of highly skewed cells contained in a particular grid, the greater the numerical error associated with the solution, thus making an unstructured mesh a prime choice for cases where geometries are complex. The authors' recommendations include creating a domain large enough which contains the hole and has realistic boundary conditions, and creating an initial mesh that has the best quality and cell concentration as possible.

Berhe and Patankar (1996) conducted various numerical film cooling simulations to investigate the general behavior of the flow on the test plate, as well as the effect of varying various parameters on film cooling effectiveness. A non-uniform structured hexahedral mesh approach was implemented, with 98 x 15 x 68 elements in the streamwise, vertical and lateral directions. The domain used in this study includes the plenum and hole regions, and extends 20D upstream of the hole exit. Turbulence modeling was achieved through the use of the standard k-ε model, with values of y^+ equal to 50, 30 and 20 for the mainstream, film hole and plenum walls respectively. By varying the plenum height, the authors found that only when this parameter was less than 2D did the plenum flow direction have an effect on the film cooling effectiveness. The authors compared their results with those from several previous experimental and computational studies; they found their computed centerline effectiveness data to be in good agreement

with the experimental data, but found that the laterally averaged values of effectiveness were underpredicted. They attribute this to the poor capabilities of the standard k-ε turbulence model to simulate lateral spreading of the jet.

Hyams et al. (1996) numerically studied four different slot geometries and examined what mechanisms affected the film cooling performance they delivered. The slots were inclined at 35 degrees and had one or more blunt edges which allow the flow to turn gradually. The turbulence is simulated using the standard k-ε turbulence model. The computational domain enclosed the mainstream, hole and plenum regions, and extended 40 slot-widths ahead of, 20 slot-widths above and 30 slot-widths downstream of the slot exit. The mesh was created using an unstructured grid with low skewness levels, which keeps y^+ values between 20 and 30 on walls inside the slot and in the mainstream bottom. According to the authors, the film cooling performance is influenced most by three characteristics of the flow, namely the separation region found at the slot inlet, the region of accelerated flow within the upstream part of the slot, and the region of high pressure gradient at the trailing edge of the slot exit. Diffusing the slot inlet or exit was found to increase the performance of film cooling, for all M tested, and this was even more so for the shaped exit cases than the shaped inlet cases. The advantage gained from shaping the slot inlet increases with increasing M, while that obtained from shaping the slot exit remains constant no matter what the blowing rate is. For both geometries the presence of competing mechanisms reduces the cooling potential of the film, but these mechanisms can be eliminated if the slot is shaped both at the inlet and the exit.

McGrath and Leylek (1998) studied the predicted flowfield around compound angle shaped holes (forward-expanded), in particular the ingestion of crossflow into the film cooling hole. The authors generated the numerical data using a 3-D computational domain constituted of 800 000 to 900 000 unstructured tetrahedral elements. The domain, which includes the plenum, extends 10D above and upstream of, and 25D downstream of the hole. The numerical results reveal that crossflow ingestion is exacerbated when the hole exit is diffused at the trailing edge, and/or when the blowing rate is high enough to cause jetting at the hole exit trailing edge.

Ferguson et al. (1998) compared and reported the performance of various versions of k-ε and RSM turbulence models in a simulation of cylindrical round film-cooling holes in a flat plate. This was done using unstructured/adaptive mesh containing 300 000 to 400 000 elements. For all cases using wall functions, the domain extends 19D upstream of, 30D downstream of and 10D above the injection location; this domain is reduced when the two-layer model for enhanced wall treatment is applied. Computations showed that turbulence levels within the hole are much lower for the RNG and RSM models than with other models. This explains the low diffusion observed in the coolant jet in simulations using these turbulence models. The authors also concluded that wall functions are better suited to deal with turbulence in the plenum that the two-layer zonal model, but they do not resolve as well such features as jet lift-off. According to the study, the simulations which matched experimental results best were those using the standard k-ε model and the two-layer model.

Hale et al. (1999) tested the standard and RNG k-ε models as well as the Reynolds Stress model several turbulence models, with non-equilibrium wall functions and two layer zonal-models for film cooling simulations of short holes (L/D = 2.91) fed by a narrow plenum of height-to-diameter equal to unity, with blowing rates between 0.5 and 1.0. Simulations were undertaken using the commercial software FLUENT with a structured non-uniform mesh composed of 600 000 to 900 000 hexahedral elements. After having compared their predictions with experimental results, they concluded that non-equilibrium walls functions do not give accurate predictions of the flowfield or adiabatic film cooling effectiveness distributions, especially in the near-hole region where the jet lifts off from the surface and a recirculation bubble is formed.

Walters and Leylek (2000), McGovern and Leylek (2000), Hyams and Leylek (2000) and Brittingham and Leylek (2000) conducted a series of computational studies concerned with the analysis of the film cooling flow obtained with streamwise or compound circular and shaped holes. The use of CFD for complex film cooling geometries was validated and a computational methodology used to predict both the adiabatic film cooling effectiveness and the heat transfer coefficient was presented. The computational domains, which included the mainstream, hole and plenum regions, were meshed using 600 000 to 800 000 tetrahedral elements. These studies give some insight on various flow mechanisms, such as vorticity generation within the film hole.

Gartshore et al. (2001) were interested in knowing whether or not prediction accuracy depends on film cooling hole cross section geometry. They modeled compound holes

with round and square cross-sections at blowing rates of 0.5, 1.0 and 1.5. The three-dimensional computational domain included solely the hole and mainstream regions, and extended 5D upstream, 25D above and 30D downstream of injection. Results were obtained using the standard k-ε turbulence model. The authors found that the accuracy in the predictions is similar for round and square holes. When comparing the spanwise averaged adiabatic effectiveness obtained at blowing rates of 0.5 and 1.5 to experimental results, the authors noted that the accuracy of prediction is improved when the blowing rate is low. It was also observed that round holes perform generally better than square holes, especially at high blowing rates.

2.4 Summary and Objectives

- Hole geometry is an important parameter for film cooling performance. Laterally-and-forward-expanded holes provide higher values of spanwise averaged effectiveness and lower values of spanwise averaged heat transfer coefficients than laterally-expanded holes. However, the former has a tendency to allow hot mainstream ingestion into the windward portion of the hole exit. Flared holes have the best overall performance, especially at high blowing rates, when compared to the standard circular film cooling hole. Their diffused exits reduce the coolant momentum, allowing it to spread laterally, thus resulting in increased film protection.

- Compound angle injection, whether for shaped or circular holes, leads to an increase in spanwise averaged effectiveness compared to that obtained with standard circular holes. However, compound jets generally produce higher values of heat transfer coefficient on the surface than do simple injection jets, and this trend is amplified as the blowing rate rises.

- Hole spacing affects the ability of adjacent jets to coalesce. Small hole spacing results in better coverage of the wall, and thus higher effectiveness values than larger ones. A pitch-to-diameter ratio of 3 was commonly used in film cooling studies.

- For standard circular holes on a flat surface with low mainstream turbulence intensities, the downstream effectiveness is optimum for blowing ratios of approximately 0.5. For blowing rates above this value, the coolant jet undergoes lift-off. This allows the hot gases to come in contact with the surface, which causes the effectiveness to decrease.

- At small blowing rates, the length-to-diameter ratio L/D generally has no major effect on the spanwise averaged effectiveness obtained for standard circular holes in a flat plate. The only exception is in the near hole region where short holes perform best. At high blowing rates, small L/D holes, for $x/D \leq 3$, perform better in terms of effectiveness in the near-hole region, however large L/D holes are more efficient further downstream. The smaller the hole length-to-diameter (L/D) ratio, the larger the effective injection angle, indicating that the jet lifts off at a smaller value of blowing ratio when the L/D ratio is small.

- An increase in mainstream turbulence intensity Ti at low blowing rates decreases the spanwise averaged adiabatic film cooling effectiveness due to the enhanced mixing of the mainstream and coolant flow. There is a critical blowing ratio for which an increase in Ti brings about an increase in spanwise averaged effectiveness. For these cases the turbulence delays the jet lift-off by pushing the detached jet back to the surface, which enhances the film coverage. Furthermore, the effectiveness is not as dependent on Ti at high blowing rates as it is at low blowing rates.

- A decrease in density ratio causes an increase in the downstream heat transfer coefficient on the film-cooled surface for the 35 degree inclined holes, however no significant effect on heat transfer coefficient for 90 degree inclined holes (normal injection) was observed. Lowering the density ratio has the same effect as increasing the momentum flux ratio, such that it reduces the lateral spreading of the jet thus lowering the spanwise averaged adiabatic film cooling effectiveness.

- All plenums with flow direction were observed to yield superior effectiveness compared to that for the standard stagnant plenum. The plenum flow direction has an effect on cooling effectiveness only when the plenum height is less than 2D. Counter-flow plenums produce better centerline effectiveness in the near-hole region than that in co-flow plenums at low and high blowing rates. However at high blowing rates, the co-flow performs best in terms of spanwise averaged effectiveness for $x/D \geq 2$.

Few studies in the open literature have focused on novel hole geometries for increased cooling performance. To date, most film cooling schemes aim to cool the turbine airfoil surface downstream of injection. With the conception of an advanced film cooling hole geometry, which extracts some cooling potential from the jet prior to being ejected into the mainstream by impinging it onto the blade material, a greater portion of the airfoil is protected. The present study will numerically investigate the effect of the blowing ratio, the hole geometry (nozzle inlet geometry and pedestal configuration), the mainstream

turbulence intensity, and the turbulence model on the downstream adiabatic film cooling effectiveness for such a geometry. The velocity, temperature, and turbulent kinetic energy fields will also be analyzed and reported in order to explain the behavior of the flow. This novel film cooling scheme is expected to provide several benefits over standard round film cooling holes since the flared hole exit, designed to reduce the coolant momentum and ensure wide lateral spreading of the coolant on the downstream surface, will provide enhanced film cooling protection both in the lateral and streamwise directions, with pedestals also inducing the lateral spreading of the flow. While the inlet nozzle geometry is expected to mainly affect the heat transfer characteristics of the impinging jet (which will be investigated in a future study), it is expected that this geometry will also influence the downstream effectiveness.

Chapter III

Numerical Analysis

3.1 Problem Description

The computational domain and film cooling geometry are depicted in Figure 3-1, Figure 3-2a and 3-2b. The domain consists of an infinite row of film cooling holes in a flat plate, such that end-wall effects are neglected. The domain dimensions are expressed in terms of D_h = 17.1 cm which is the hole exit hydraulic diameter (at y/Dh = 0). Since all results in the present study are presented in a dimensionless form, they are not dependent on the value of D_h. This was confirmed when results obtained from simulations of cases using different values of D_h (at constant Reynolds number based on D_h) were compared and found to be identical. The dimensions of the hole shown in Figure 3-2a and 3-2b are expressed in terms of $D = D_h/17.1$. This is not a major parameter as it is used for scaling purposes only, and not for any result presentation.

The various hole configurations are summarized in Table 3-1. Each case is designated by a two-part nomenclature. For example, NOV1-4p refers to the geometry possessing a three-impingement-hole inlet and four pedestals. The suffix refers to the pedestal configurations, with -4p, -2p and -0p corresponding to the four-pedestal, two-pedestal and no-pedestal arrangements, respectively. In the -2p configuration, the two outer pedestals have been removed. The computational domain extends $21D_h$ upstream, $32D_h$

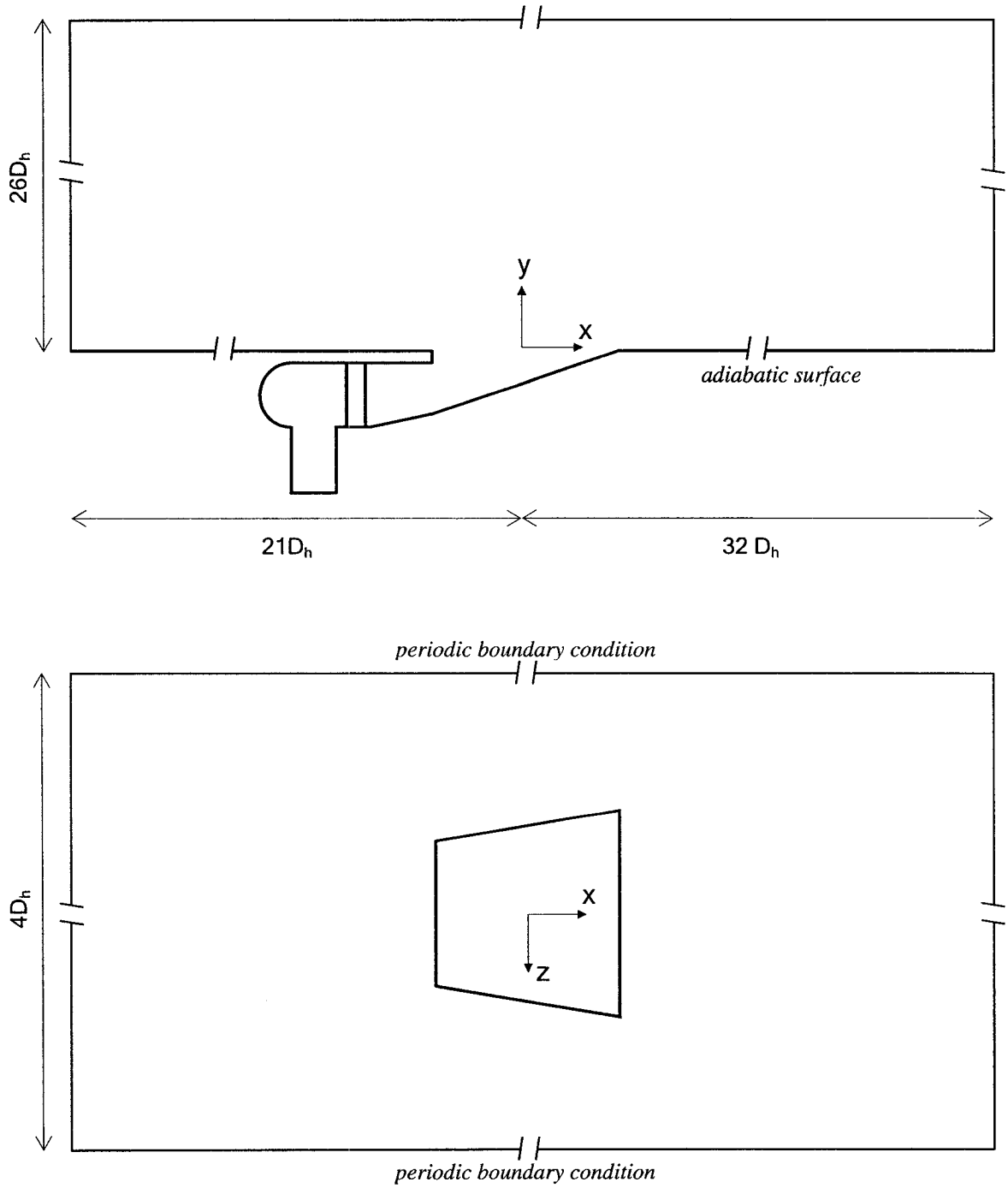

Figure 3-1. Computational domain.

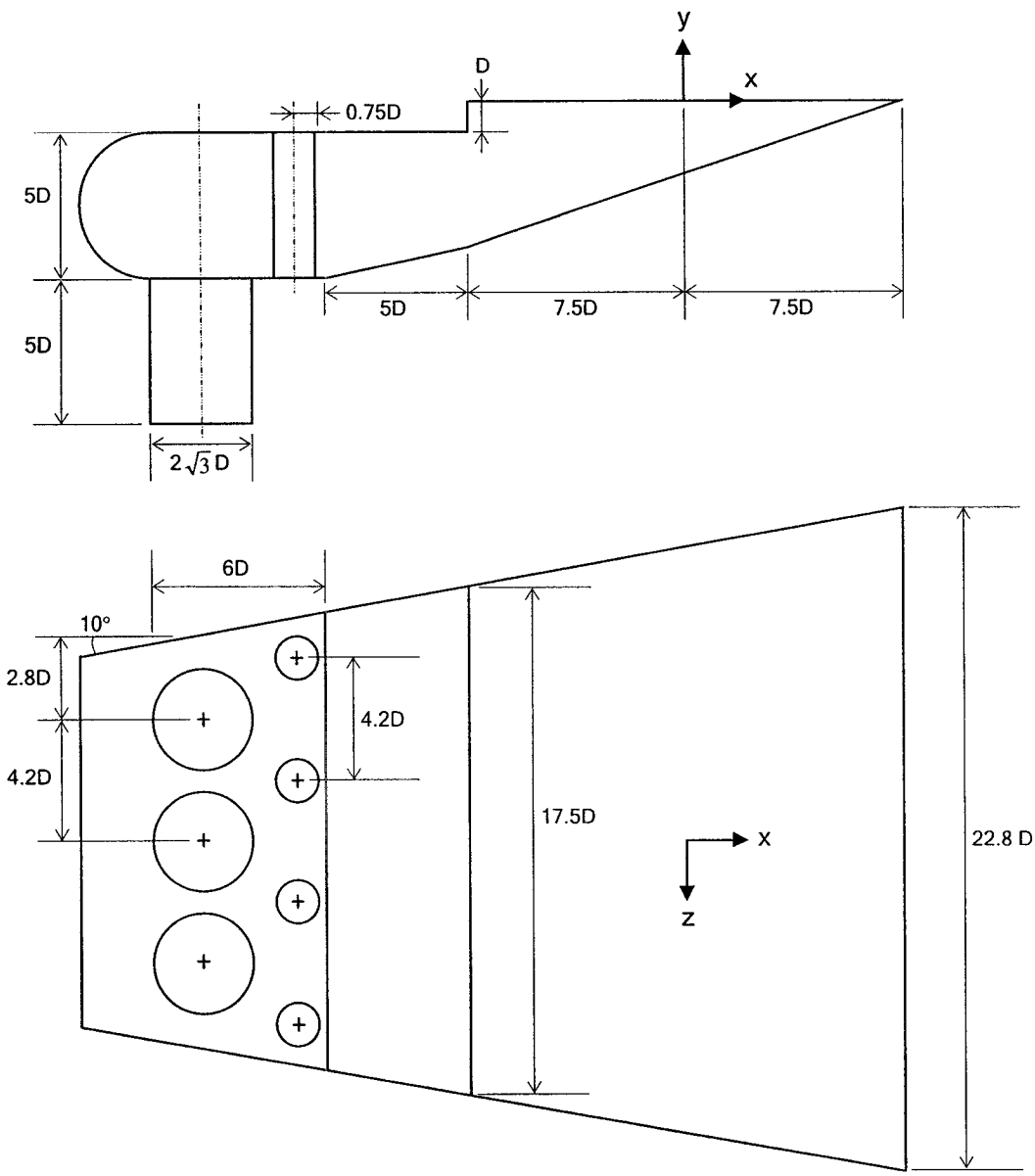

Figure 3-2a. Hole geometry (NOV1-4p configuration).

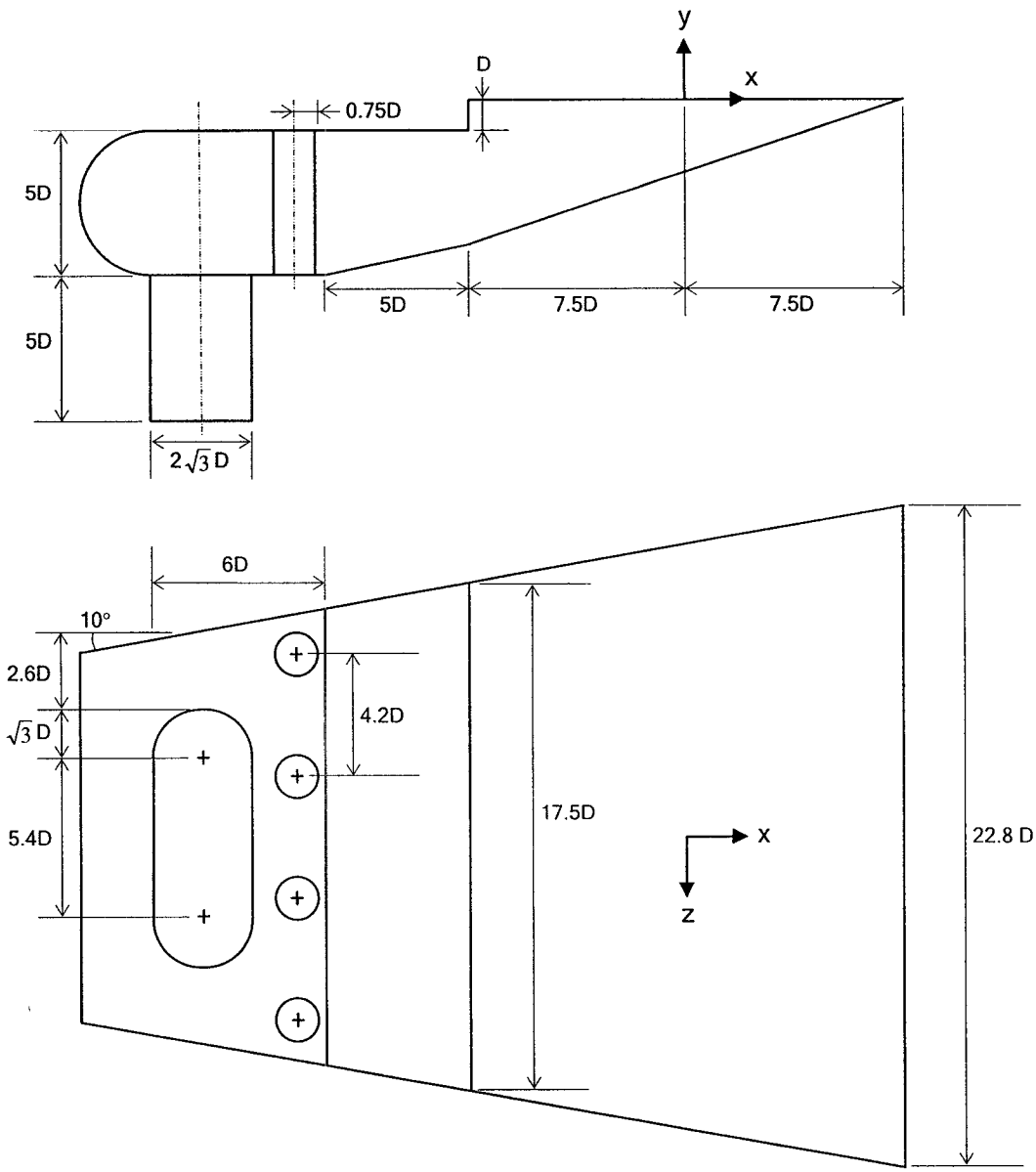

Figure 3-2b. Hole geometry (NOV2-4p configuration).

Table 3-1. Film cooling hole nomenclature.

Geometry	Description
NOV1-4p	Three inlet impingement holes Four pedestals
NOV1-2p	Three inlet impingement holes Two pedestals
NOV1-0p	Three inlet impingement holes No pedestals
NOV2-4p	One inlet impingement slot Four pedestals

downstream and $26D_h$ above the locus of injection, while the hole pitch-to-diameter ratio is $4D_h$. It was possible to reduce the size of the domain due to the periodic nature of the flow. To reduce the computational effort, the domain is centered about one hole centerline and is periodic about the planes $y/D_h = 2.1$ and $y/D_h = -2.1$. The hole is oriented in the same direction as the mainstream flow and the top mainstream boundary satisfies a free-slip condition ($\partial u/\partial y = 0$). All walls are treated as adiabatic with a non-slip condition.

Cooling air enters the hole with uniform velocity in the y-direction through either three impingement tubes or an impingement slot of identical area, with a turbulence intensity of 3% and a turbulent viscosity ratio μ_T/μ of 5. Mainstream air enters the domain with uniform velocity in the x-direction, with a turbulence intensity of 3% or 10% and a turbulent viscosity ratio of 5. For all computational cases, the mainstream and coolant inlet temperatures were set to 1300 K and 750 K, respectively. The coolant inlet velocity was maintained at 3 m/s, while the mainstream inlet velocity was varied between 1 m/s and 6 m/s, corresponding to blowing rates M_i between 0.87 and 5.22 based on hole inlet conditions. The flow is considered incompressible since the Mach number for both the coolant and the mainstream is inferior to 0.02.

3.2 Numerical Grid

Numerical results in this study were obtained using the commercial CFD package which includes the CFD solver FLUENT 6.1 and the mesh generation preprocessor software Gambit 2.0.4. The preprocessor Gambit, which allows the use of several element types

(hexahedrons, wedges, tetrahedrons or pyramids - Figure 3-3), as well as various meshing schemes, was used to design the computational domain and create a hybrid mesh of tetrahedral/wedge elements. An unstructured grid approach with tetrahedral element offers excellent flexibility to discretize complex geometries. However the advantage of this approach is offset by a lower control in node placement when compared to the structured grid approach. This limits the capacity to adjust the height of the nodes adjacent to the wall surfaces of the domain, a key criterion for the validity of the turbulence models used in this study. Section 3.2.3 explains the use of the structured part of the mesh (the wedge-type elements) to work around this problem. The density, shape and distribution of the elements are some factors that affect the accuracy of the numerical solution.

The grid was generated in the following manner. Nodes were equally-spaced or with an exponential distribution on all edges. Faces were then meshed into triangular elements using the "Tri-pave" scheme specified in Gambit. The meshing is identical on periodic faces of the domain. The interior of the domain was meshed into tetrahedral and wedge elements using the "Tet/Hybrid-TGrid" scheme specified in Gambit. It should be noted that the words "grid" and "mesh" are equivalent and used interchangeably in this study.

3.2.1 Grid Density

Numerical (or false) diffusion is inversely proportional to the density of the grid. However, the grid does not require the same fineness

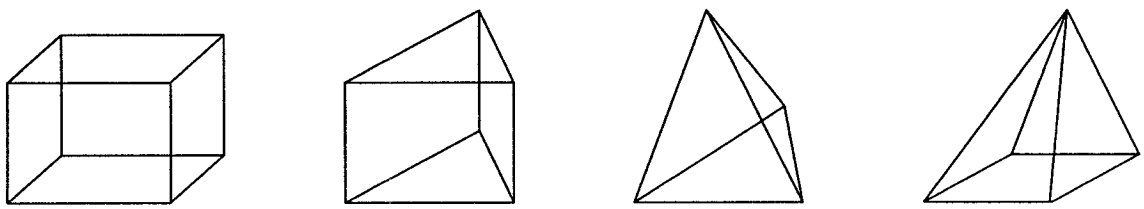

Figure 3-3. Various mesh element types.

everywhere, and the mesh may be coarser in regions where the flow is unchanging, in order to save computational time. The computational grid should be fine enough to minimize errors and ensure that the solution is accurate and grid-independent, especially in regions of strong curvature and gradients. For this reason, it is desirable to concentrate the mesh elements near walls in particular, in order to capture the changing behavior of the fluid.

A study was conducted to determine the minimum number of elements required in the domain in order to obtain a grid-independent solution. Several meshes were generated different numbers of elements, and the numerical results were obtained and compared. Grid independence was asserted when the difference between solutions was considered sufficiently small. A sample grid generated for this study is shown in Figures 3-4a and 3-4b. Grid refinement was performed manually in Gambit, by successively increasing the number of nodes in the vicinity of the bottom mainstream wall and the film cooling hole.

Solutions for the grid-independence study were compared in terms of two parameters. The first is the centerline adiabatic film-cooling effectiveness downstream of injection η. The downstream variation of the centerline adiabatic film cooling effectiveness for the NOV1-4p geometry at M_i = 3.48 and Ti = 3%, calculated with the realizable k-ε turbulence model, using grids containing 36153, 633620, 739510 and 819675 elements is shown in Figure 3-5. It can be seen from this figure that the 633620-element, 739510-element and 819675-element grids yield similar results. Even though there is a 30%

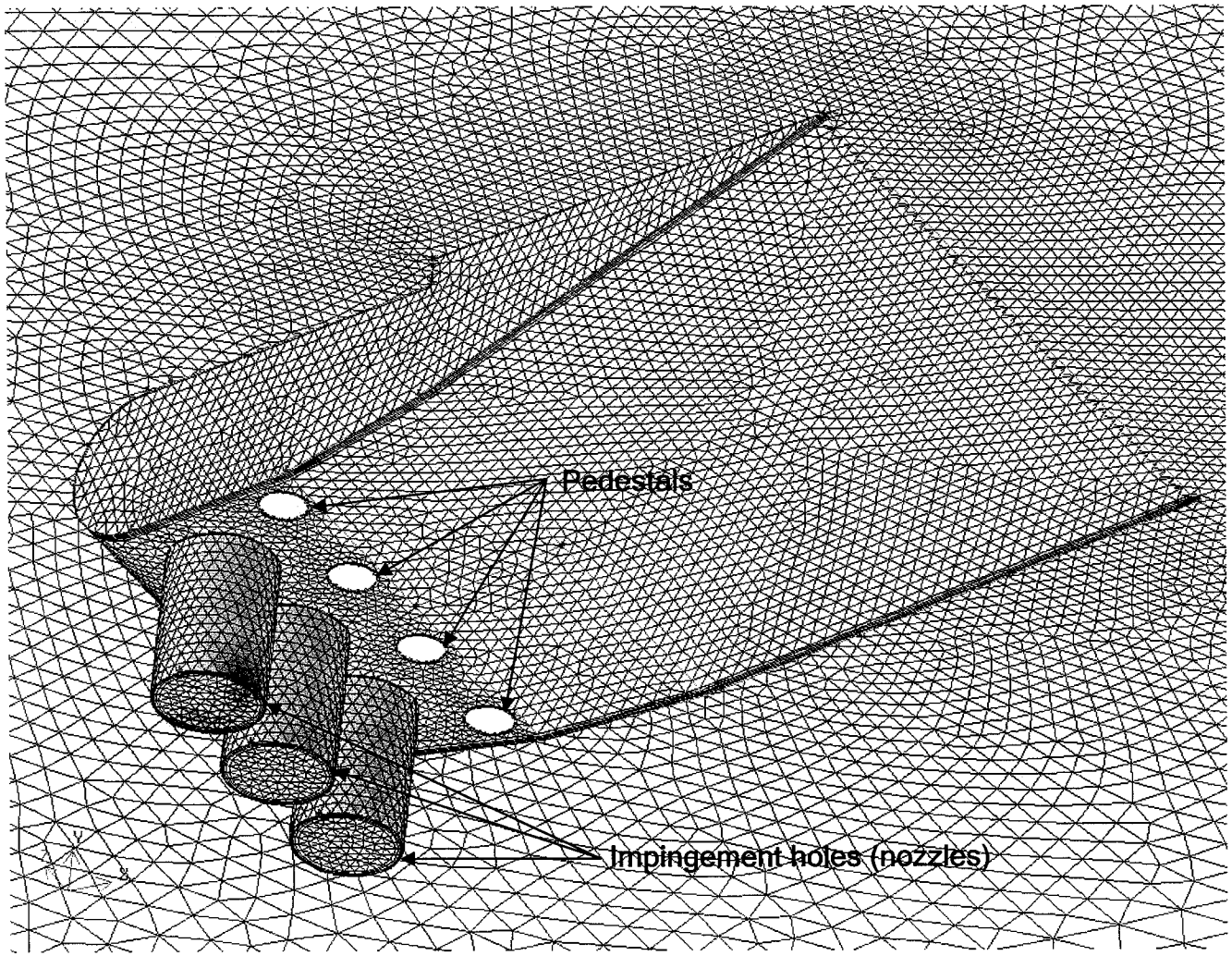

Figure 3-4a. Computational grid in the near hole region.

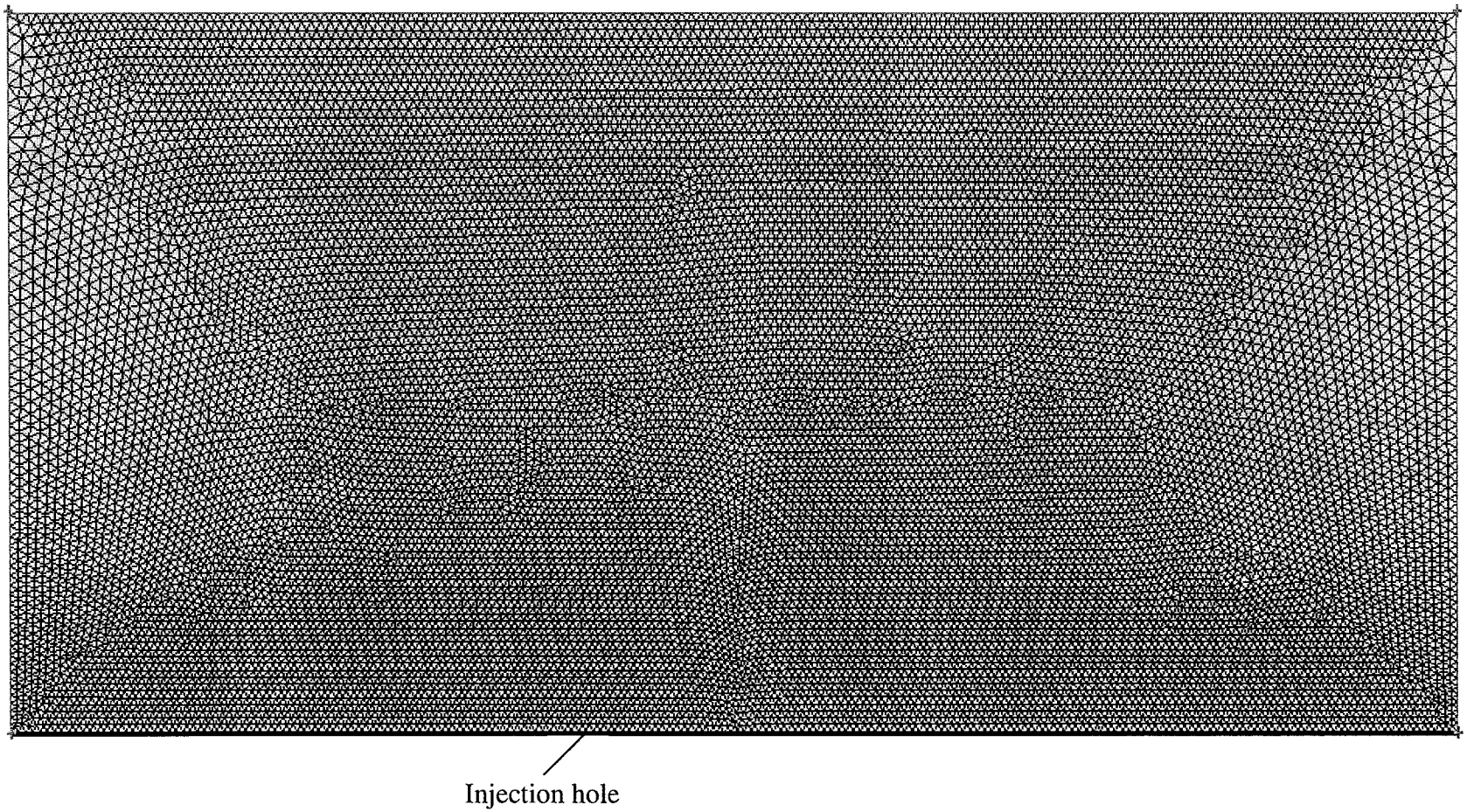

Figure 3-4b. Computational grid in the mainstream region.

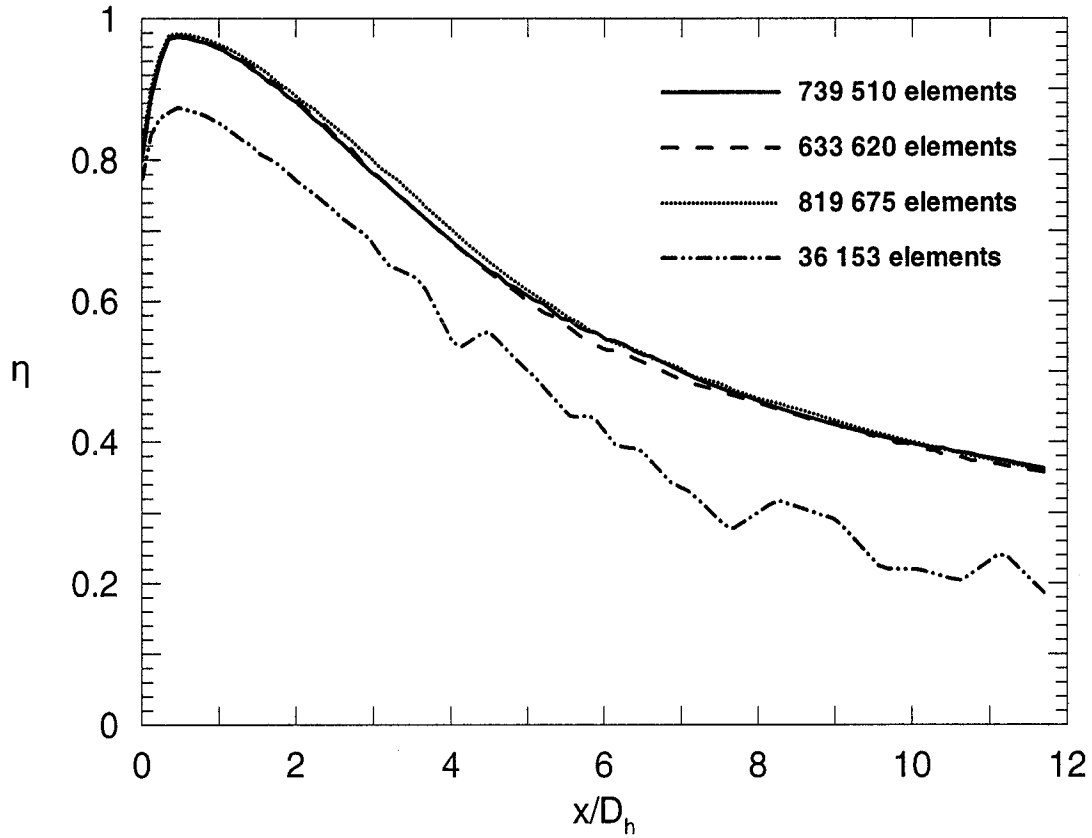

Figure 3-5. Centerline adiabatic film cooling effectiveness for various grid densities at $M_i = 3.48$ for the NOV1-4p geometry (Ti = 3%, realizable k-ε turbulence model).

increase in number of elements between the 633620-element and the 819675-element grids, the discrepancy in the centerline effectiveness remains below 3%.

The second parameter used for comparison in the grid-independence study is the lateral distribution of adiabatic effectiveness at various downstream locations in the domain (x/Dh = 1, 3 and 8), and the results are shown in Figure 3-6 for the same cases. Results confirm that the solution is grid-independent for a mesh of at least 633620 elements. Figure 3-6 shows that the difference between the effectiveness predicted by the 36153-element grid and that predicted by the other grids increases at regions more downstream of the hole. This is due to the fact that the mesh inside the hole is much finer than in the mainstream, thus it propagates in the near-hole region. For coarse meshes, this fine mesh propagation reduces the numerical error of the solution near the hole.

3.2.2 Grid Quality

Grids were optimized in terms of quality in order to reduce numerical errors. The smoothness of the mesh and element skewness both have a significant impact on the solution accuracy. Smoothness in a mesh is characterized by a gradual change in volume in adjacent elements, which helps minimize the truncation error. This error is defined as the difference between the partial differential equations and the finite difference equations. Element equivolume skewness compares the difference in volume between a given cell and an equilateral cell inscribed in a sphere of radius identical to that

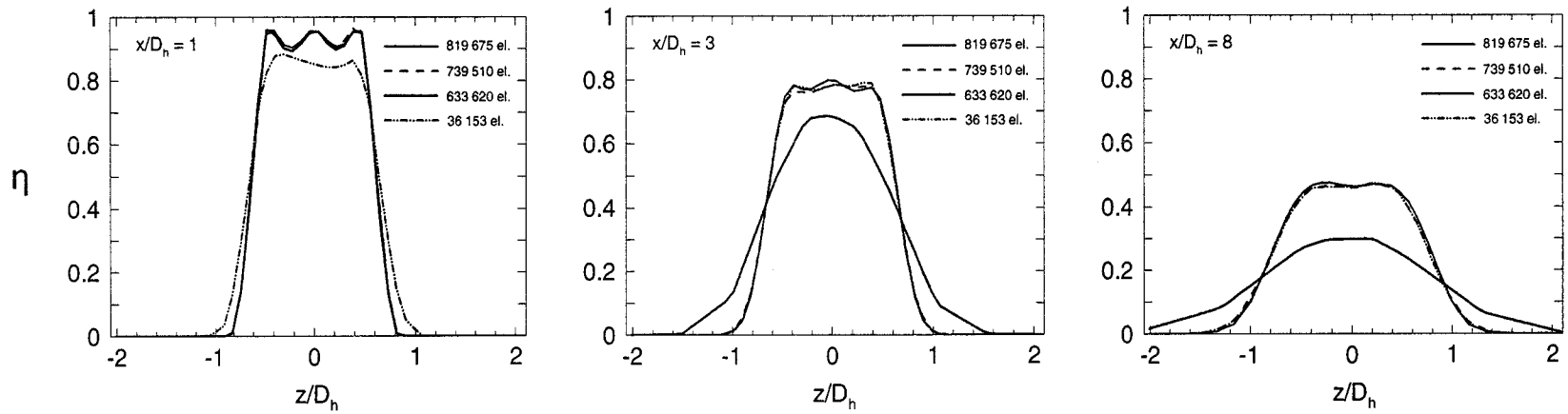

a) $x/D_h = 1$ b) $x/D_h = 3$ c) $x/D_h = 8$

Figure 3-6. Lateral ditribution of adiabatic film cooling effectiveness for the NOV1-4p geometry at various downstream planes: a) $x/D_h = 1$, b) $x/D_h = 3$, c) $x/D_h = 8$ ($M_i = 3.48$, Ti = 3%, realizable k-ε turbulence model).

circumscribing the given cell. This can be summarized by the following scaled parameter:

$$\text{Element equivolume skewness} = \frac{\text{Equilateral} \cdot \text{cell} \cdot \text{volume} - \text{cell} \cdot \text{volume}}{\text{Equilateral} \cdot \text{cell} \cdot \text{volume}} \tag{3.1}$$

An equivolume skewness of 0 corresponds to an equilateral tetrahedral element; this value increases as the element collapses, until finally it becomes unity for a degenerate element (whose nodes are coplanar). Similarly, the element equiangle skewness indicates the skewness levels in faces of elements only. It is defined as:

$$\text{Face equiangle skewness} = \text{Max}\left[\frac{\theta_{max} - \theta_e}{180 - \theta_e}, \frac{\theta_e - \theta_{min}}{\theta_e}\right] \tag{3.2}$$

Where

θ_e = 60 (angle of an equilateral triangular face)

θ_{max} = largest angle in the face

θ_{min} = smallest angle in the face

An equiangle skewness of 0 corresponds to an equilateral face, while an equiangle skewness of 1 is attributed to a degenerate face, whose nodes are coplanar. It is desired to reduce the skewness levels in the grid, since an increase in the number of highly skewed cells in the domain reduces the accuracy of the solution due to an increase in the

numerical error. Mesh smoothing and cell swapping are tools available in Fluent 6.1 to improve the quality of the mesh. Skewness smoothing was used to reposition nodes such that the average levels of equiangle and equivolume skewness in the mesh were reduced. The smoothing operation was followed by face swapping, which involves repositioning element edges and faces such that the grid is optimized in terms of skewness for a fixed node distribution. Since smoothing and swapping are time consuming and tend to even out the mesh in terms of element concentration, only four iterations of smoothing followed by the swapping procedure were performed on cells of equivolume skewness superior to 0.8. The process was repeated once more on cells of equivolume skewness superior to 0.6. This procedure resulted in a reduction by approximately 2.76% and 0.46% of the equivolume skewness and equiangle skewness levels in the grid, respectively.

3.2.3 Mesh Boundary Layer

Five layers of wedge-type mesh elements were placed adjacent to most wall surfaces to ensure a minimum of 10 elements in the viscosity affected region. This study uses turbulence models with enhanced wall treatment, which require to be valid $y^+ \approx 1$ (with $y^+ < 5$ acceptable, as stated in FLUENT 6.1 Documentation, 2003). This parameter is defined as following:

$$y^+ = \frac{\rho u_\tau y_p}{\mu} \tag{3.3}$$

where $u_\tau = \sqrt{\tau_w/\rho_w}$, y_p is the height of the first node P off the wall and ρ and μ are the fluid density and viscosity at this node, respectively. In order to achieve a wall $y^+ \approx 1$ solely with tetrahedral elements, the element density can become very large. This is due to the fact that, for tetrahedral grids, the height of the elements is inversely proportional to the grid density in the computational domain.

The wedge elements, unlike tetrahedral elements, have a fixed height on a given layer, and this height gradually increases with the distance from the surface. This allows good control on the height y_p of the first node next to the wall while minimizing the number of elements. The value of y_p for which y^+ is around unity, was determined by iteration by measuring the value of y^+ obtained on all surfaces after convergence and correcting the height of the first layer of wedge elements in Gambit. The mesh boundary layer of wedge elements was omitted on surfaces where the tetrahedrons were small enough, and thus the element density being high enough, to ensure valid turbulence modeling. Table 3-2 presents values of y^+ for typical simulations.

3.3 Numerical Model

The present film cooling study involves fluid which is steady, Newtonian, three-dimensional, incompressible and turbulent. Such fluid behaves according to three fundamental laws, namely the laws of continuity, conservation of momentum, and conservation of energy. These laws are expressed as follows:

Continuity

$$\frac{\partial}{\partial x_j}\left(\rho u_j\right) = 0 \tag{3.4}$$

Momentum

$$\frac{\partial}{\partial x_j}\left(\rho u_i u_j\right) = -\frac{\partial P}{\partial x_i} + \frac{\partial}{\partial x_j}\left(\mu \frac{\partial u_i}{\partial x_j} - \rho \overline{u_i' u_j'}\right) \tag{3.5}$$

Energy

$$\frac{\partial}{\partial x_j}\left(\rho T u_j\right) = \frac{\partial}{\partial x_j}\left(\frac{\mu}{Pr}\frac{\partial T}{\partial x_j} - \rho \overline{\theta u_j'}\right) \tag{3.6}$$

Table 3-2. Typical values of wall y^+ obtained with the final mesh.

Case	Area-weighted average of y^+ on the downstream surface	Area-weighted average of y^+ on surfaces inside the hole	Total area-weighted average of y^+
NOV1-4p, $M_i = 0.87$	2.4609	2.1863	2.4559
NOV1-4p, $M_i = 5.22$	0.6005	2.1210	0.6283

where Pr is the molecular Prandtl number, $\overline{u_i' u_j'}$ is the Reynolds-stress tensor and $\overline{\theta u_j'}$ is the turbulent heat flux. FLUENT 6.1 is used to solve these governing equations inside the film-cooling computational domain. The software discretizes the equations and solves them using a finite volume approach. In the present study, equations were discretized implicitly and solved sequentially for the dependent variables using a Gauss- Seidel method in conjunction with an algebraic multigrid method (FLUENT 6.1 Documentation, 2003). The viscosity μ, thermal conductivity K and specific heat Cp were approximated as piecewise-linear functions of temperature. Each function was defined using nine data points as shown in Table 3-3.

3.3.1 Pressure-Velocity Coupling Algorithm

The Pressure-Implicit with Splitting of Operators (PISO) algorithm was chosen as the pressure-velocity coupling method. This algorithm provides more efficient calculations than the SIMPLE and SIMPLEC algorithms, thus reducing the number of iterations required for convergence. FLUENT offers two refinements for this option, i.e. neighbor correction and skewness correction, which were both applied in this study. The PISO neighbor correction option adjusts the velocity during each iteration, such that it satisfies the continuity and momentum equations more closely. Although this procedure uses more

Table 3-3. Fluid properties at various temperatures (Holman (1997)).

Temperature (K)	Cp (kJ/kg·K)	K (W/m·K)	μ (kg/m·s)
750	1.0856	0.05509	$3.481*10^{-5}$
800	1.0978	0.05779	$3.625*10^{-5}$
850	1.1095	0.06028	$3.765*10^{-5}$
900	1.1212	0.06279	$3.899*10^{-5}$
950	1.1321	0.06525	$4.023*10^{-5}$
1000	1.1417	0.06752	$4.152*10^{-5}$
1100	1.160	0.0732	$4.44*10^{-5}$
1200	1.179	0.0782	$4.69*10^{-5}$
1300	1.197	0.0837	$4.93*10^{-5}$

CPU time per iteration, it permits a reduction in the number of iterations required to achieve convergence so that convergence is achieved in less time overall. This is advantageous for steady state problems, even though transient problems benefit more from this correction. The PISO with skewness correction allows easier and faster convergence for steady state problems that involve meshes with some level of cell skewness, by reducing the total number of iterations needed (FLUENT 6.1 Documentation, 2003). This correction complements the smoothing and swapping operations, thus maximizing the grid quality.

3.3.2 Discretization and Under-Relaxation Factors

It was shown by Walters et al. (1995) that higher order discretization schemes are among factors that lead to more accurate results in simulations of a film-cooling jet in crossflow. The use of the second order upwind scheme to discretize the equations leads to less numerical diffusion in the solution, since this scheme has second-order accuracy, while the first order upwind scheme has only first-order accuracy. This is of course only valid if the grid is fine enough (Patankar, 1980). One drawback associated with this scheme is that it fosters more instability in the convergence process than the first order scheme.

Numerical simulations of the film cooling geometry studied by Sinha et al. (1991) were conducted and the spanwise-averaged adiabatic film cooling effectiveness was obtained and compared to the experimental results. Three discretization schemes were used for comparison, namely first-order upwind, second-order upwind and power law schemes.

Figure 3-7 presents these results as well as the experimental data found by Sinha et al. (1991). All three schemes give very similar predictions of downstream centerline effectiveness except near $x/D_h = 0$ (where the prediction using the first order upwind scheme was furthest from experimental results). The power law scheme requires more computational time to achieve convergence than the first and second order schemes. Therefore the second-order upwind scheme was found to be a good comprise between good accuracy and fast convergence time, and was the discretization scheme of choice throughout this study. In numerical computations, it may be desirable to slow down the change in value of the dependent variables from one iteration to the next. At a given iteration n, the new value of each dependent variable is adjusted by a coefficient (relaxation factor) which dictates how much this value changes compared to the value at iteration n-1. The smaller the relaxation factor, the smaller the change in value of the dependent variable from iteration n-1 to iteration n. FLUENT only allows for relaxation factors less than or equal to one; these are termed under-relaxation factors. Lowering under-relaxation factors helps in the convergence of the solution, especially for strongly non-linear problems. However, this benefit is drawn back by an increase in computational time (Patankar, 1980). In this study under-relaxation factors were set as follows: 0.3 for pressure, 0.7 for momentum, 0.6 for turbulence kinetic energy, 0.6 for turbulence dissipation rate, 0.5 for turbulent viscosity and 0.8 for energy. Density and buoyancy were not relaxed. These values were found to ensure a good compromise between computing time and stability in the convergence process.

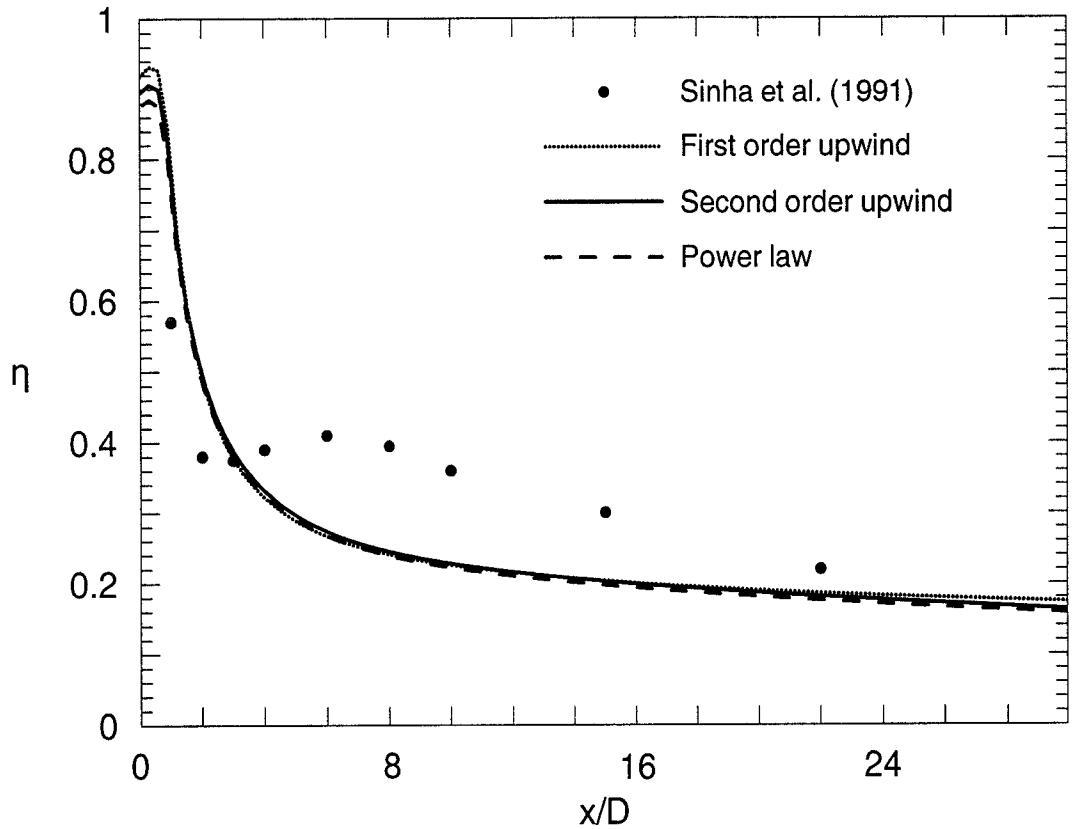

Figure 3-7. Centerline adiabatic film cooling effectiveness for the simple injection circular hole, obtained with three discretization schemes, at M = 1.0.

3.3.3 Convergence Criteria

A necessary condition for convergence is met when the values of the dependent variables remain almost unchanged from one iteration to the next, i.e. they are considered to be the correct solution to the governing equations for the problem studied. The exact solution will of course never be reached, as there will always be small numerical errors remaining in the solution. Moreover, the solution may never even reach convergence, and this happens if the variation in solution from one iteration to the next increases, in which case one speaks of divergence. Many factors affect convergence, including mesh quality, discretization schemes, pressure-velocity coupling algorithm, under-relaxation factors, and initialization among others. Convergence is evaluated by two necessary conditions:

Low and Stable Residuals

The algebraic form of the conservation equation for any variable Φ at each element C in the computational domain is of the form:

$$a_C \Phi_C = \sum_{nb} a_{nb} \Phi_{nb} + b \tag{3.7}$$

where *nb* denotes a neighbor element of C, and b is a constant. As long as the solution has not converged, this equality is not satisfied, and equation (3.7) thus becomes:

$$a_C \Phi_C = \sum a_{nb} \Phi_{nb} + b + R \tag{3.8}$$

where R is the imbalance in the element C. Thus the residual R^{Φ} of a given variable Φ over the entire computational domain is defined as:

$$R^{\Phi} = \sum_{all\_cells} \left| \sum_{nb} a_{nb}\Phi_{nb} + b - a_C\Phi_C \right| \tag{3.9}$$

Residuals measure how large the error in the solution is. After each iteration, FLUENT evaluates the algebraic form of the conservation equation for each dependent variable in every element of the domain, and compares it to what it should be if the solution was exact. Residuals can be scaled and/or can be normalized.

Scaled residuals are defined as:

$$R^{\Phi} = \frac{\sum_{all\_cells} \left| \sum_{nb} a_{nb}\Phi_{nb} + b - a_C\Phi_C \right|}{\sum_{all\_cells} |a_C\Phi_C|} \tag{3.10}$$

While normalized residuals are defined as:

$$\overline{R}^{\Phi} = \frac{R^{\Phi}_{iteration\_n}}{R^{\Phi}_{iteration\_m}} \tag{3.11}$$

where m is the number of iterations for which the residual is maximal. In the present study, the solution was considered converged when the scaled residuals of each variable reached at least $1.6*10^{-4}$ (and at least 10^{-6} for energy) while displaying a stable trend.

Constant Mass Flow Rate

The imbalance in mass flow rate was monitored at the film-hole exit plane at each iteration during the whole iterative process. Convergence was assumed when this imbalance was reduced to less than 0.001%. Figure 3-8 shows the change in centerline effectiveness depending on the value of the residuals. For cases where residuals are higher than $1.6*10^{-4}$, the solution is different for each case, even though the imbalance in mass flow rate may be lower than 0.001%. However for cases where residuals are lower than $1.6*10^{-4}$ (and for which the flow rate imbalance is lower than 0.001%), the change in solution is considered insignificant.

3.3.4 Turbulence Modeling

Turbulence modeling is one of the most challenging aspects of CFD, due to the fluctuating, random nature of turbulence. Flow turbulence is characterized by variations in the velocity fields. Three Reynolds-averaged Navier-Stokes (RANS) turbulence models, which employ averaged governing equations to solve for the mean flow quantities, were used in this study, namely the standard k-ε model (Launder and Spalding,

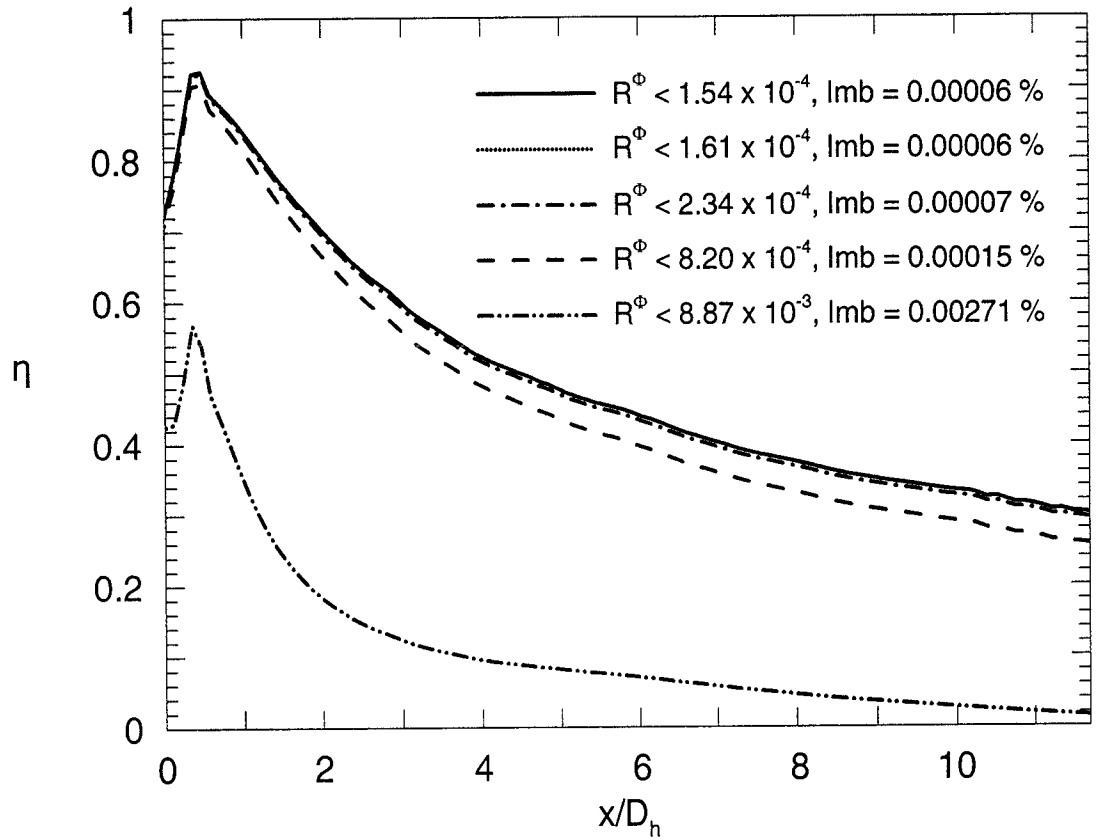

Figure 3-8. Centerline adiabatic film cooling effectiveness obtained for various values of residuals (NOV1-4p geometry, $M_i = 5.22$, Ti = 3%, realizable k-ε turbulence model).

1974), the renormalization group (RNG) k-ε model (Yakhot and Orszag, 1989) and the realizable k-ε model (Shih et al., 1995). These models solve transport equations for the turbulent kinetic energy k and the turbulent dissipation rate ε.

For the standard k-ε model, the transport equations are expressed as follows:

$$\frac{\partial}{\partial t}(\rho k)+\frac{\partial}{\partial x_j}(\rho k u_j) = \frac{\partial}{\partial x_i}\left[(\mu+\frac{\mu_T}{\sigma_k})\frac{\partial k}{\partial x_i}\right] - \rho\varepsilon + G_k + G_b + S_k - Y_M \qquad (3.14)$$

$$\frac{\partial}{\partial t}(\rho \varepsilon)+\frac{\partial}{\partial x_j}(\rho \varepsilon u_j) = \frac{\partial}{\partial x_i}\left[(\mu+\frac{\mu_T}{\sigma_\varepsilon})\frac{\partial k}{\partial x_i}\right] + C_{1\varepsilon}\frac{\varepsilon}{k}[G_k + C_{3\varepsilon}G_b] - \rho C_{2\varepsilon}\frac{\varepsilon^2}{k} + S_\varepsilon \qquad (3.15)$$

where G_k and G_b are the generation of turbulence kinetic energy due to the mean velocity gradients and due to buoyancy, respectively. The term Y_M represents the contribution of the fluctuating dilatation in compressible turbulence to the overall dissipation rate, while σ_k and σ_ε denote the turbulent Prandtl numbers for k and ε equal to 1.0 and 1.3, respectively. The symbols S_ε and S_k represent user-defined source terms, while $C_{1\varepsilon}$ = 1.44, $C_{2\varepsilon}$ = 1.92, C_μ = 0.09 and $C_{3\varepsilon}$ = 0.

For the RNG k-ε model, the transport equations are expressed as follows:

$$\frac{\partial}{\partial t}(\rho k)+\frac{\partial}{\partial x_j}(\rho k u_j) = \frac{\partial}{\partial x_i}\left[\alpha_k \mu_{eff}\frac{\partial k}{\partial x_i}\right] - \rho\varepsilon + G_k + G_b + S_k - Y_M \qquad (3.16)$$

$$\frac{\partial}{\partial t}(\rho\varepsilon)+\frac{\partial}{\partial x_j}(\rho\varepsilon u_j)=\frac{\partial}{\partial x_i}\left[\alpha_\varepsilon\mu_{eff}\frac{\partial\varepsilon}{\partial x_i}\right]+C_{1\varepsilon}\frac{\varepsilon}{k}[G_k+C_{3\varepsilon}G_b]-$$

$$\rho\frac{\varepsilon^2}{k}\left[C_{2\varepsilon}+\frac{\rho C_\mu(Sk/\varepsilon)^3[1-(Sk/\varepsilon)/a_0]}{1+b(Sk/\varepsilon)^3}\right]+S_\varepsilon \qquad (3.17)$$

where S is the modulus of the mean rate-of-strain tensor. In addition, $a_0 = 4.38$, $b = 0.012$, while α_k and α_ε are the inverse effective Prandtl numbers for k and ε, respectively. Finally, $C_{1\varepsilon} = 1.42$, $C_{2\varepsilon} = 1.68$ and $C_\mu = 0.0845$.

For the realizable k-ε model, the transport equations are expressed as follows:

$$\frac{\partial}{\partial t}(\rho k)+\frac{\partial}{\partial x_j}(\rho k u_j)=\frac{\partial}{\partial x_i}\left[(\mu+\frac{\mu_T}{\sigma_k})\frac{\partial k}{\partial x_i}\right]-\rho\varepsilon+G_k+G_b+S_k-Y_M \qquad (3.18)$$

$$\frac{\partial}{\partial t}(\rho\varepsilon)+\frac{\partial}{\partial x_j}(\rho\varepsilon u_j)=\frac{\partial}{\partial x_i}\left[(\mu+\frac{\mu_T}{\sigma_\varepsilon})\frac{\partial k}{\partial x_i}\right]+C_{1\varepsilon}\frac{\varepsilon}{k}C_{3\varepsilon}G_b+$$

$$\rho C_1 S\varepsilon - \rho C_2\frac{\varepsilon^2}{k+\sqrt{\nu\varepsilon}}+S_\varepsilon \qquad (3.19)$$

where $C_1 = \max[0.43, \frac{(Sk/\varepsilon)}{(Sk/\varepsilon)+5}]$, $C_{1\varepsilon} = 1.44$, $C_2 = 1.9$, $\sigma_k = 1.0$, and $\sigma_\varepsilon = 1.2$.

All simulations involved any one of these models in conjunction with enhanced wall treatment. The film cooling configuration studied experimentally by Sinha et al. (1991) was simulated using each of the turbulence models mentioned above. Figure 3-9

compares the centerline adiabatic film cooling effectiveness for M = 1, obtained experimentally by Sinha et al. (1991) and numerically by Walters and Leylek (2000), to the results obtained in the present study. It was found that the realizable k-ε model provided the best prediction of centerline adiabatic film cooling effectiveness, followed closely by the RNG k-ε model (c.f. Appendix section for more detail on the benchmark studies). These two turbulence models were therefore used in most of the simulations in the present study.

The details of the numerical computations are summarized in Table 3-4. A total of twenty cases were simulated for the novel film cooling geometry. Computations were performed on DELL Precision Workstations PWS350 equipped with one or two 3.06 GHz processors. Typically each case reached convergence after approximately 2000 iterations, equivalent to 17 hours of numerical computation.

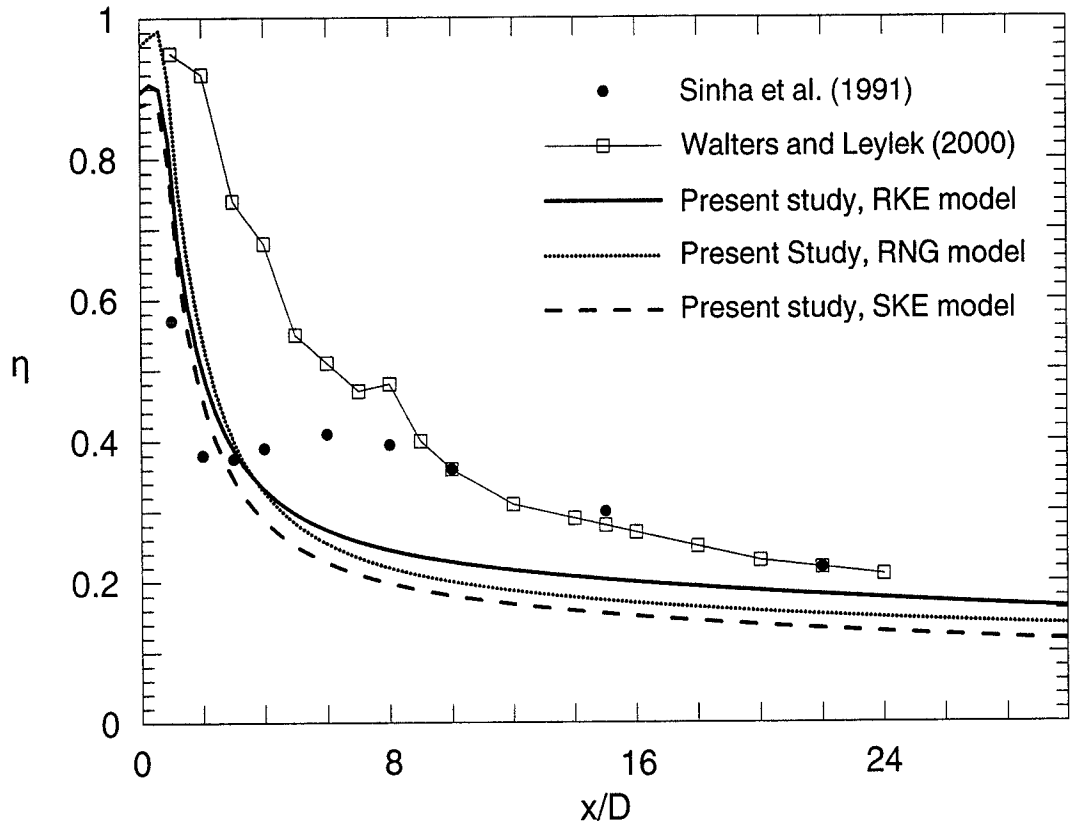

Figure 3-9. Centerline adiabatic film cooling effectiveness for the simple injection circular hole, obtained with various turbulence models, at M = 1.0.

Table 3-4. Test matrix.

Hole geometry	Coolant velocity U_j (m/s)	Mainstream velocity U_∞ (m/s)	Blowing ratio M_i	Mainstream Ti (%)	Turbulence model and wall treatment
NOV1-4p	3	1	5.22	3	Realizable k-ε with enhanced wall treatment
NOV1-4p	3	1.5	3.48	3	Realizable k-ε with enhanced wall treatment
NOV1-4p	3	3	1.74	3	Realizable k-ε with enhanced wall treatment
NOV1-4p	3	6	0.87	3	Realizable k-ε with enhanced wall treatment
NOV1-4p	3	1	5.22	3	RNG k-ε with enhanced wall treatment
NOV1-4p	3	6	0.87	3	RNG k-ε with enhanced wall treatment
NOV1-4p	3	1	5.22	3	standard k-ε with enhanced wall treatment
NOV1-4p	3	6	0.87	3	standard k-ε with enhanced wall treatment
NOV1-4p	3	1	5.22	10	Realizable k-ε with enhanced wall treatment
NOV1-4p	3	6	0.87	10	Realizable k-ε with enhanced wall treatment
NOV1-4p	3	1	5.22	10	RNG k-ε with enhanced wall treatment
NOV1-4p	3	6	0.87	10	RNG k-ε with enhanced wall treatment
NOV1-0p	3	1	5.22	3	Realizable k-ε with enhanced wall treatment
NOV1-0p	3	6	0.87	3	Realizable k-ε with enhanced wall treatment
NOV1-2p	3	1	5.22	3	Realizable k-ε with enhanced wall treatment
NOV1-2p	3	6	0.87	3	Realizable k-ε with enhanced wall treatment
NOV2-4p	3	1	5.22	3	Realizable k-ε with enhanced wall treatment
NOV2-4p	3	1.5	3.48	3	Realizable k-ε with enhanced wall treatment
NOV2-4p	3	3	1.74	3	Realizable k-ε with enhanced wall treatment
NOV2-4p	3	6	0.87	3	Realizable k-ε with enhanced wall treatment

3.3.5 Calculation of $\overline{\eta}$

The spanwise-averaged adiabatic film-cooling effectiveness downstream of injection $\overline{\eta}$ represents the average adiabatic film cooling effectiveness in the z-direction measured at a given x/D_h. This parameter is found by determining the lateral (z-direction) distribution of temperature at the wall ($y/D_h = 0$) at a given x/D_h. The average temperature $\overline{T}_{aw}$ at this location is then substituted in the following equation to obtain $\overline{\eta}$:

$$\overline{\eta} = \frac{\overline{T}_{aw} - T_{\infty}}{T_j - T_{\infty}} \tag{3.20}$$

Temperature is sampled at typically 100 data points in the z-direction. Since the spanwise distribution of temperature is generally not uniform downstream of the film hole exit, a program was written in Visual Fortran to calculate the average temperature at the wall at any given x/D_h. This program uses a combination of three numerical integration schemes (Simpson's 1/3 rule, 3/8 rule and the trapezoidal rule) to compute the average temperature $\overline{T}_{aw}$, depending on the number of data points and how far apart they are from each other.

Chapter IV

Results and Discussion

The following section presents the analysis of the adiabatic film cooling effectiveness obtained with the novel hole geometry for blowing rates based on hole inlet conditions M_i = 5.22, 3.48, 1.74 and 0.87, with mainstream turbulence intensity Ti = 3% and 10%, successively. Results are obtained for two different hole inlets, as well as three different pedestal arrangements, and were computed with three different turbulence models. In order to explain the physics of the flow, the velocity field, turbulent kinetic energy field and temperature field at various locations in the domain were studied in detail.

4.1 Effect of Blowing Ratio

In the present study, the blowing rate is calculated using conditions at the hole inlet, because the complexity of the geometry renders the analytical calculation of jet exit conditions difficult. These conditions are different than those at the hole inlet due to the changes in cross section of the hole. Based on hole inlet conditions, the blowing ratio M_i varies between 0.87 and 5.22. More practically, this corresponds to a range of blowing rates M_e varying from 0.44 to 1.77, when the blowing rate is calculated based on hole exit

conditions, i.e.,

$$M_e = \frac{\rho_{j_e} U_{j_e}}{\rho_\infty U_\infty} \tag{4.1}$$

where ρ_{j_e} and U_{j_e} are the area-weighted average of velocity magnitude and density on the hole exit plane, respectively. Table 4-1 recapitulates the various blowing rate.

Figure 4-1 presents the downstream centerline adiabatic film cooling effectiveness obtained with the NOV1-4p geometry, at various blowing rates. All cases show a gradual decrease in effectiveness with increasing downstream position. As the blowing ratio M_i increases from 0.87 to 5.22 (equivalent to M_e increasing from 0.44 to 1.77), the centerline effectiveness increases at all downstream positions, except for when $x/D_h \leq 2$, in which case the effectiveness remains constant from $M_i = 3.48$ to $M_i = 5.22$. Many studies have shown that jet lift-off occurs for blowing rates of approximately 0.5, for cylindrical film cooling holes (Bergeles et al., 1977; Forth and Jones, 1988). For these cylindrical holes, a drop in effectiveness in the near-hole region is observed as a result of this lift-off. This is due to the fact that the hot mainstream gases are able to slip underneath the jet, thus reducing its cooling performance. In addition, the jet lift-off continues to intensify as the blowing rate increases beyond 0.5. With the present hole geometry, the coolant jet has not experienced any similar liftoff from the surface at any blowing rate studied, which would have otherwise caused a drop in centerline effectiveness in the near-hole region. The advantage of the forward expansion in the hole design is conveyed as an

Table 4-1. Blowing ratio based on hole inlet and exit conditions.

Coolant inlet velocity U_{j_i} (m/s)	**Mainstream inlet velocity U_∞ (m/s)**	**Velocity at hole exit U_{j_e} (m/s)**	**Density at hole exit ρ_{j_e} (kg/m^3)**	**Blowing rate $M_i = \frac{\rho_{j_i} U_{j_i}}{\rho_\infty U_\infty}$**	**Blowing rate $M_e = \frac{\rho_{j_e} U_{j_e}}{\rho_\infty U_\infty}$**
3	6	1.94	0.37	0.87	0.44
3	3	1.40	0.39	1.74	0.67
3	1.5	1.24	0.40	3.86	1.22
3	1	1.20	0.40	5.22	1.77

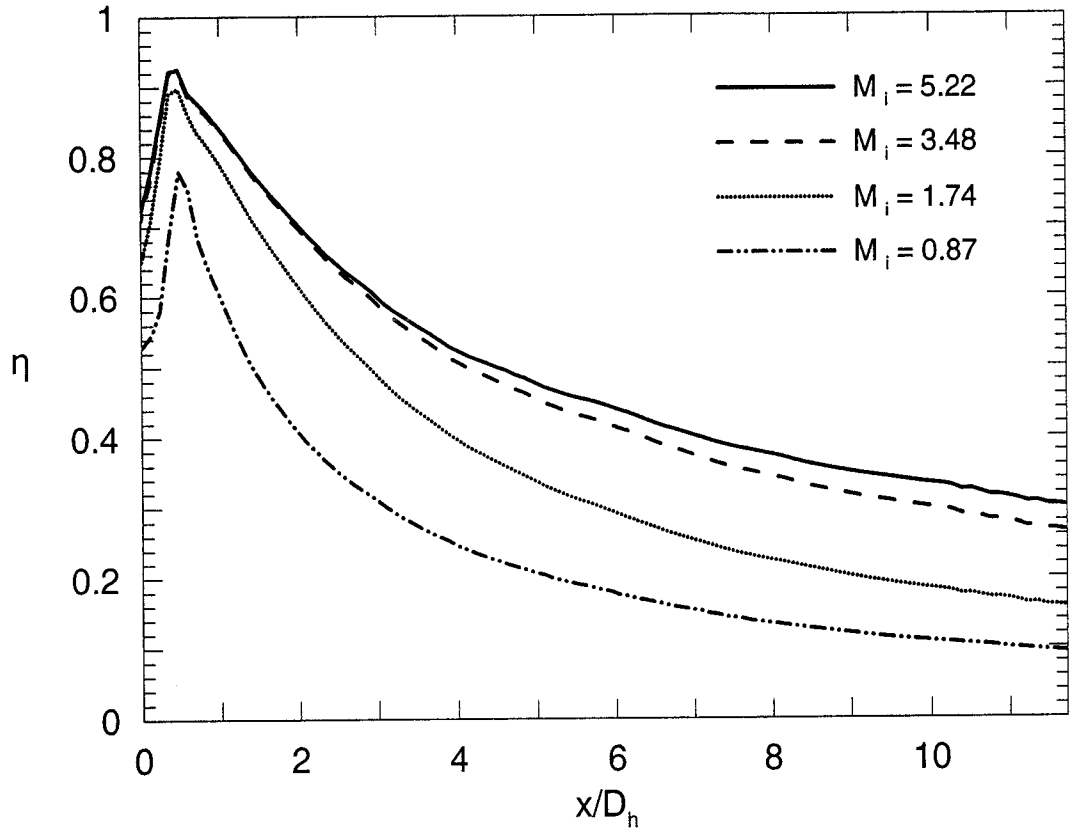

Figure 4-1. Centerline adiabatic film cooling effectiveness for the NOV1-4p geometry at various M_i (Ti = 3%, realizable k-ε turbulence model).

increased adherence of the film at high blowing rates. Due to the flared hole exit, the coolant momentum is reduced, allowing it to spread laterally onto the surface, thus enhancing the cooling performance. The rate at which the centerline effectiveness decreases is reduced as the blowing ratio rises, according to Figure 4-1. As the coolant gains momentum with respect to the mainstream, the jet dilution is delayed as more coolant is convected downstream. This provides an enhanced protection of the wall in the streamwise direction.

As shown in Figure 4-1, there is no significant difference in the centerline effectiveness obtained at $M_i = 3.48$ and $M_i = 5.22$, for $x/D_h \leq 2$. While the centerline effectiveness in this region plateaus for blowing rates above 3.48, the jet continues to swell vertically and its protective action grows at locations farther downstream. Figure 4-2 depicts the contours of effectiveness on the downstream surface for all blowing rates. This figure shows the gradual increase of effectiveness in the streamwise direction as the blowing rate is increased, denoting the improving performance of the jet. Effectiveness values of 4% just barely reach $x/D_h = 25$ at $M_i = 0.87$ while for $M_i = 5.22$ they extend past $x/D_h = 30$. Figure 4-3 provides an overall outlook on the temperature field at various cross-stream planes downstream of injection at all blowing rates. The contours show the interaction of the coolant and mainstream flows, as well as the growing impact of the jet on the temperature field. The thermal dilution of the coolant resulting from the mixing between the coolant flow and the mainstream flow is visible at $x/D_h = 5$. The gradients of temperature at this location are lessened and the film temperature is warmer than at injection, hence degrading the film effectiveness. The increase in lateral coolant coverage

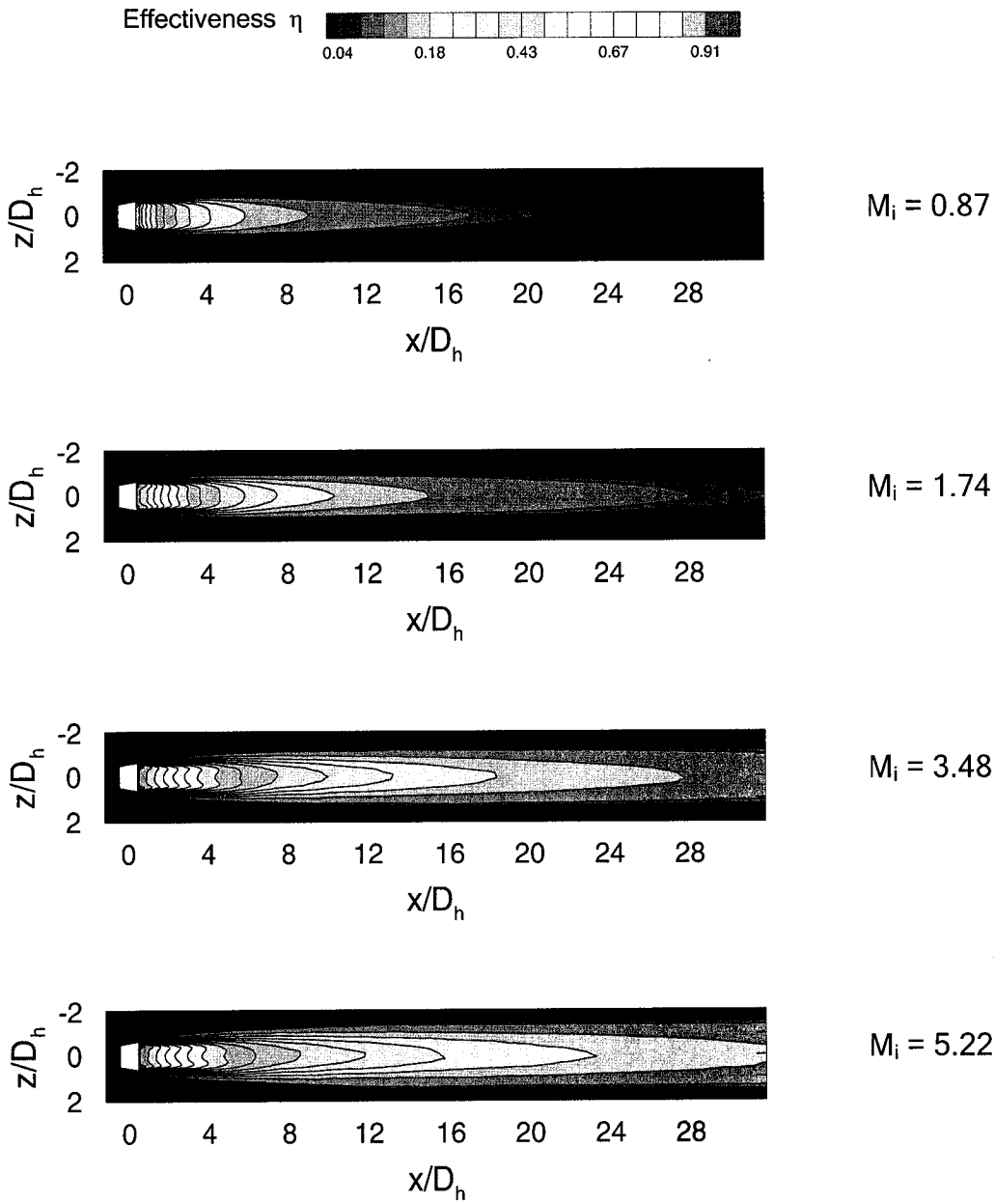

Figure 4-2. Contours of adiabatic film cooling effectiveness downstream of injection at $y/D_h = 0$, for various blowing rates (NOV1-4p, Ti = 3%, realizable k-ε turbulence model).

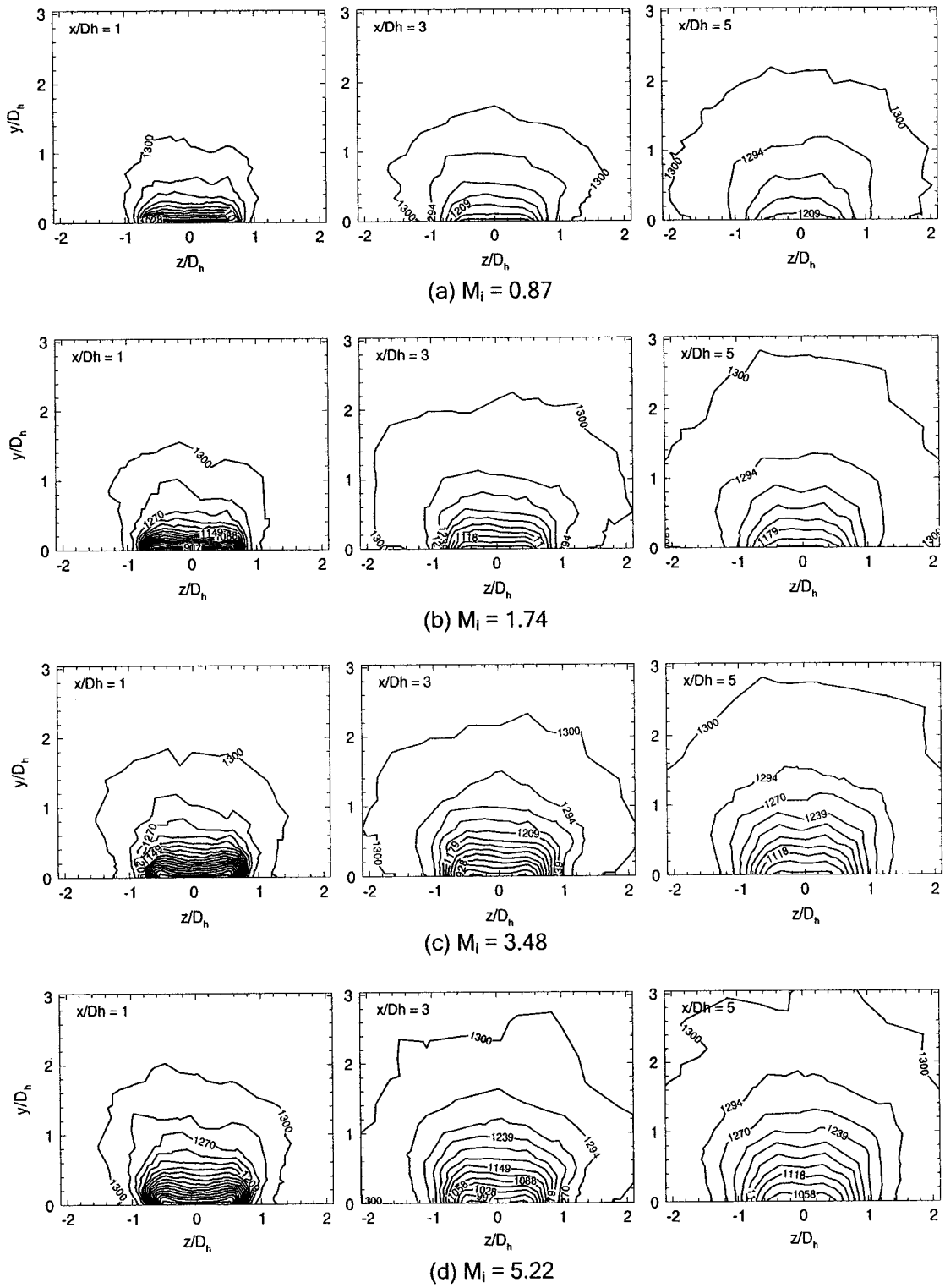

Figure 4-3. Temperature contours on planes downstream of injection, at various blowing rates (NOV1-4p, Ti = 3%, realizable k-ε turbulence model).

is most visible at $x/D_h = 3$ and $x/D_h = 5$. At $x/D_h = 1$, some lateral spreading is observed as the blowing rate increases from $M_i = 0.87$ to $M_i = 3.48$. When the blowing rate reaches 5.22 however, the lateral spreading levels out, while the jet continues to grow in the vertical direction. This contraction and rise of the jet, accompanied by a stall in the growth of centerline effectiveness as shown in Figure 4-1, denotes that jet lift-off is imminent.

Figure 4-4 shows the spanwise averaged film cooling effectiveness as a function of the downstream position for all blowing rates. It was observed that the spanwise averaged effectiveness for $x/D_h \leq 1.7$ is lower at $M_i = 5.22$ than at $M_i = 3.48$. It was concluded previously that the centerline effectiveness is not affected significantly by the blowing ratio in that region. This suggests that the jet edges have started to detach from the surface in the near-hole region, thus allowing hot gas to slip beneath it and come in contact with the surface. It is for this reason that there is an overall degradation in the effectiveness in this region. For $x/D_h \geq 1.7$, the spanwise averaged effectiveness increases steadily with stronger blowing ratios. As the coolant is convected downstream, it loses some momentum, and so the jet edges are pushed back onto the wall. The larger coolant flow also ensures a wider lateral spreading of the jet for a given x/D_h, resulting in higher effectiveness values for $M_i = 5.22$ than for $M_i = 3.48$. As a note, low levels of spanwise-averaged effectiveness (less than 30%) are expected since the hole spacing is equal to $p/D_h = 4$, which is higher than the typical distance of 3 diameters used in film cooling experiments.

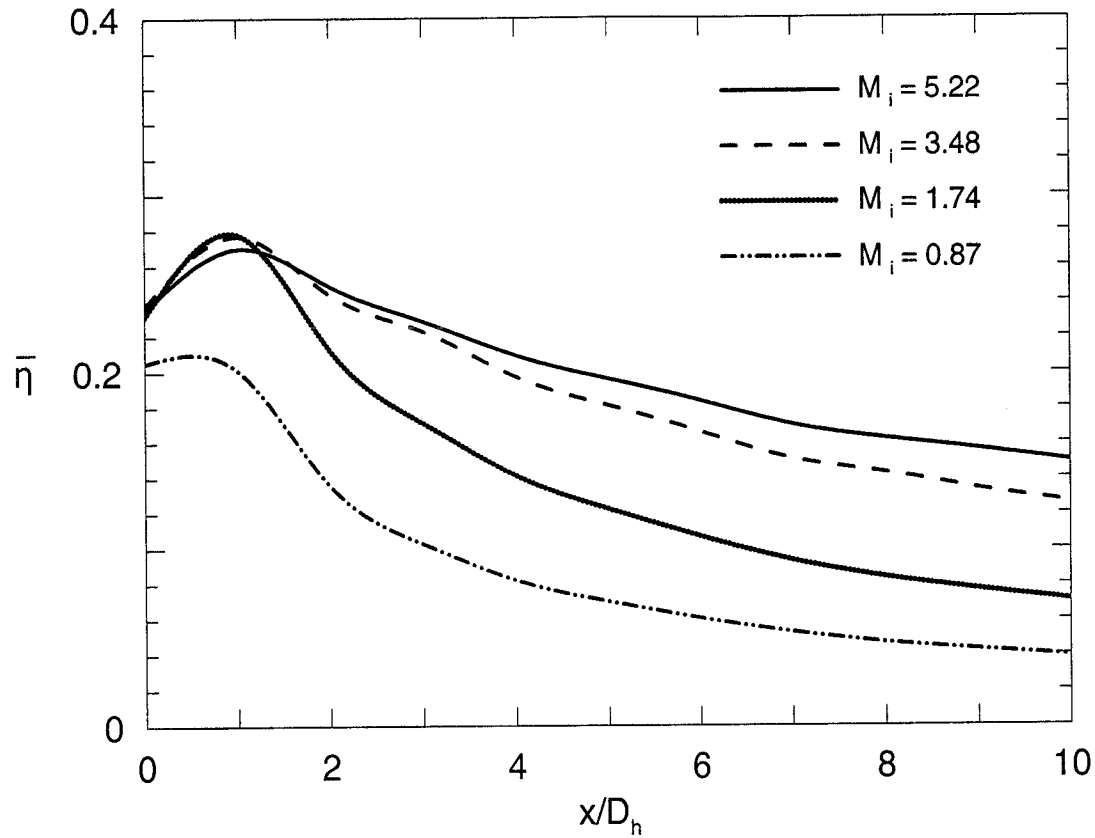

Figure 4-4. Spanwise averaged adiabatic film cooling effectiveness for the NOV1-4p geometry at various M_i (Ti = 3%,realizable k-ε turbulence model).

Figure 4-5 presents superimposed temperature contours and velocity vectors in the cross-stream plane $x/D_h = 1$, obtained for all blowing rates. These contours permit the visualization of the flow structure and its effects on the temperature field. Counter-rotating structures or kidney vortices, associated with any crossflow jets, are visible at the edges of the jet, especially at high blowing rates. This secondary flow motion caused by the strong interaction between the mainstream and coolant intensifies the mixing between the two streams. At $M_i = 5.22$, the kidney vortices are higher and stronger than for any other blowing rate. Comparison of the flow structure at $x/D_h = 1$ for $M_i = 0.87$ and $M_i = 5.22$ shows that, as M_i gains importance, the coolant gains vertical momentum as its edges lose some lateral momentum. Examination of the temperature contours in the same figure confirms that the stronger counter-rotating vortices propel the coolant higher upwards, resulting in cooler temperatures for equivalent y/D_h values. The contours also show the contraction of the jet near the wall for $M_i = 5.22$ as a result of the jetting effect.

The lateral distribution of adiabatic film cooling effectiveness at various downstream positions is shown in Figure 4-6. At increasing downstream positions, the effectiveness increases at lateral positions while decreasing in the centerline for all blowing rates, denoting that the lateral coverage of the jet is enhanced. This jet spreading is due to a reduction in coolant momentum through dissipation losses, and induces a thinning of the jet in the centerline as the coolant travels to larger z/D_h values. Peaks of effectiveness, symmetrical about the centerline, are observed on the effectiveness distributions. These are most pronounced at $x/D_h = 1$, and gradually fade with increasing downstream position. As the jet momentum increases, the peaks of effectiveness at $x/D_h = 1$ move

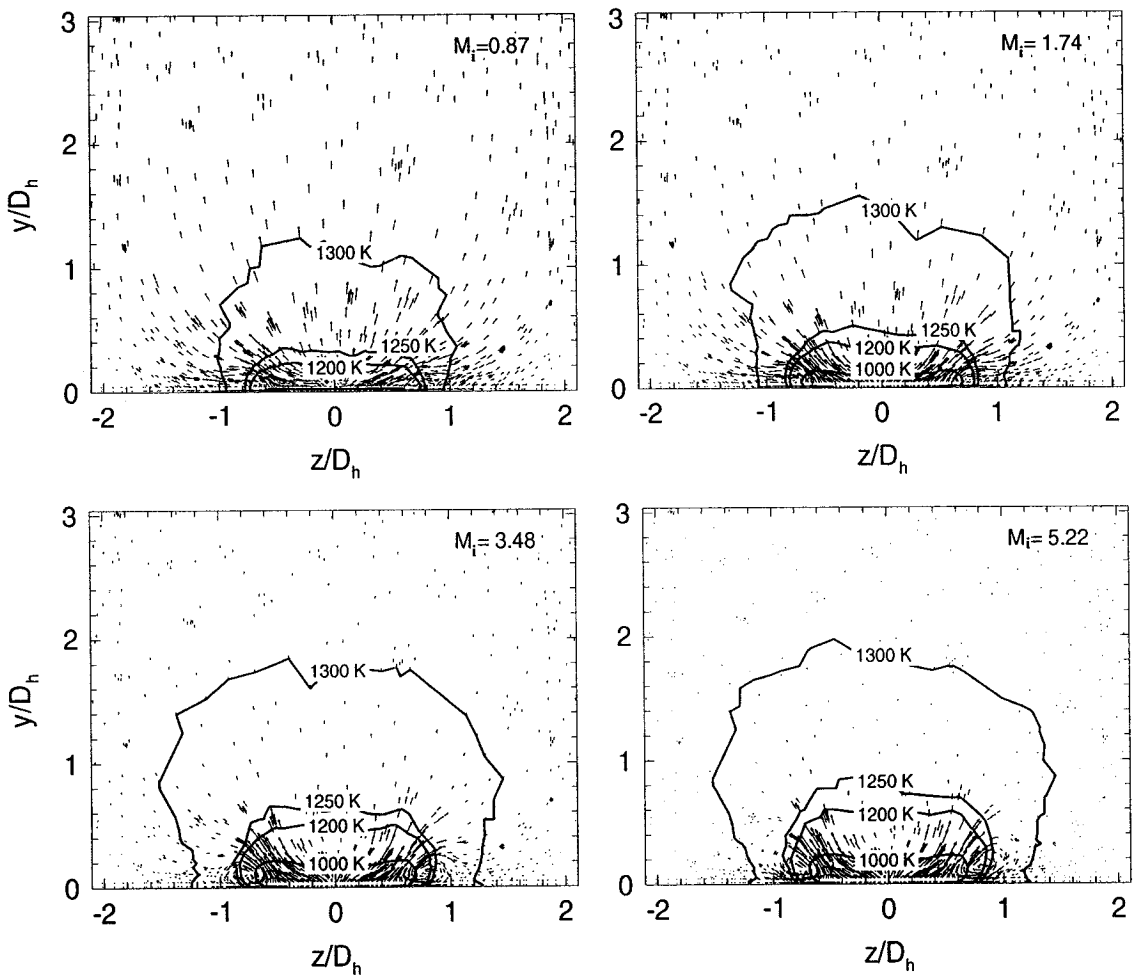

Figure 4-5. Superimposed temperature contours and velocity vectors at $x/D_h = 1$, for all blowing rates (NOV1-4p geometry, Ti = 3%, realizable k-ε turbulence model).

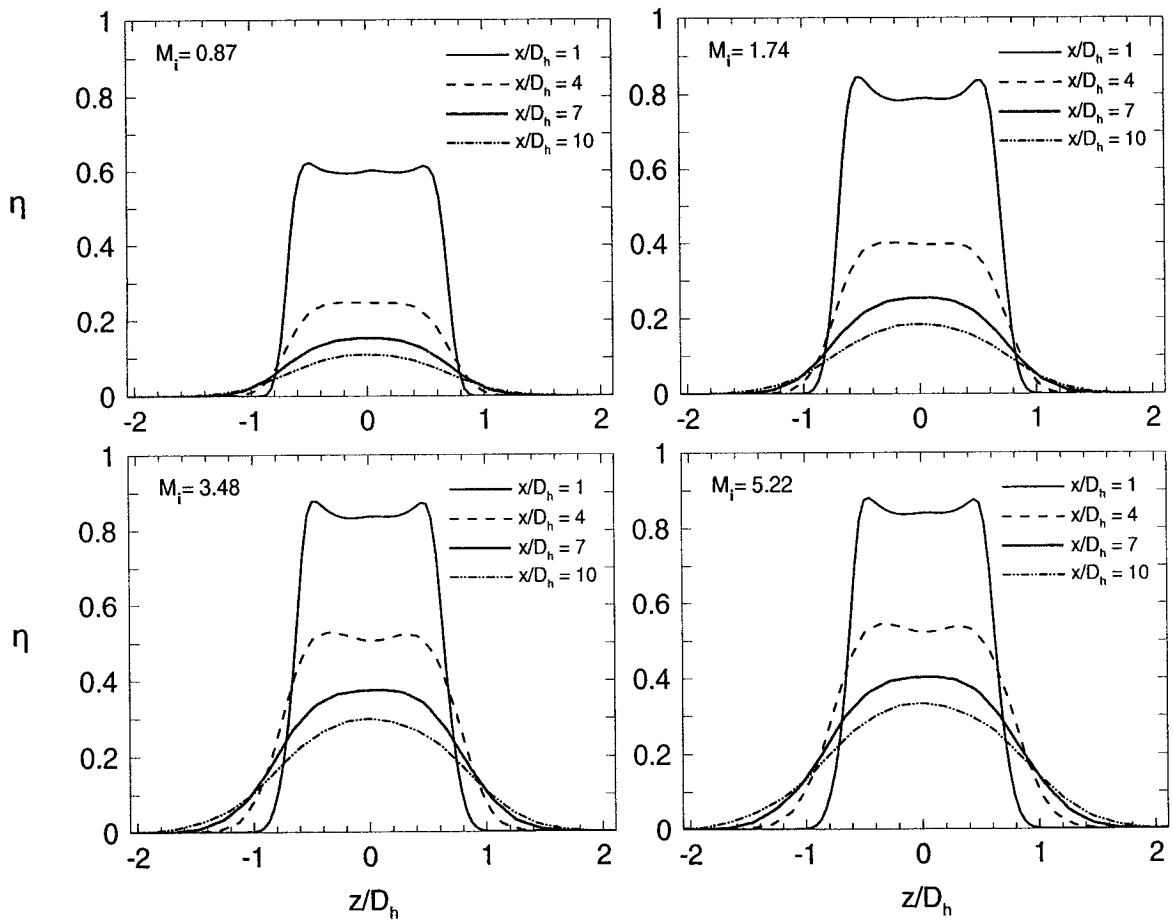

Figure 4-6. Spanwise distribution of adiabatic film cooling effectiveness at various downstream positions and for all blowing rates (NOV1-4p, Ti = 3%, realizable k-ε turbulence model).

closer together due to the jetting effect, which prevents the coolant from spreading laterally. As M_i increases from 0.87 to 3.48, the reduction of the high effectiveness region between the peaks is offset by an overall rise in effectiveness values, so that the spanwise averaged effectiveness at $x/D_h = 1$ increases steadily. As M_i increases from 3.48 to 5.22, the peaks continue to move inwards, hence reducing the region of high effectiveness between them. However, the overall effectiveness does not increase enough to overcome this deficit, and this translates to a net decrease in spanwise averaged effectiveness at $x/D_h = 1$. The benefits of this high blowing ratio are observed far downstream of injection ($x/D_h = 10$), where the distribution of effectiveness is the highest over the widest span for all cases. Since the jet core is larger, coolant dilution is hindered, and so the influence of the jet is felt at wider and longer distances downstream of injection. However, it also ensures less dilution of the jet, so that it is able to reach regions farther downstream of injection.

The peaks of effectiveness visible at the edges of the regions of high effectiveness, as shown in Figure 4-6, are evidence that the flow does not exit the hole uniformly, especially at high blowing rates. This is confirmed when examining the contours of normalized velocity magnitude at the hole exit plane ($y/D_h = 0$) in Figure 4-7. The velocity magnitude is divided by the reference velocity magnitude for each case, as sampled at $(x/D_h, y/D_h, z/D_h) = (-10, 10, 0)$ in the computational domain. The contours shown in this figure reveal that the jet exit velocity is relatively uniform at $M_i = 0.87$, but as the blowing rate increases, the coolant is redistributed and the jet exits mainly in the leeward portion of the hole. At $M_i = 0.87$, the mainstream momentum is comparatively

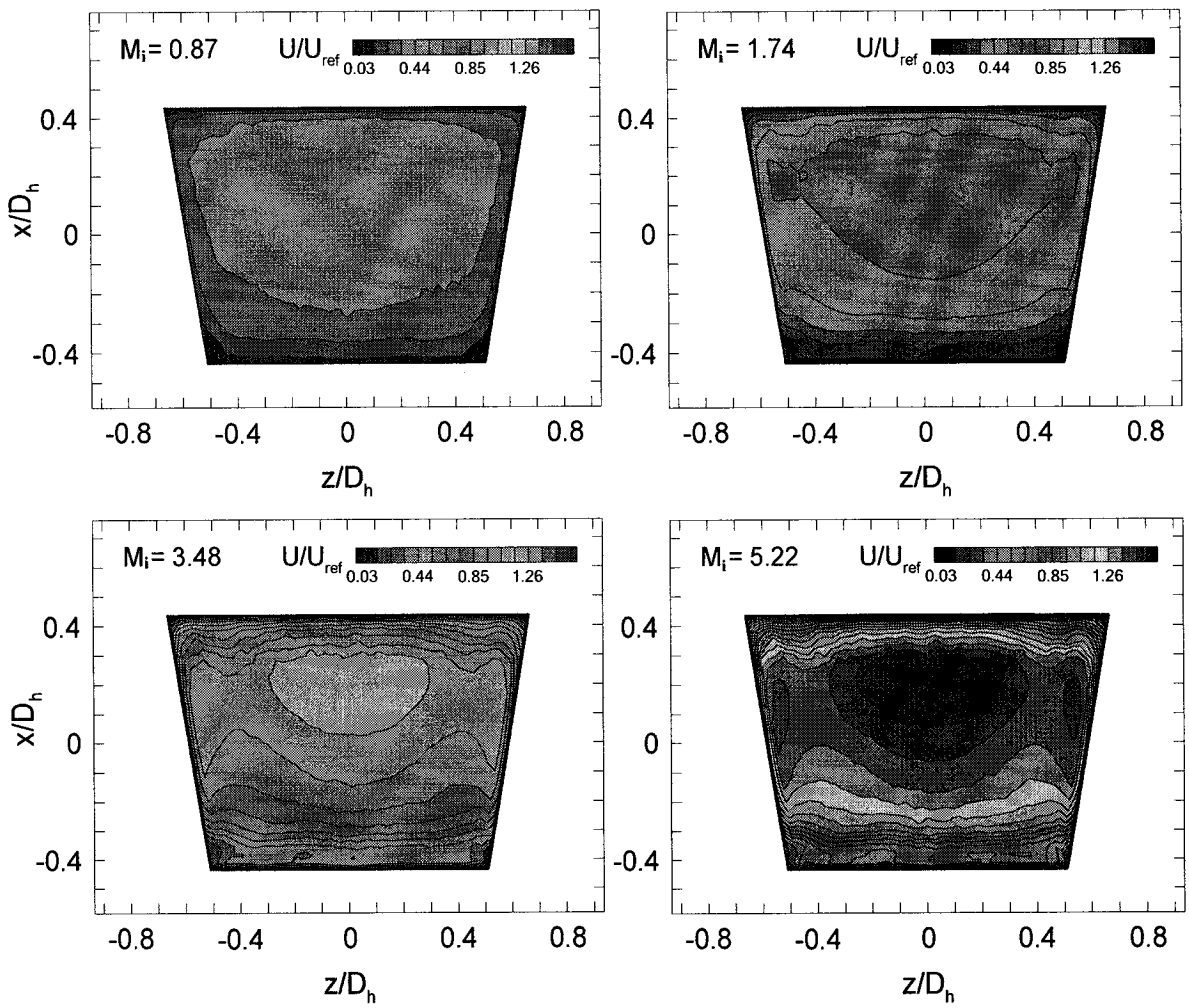

Figure 4-7. Normalized velocity magnitude contours on the hole exit plane for all blowing rates (NOV1-4p, Ti = 3%, realizable k-ε turbulence model).

large with respect to that of the coolant. Crossflow blockage prevents the coolant from penetrating into the mainstream up to a certain degree. The mainstream/coolant interactions are minimum, and the coolant velocity assumes a relatively homogeneous distribution at the hole exit. As the jet momentum increases, the mainstream blockage becomes less significant, due to the reduced constraint, the coolant shoots out of the hole in the centerline with a rising trajectory instead of expanding along the sides of the hole. Figure 4-7 also reveals that the flow accelerates along the edges of the hole, especially at high blowing ratio. This phenomenon is caused by the blockage brought on by the presence of the jet inside the mainstream. The coolant jet is a growing obstacle in the mainstream as the blowing rate increases, much like a cylinder in crossflow. As the jet becomes higher and stronger, it diverts the mainstream, which must accelerate around its edges in order to satisfy continuity. This phenomenon also generates secondary flow (vortices) in the wake region of the jet.

The jetting phenomenon observed in Figure 4-7 allows for hot gas ingestion in the upstream portion of the hole exit. Figure 4-8 depicts contours of normalized vertical velocity in the centerline plane ($z/D_h = 0$) at high and low blowing rates. The velocity contours show the increased vertical momentum of the coolant in the downstream portion of the hole exit at $M_i = 5.22$ compared to that at $M_i = 0.87$. This strong motion depletes the coolant from the upstream part of the hole, which entrains the mainstream gas to fill this space. This downward plunge of the mainstream is conveyed by the contours of negative normalized vertical velocity in Figure 4-8(b). The effect of mainstream blockage is observed in Figure 4-8(a), with lower contours of vertical velocity at $M_i = 0.87$. The

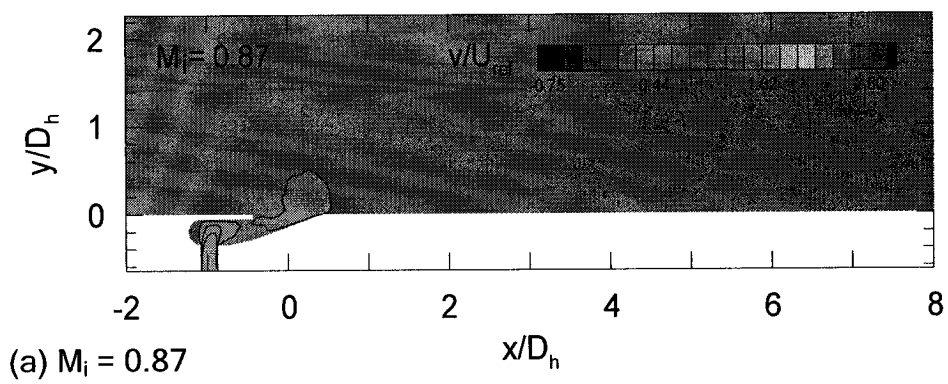

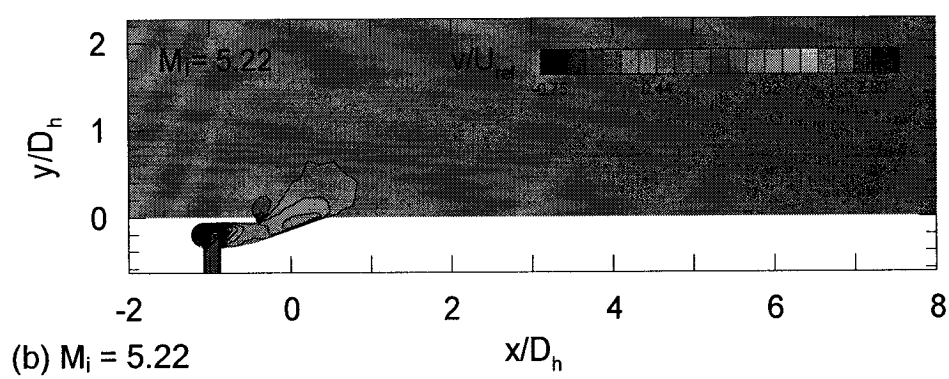

Figure 4-8. Contours of the normalized vertical component of velocity in the centerline plane at (a) $M_i = 0.87$, and (b) $M_i = 5.22$ (NOV1-4p, Ti = 3%, realizable k-ε turbulence model).

mainstream tends to maintain its flow direction due to its high relative momentum, and is not easily deflected by the coolant motion. This limits the ingestion of hot fluid into the hole at this locus (Figure 4-8(a)).

4.2 Effect of Pedestals

It can be foreseen that the presence of pedestals will change the structure of the flow. This section will investigate the degree to which these devices alter the flow patterns and their effects on the resulting adiabatic film cooling effectiveness. The centerline adiabatic film cooling effectiveness obtained for holes with four pedestals (NOV1-4p), two pedestals (NOV1-2p) and no pedestals (NOV1-0p), at high and low blowing rates, is presented in Figure 4-9. This figure reveals that pedestals affect the flow differently at high and low blowing rates. For M_i = 0.87, there is a very slight discrepancy in the centerline effectiveness for $x/D_h \leq 4$ obtained with the three geometries. Further downstream, the difference in results is considered to be negligible. At M_i = 5.22, the NOV1-4p geometry performs the worst of all three geometries, while the highest centerline adiabatic film cooling effectiveness is attributed the NOV1-2p hole configuration. In order to understand the flow mechanisms, the behavior of the flow at injection and just downstream of injection is further investigated.

Figure 4-10 presents contours of normalized velocity magnitude on the hole exit plane at M_i = 5.22, for the NOV1-4p, NOV1-2p and NOV1-0p geometries. This figure confirms that the coolant flow is indeed disturbed by the presence of the pedestals. As opposed to

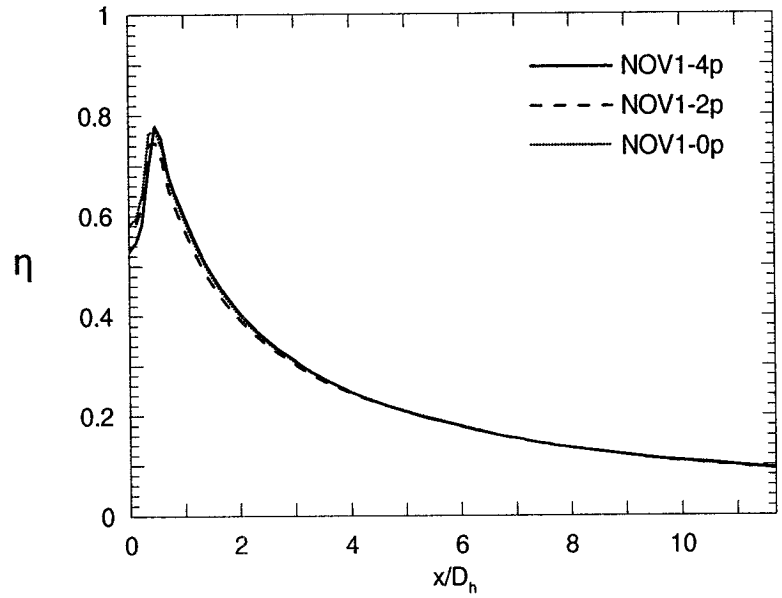

(a) $M_i = 0.87$

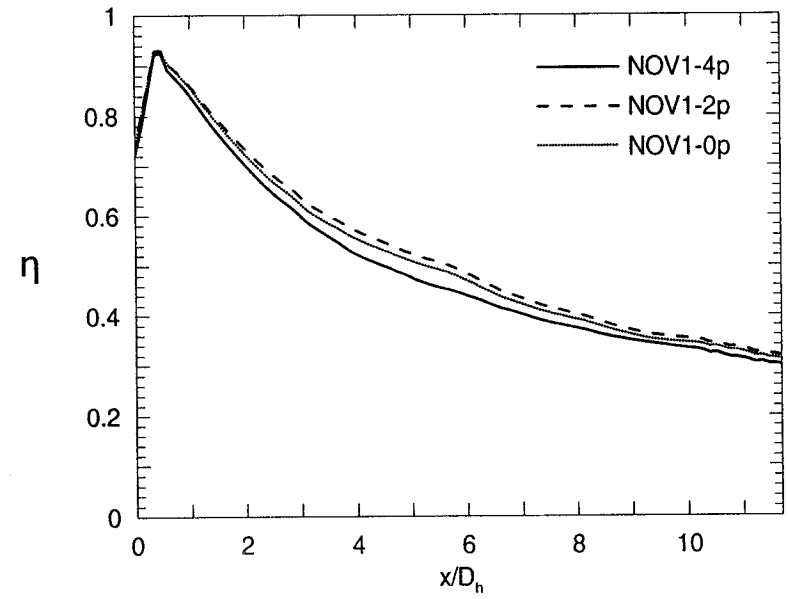

(b) $M_i = 5.22$

Figure 4-9. Centerline adiabatic film cooling effectiveness for three pedestal configurations: (a) $M_i = 0.87$, (b) $M_i = 5.22$ (Ti = 3%, realizable k-ε turbulence model).

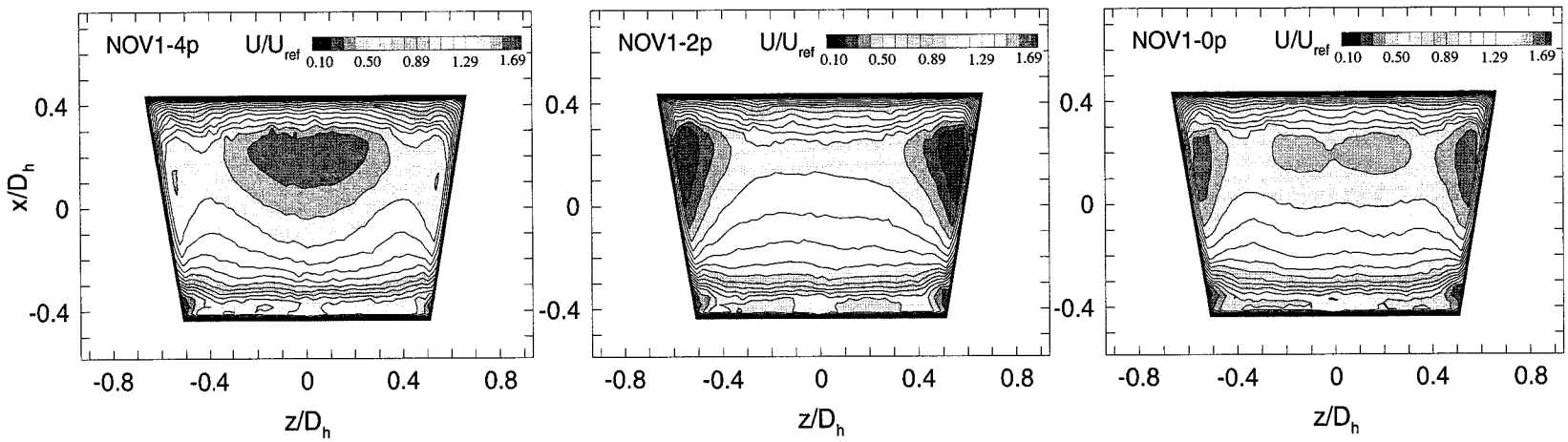

Figure 4-10. Normalized velocity magnitude contours on the hole exit plane for three pedestal configurations (M_i = 5.22, Ti = 3%, realizable k-ε turbulence model).

the NOV1-4p case, where the flow exits mainly in the leeward and centerline portion of the hole, the flow is forced to accelerate along the sides of the hole in the NOV1-2p case. Due to the absence of side pedestals, the coolant tends to by-pass the two center pedestals, thus deflecting towards the walls of the hole. As it exits along the outer edges of the hole, the coolant is further entrained by the mainstream flow which accelerates around the corners of the hole. In the NOV1-0p case, the velocity distribution at the hole exit is the most uniform of all three cases, at this blowing rate. The three coolant jets originating from the impingement tubes coalesce to form two median streams and two outer streams. This is due to the increase in cross-sectional area inside the hole. The flow of the coolant mostly follows the gradual expansion of the hole. However, the jet originating from the middle impingement tube separates into two streams in an attempt to expand to the side wall. These streams entrain the innermost part of the fluid from the other two jets, and exit around the midline of the hole. In terms of centerline effectiveness, the NOV1-2p configuration is the most effective design, since lower centerline velocity promotes less mixing of the coolant and hence produces a more effective film protection.

Figure 4-11 shows the contours of normalized streamwise velocity in the centerline for the three pedestals configurations at $M_i = 5.22$. The contours show a substantial increase in streamwise velocity for the NOV1-4p case, as compared to the case where the hole contains no pedestals. This is due to the bulk of the coolant exiting in the centerline in the NOV1-4p case. However, for the NOV1-2p case, the velocity contours disclose a slower centerline flow than for the NOV1-0p case, since the flow is deviated towards the edges

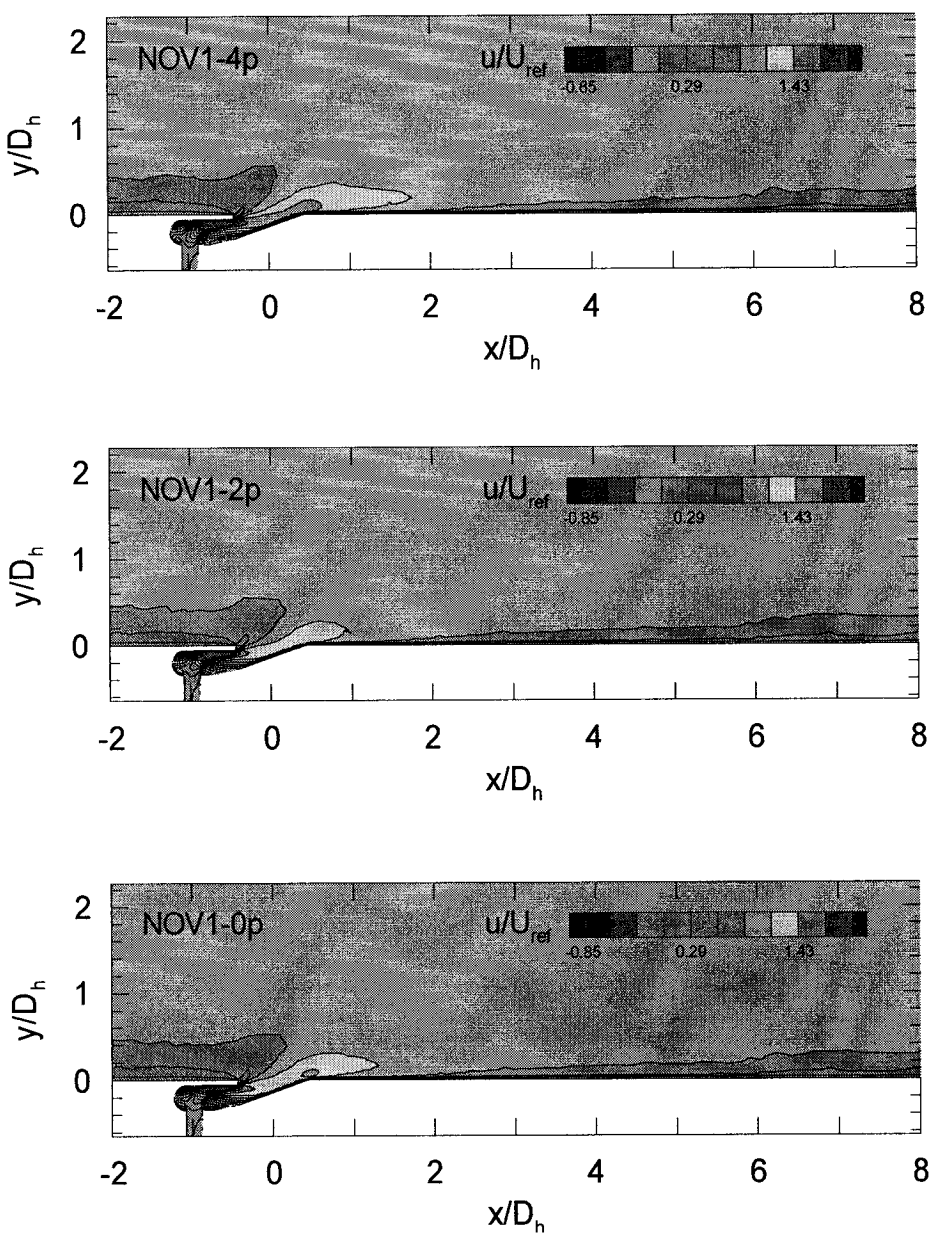

Figure 4-11. Contours of the normalized streamwise velocity in the centerline plane for three pedestal configurations (M_i = 5.22, Ti = 3%, realizable k-ε model).

of the hole by the two center pedestals. Figure 4-12 shows the profiles of normalized streamwise velocity in the centerline, at various downstream positions for the three pedestal arrangements. This complements the previous figure and provides a quantitative depiction of the behavior of the flow at the centerline after injection. The profiles show a 12% increase approximately in streamwise velocity for the NOV1-4p when compared to the NOV1-2p geometry. The addition of the two outer pedestals obstructs the path of the coolant and provokes a constricting effect on the jet due to the increase in velocity that ensues. As the jet moves downstream and loses momentum, the streamwise velocity profiles become similar.

Figure 4-13 shows the structure of the jet just after it penetrates into the mainstream. This figure shows vectors of velocity at $x/D_h = 1$ for the three pedestal configurations tested. The interaction of the coolant jet with the mainstream can be observed at the edges of each jet. Analysis of the structure of the flow at this location reveals that the coolant is closer to the wall and has more lateral momentum for the NOV1-4p configuration than for the other hole geometries. The strong lateral velocities for this case enhance the degree of mixing between the coolant and the mainstream. The jet velocity vectors show the least amount of lateral momentum for the NOV1-2p. This is due to the lower centerline velocities and to the fact that the bulk of the flow exits mainly along the outer edges of the hole and therefore slows down from the widening of the hole exit, as opposed to a flow which exits mainly through the midline of the hole.

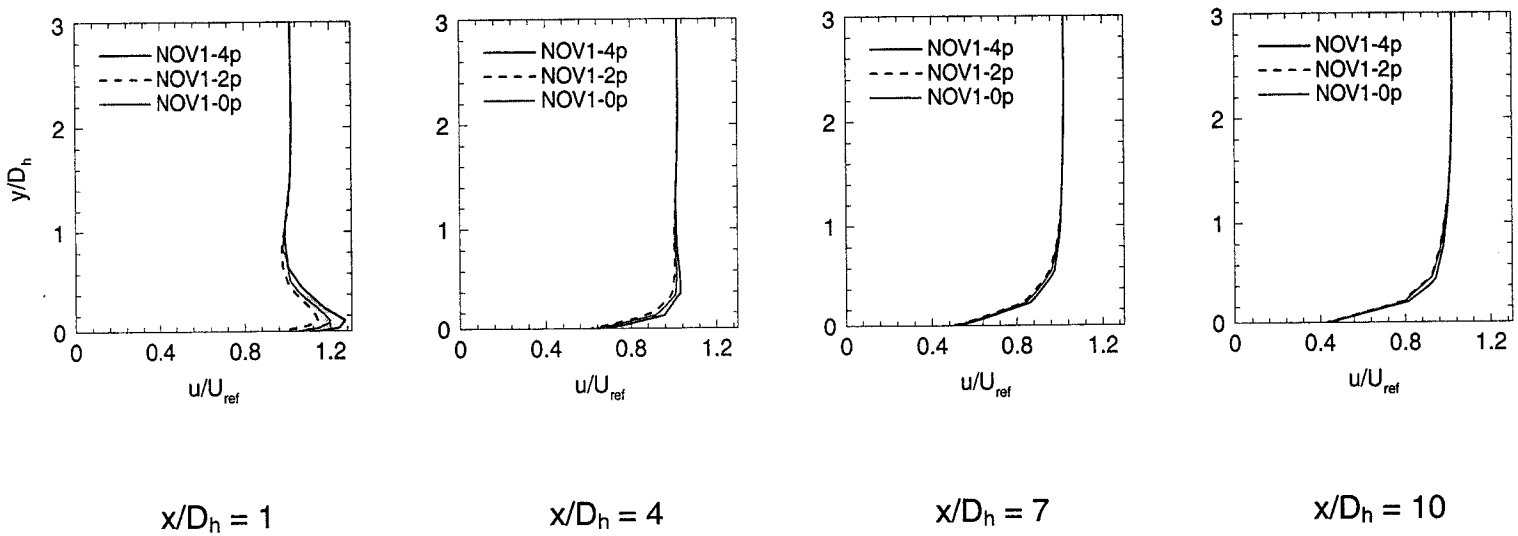

Figure 4-12. Centerline profiles of normalized streamwise velocity for three pedestal configurations (M_i = 5.22, Ti = 3%, realizable k-ε turbulence model).

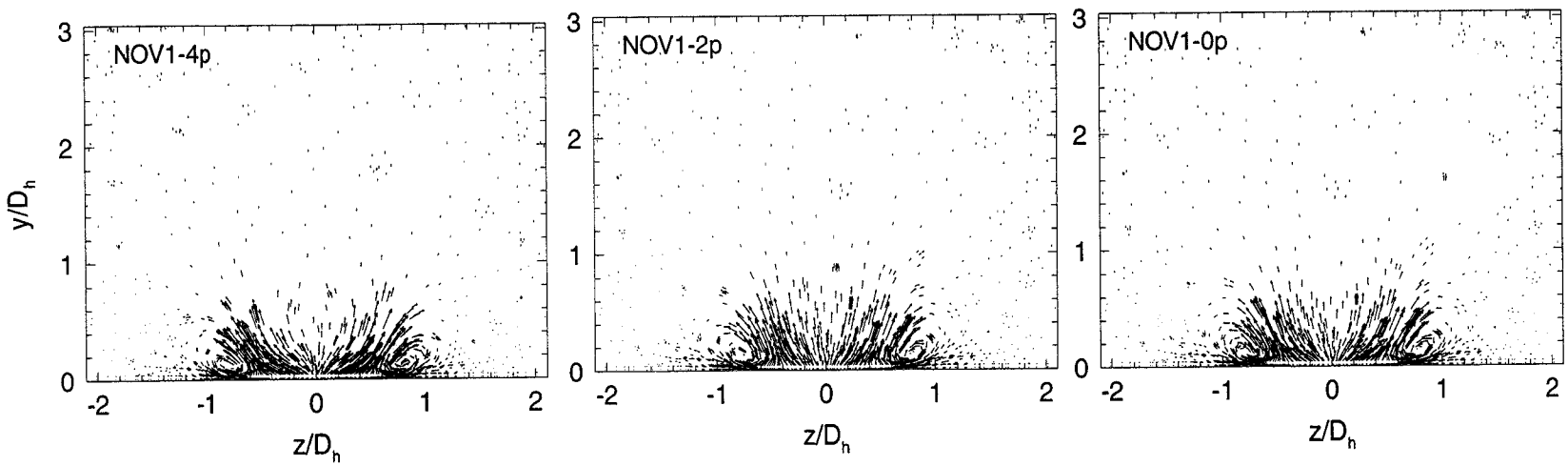

Figure 4-13. Velocity vectors in the mainstream at $x/D_h = 1$ for three pedestal configurations ($M_i = 5.22$, Ti = 3%, realizable k-ε turbulence model).

Figure 4-14 depicts the lateral distribution of effectiveness at various downstream positions obtained at $M_i = 5.22$, for the three pedestal configurations. According to these plots, the effectiveness in the centerline is systematically lowest for the NOV1-4p geometry. It was noticed that four pedestals enhance the interaction between the mainstream and coolant, thus degrading the performance of the film at $x/D_h = 1$. The set-back brought on by this mixing is offset by the ability of the jet to cover a wider surface as it moves further downstream. This translates into higher values of effectiveness at lateral positions for the NOV1-4p geometry, visible at $x/D_h = 4$, $x/D_h = 7$ and $x/D_h = 10$.

Figure 4-15 presents contours of normalized vertical and lateral velocity at $x/D_h = 1$ for the three pedestal configuration. This figure corroborates the conclusions found from Figure 4-13. The coolant for the four-pedestal geometry tends to spread more laterally and remains closer to the surface than for the other cases. Even though the centerline velocity magnitude is highest for the NOV1-4p case, as shown in Figure 4-10, the penetration is lowest because the coolant changes direction quickly after being injected into the mainstream. Both the NOV1-2p and NOV1-0p configurations produce a coolant jet with a trajectory 20% higher than that for the NOV1-4p hole at $x/D_h = 1$ (Figure 4-15(a)). The contours on Figure 4-15(b) prove that the lateral velocity at $x/D_h = 1$ for the NOV1-4p case is overall the highest. This increased lateral momentum deprives the centerline of coolant, thus rendering the film thinner there, and resulting in a lower centerline effectiveness. The coolant for the NOV1-2p case displays the least amount of spreading, from the low contours of lateral velocity as presented in Figure 4-15(b).

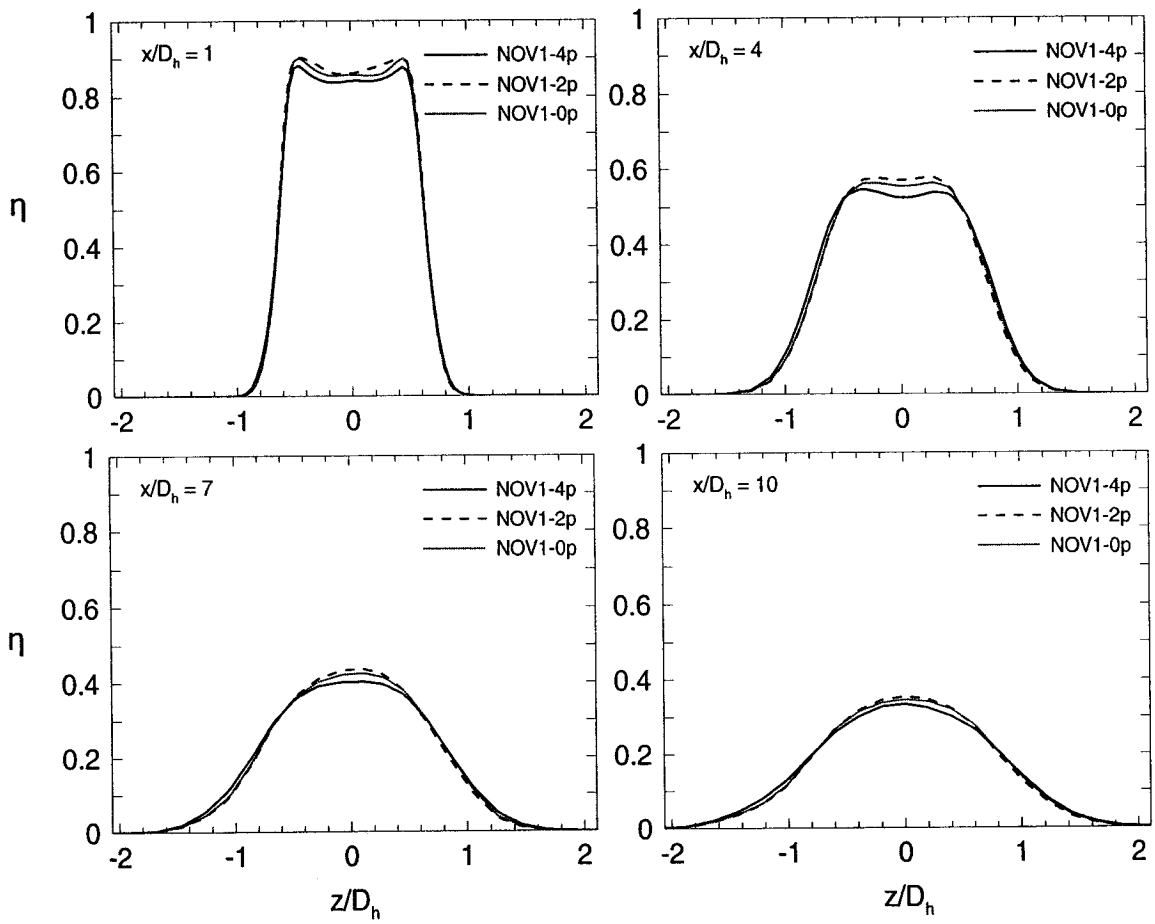

Figure 4-14. Spanwise distribution of adiabatic film cooling effectiveness at various downstream positions for three pedestal configurations (M_i = 5.22, Ti = 3%, realizable k-ε model).

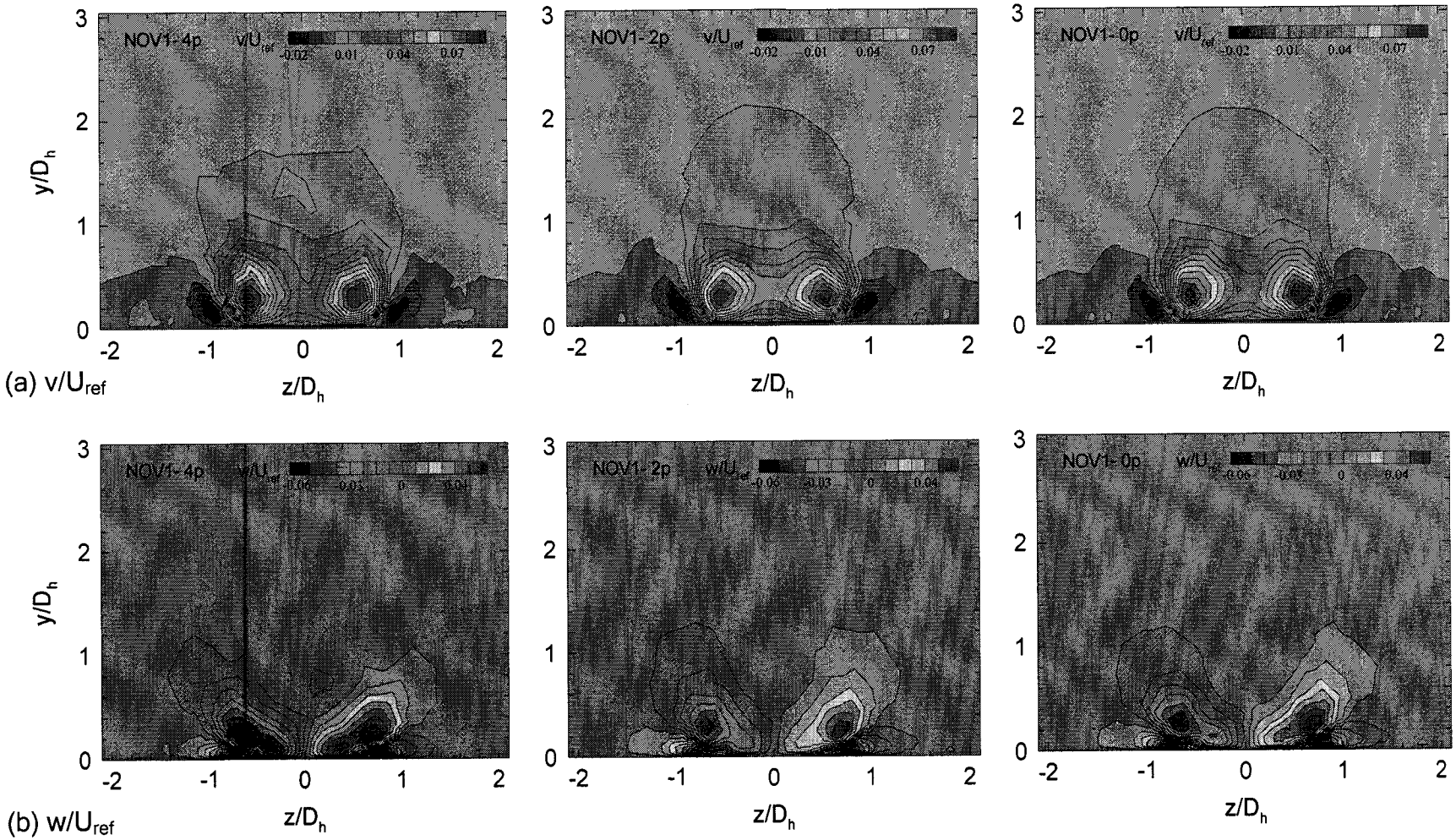

Figure 4-15. Contours of velocity components at $x/D_h = 1$, for three pedestal configurations: (a) vertical normalized velocity, (b) lateral normalized velocity ($M_i = 5.22$, Ti = 3%, realizable k-ε turbulence model).

Combined with a low centerline streamwise velocity, this indicates that the film protection at the centerline is superior to that for both the NOV1-0p and NOV1-4p cases.

Figure 4-16 shows the downstream spanwise averaged adiabatic film cooling effectiveness for the three pedestal configurations, at $M_i = 0.87$ and $M_i = 5.22$. The three configurations result in similar spanwise averaged effectiveness at low blowing rate. This confirms that the pedestals do not have a significant effect on the flow structure and its ability to protect the surface. For $M_i = 5.22$, the difference in spanwise averaged effectiveness is insignificant except for $x/D_h \leq 2$. As was seen previously, the pedestals do affect the flow structure and effectiveness distribution downstream of injection. In the near-hole region, the NOV1-2p performs best because it promotes less mixing of the coolant with the mainstream. Farther downstream, the benefits and detriments for each case cancel each other out such that the film performance is essentially equivalent for all three configurations.

4.3 Effect of Hole Inlet

The geometry of the inlet passage of the hole is expected to influence the cooling performance of the flow. Obot et al. (1979) showed that the nozzle geometry has an effect on the heat transfer coefficient on an impingement plate in a simple impinging jet problem. The present study will only investigate the effect of the nozzle (or hole inlet passage) geometry on the coolant downstream of injection in terms of adiabatic film cooling effectiveness. The cooling potential of the impingement jet for the inner blade

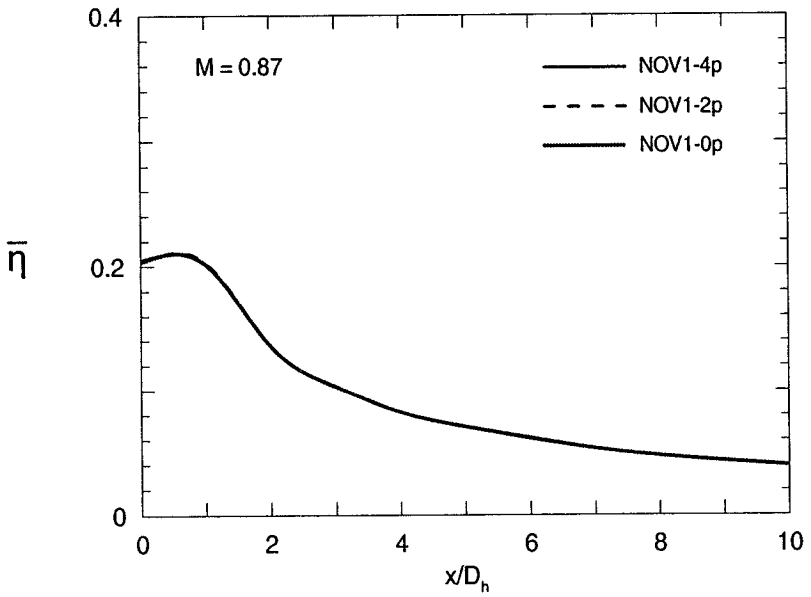

(a) $M_i = 0.87$

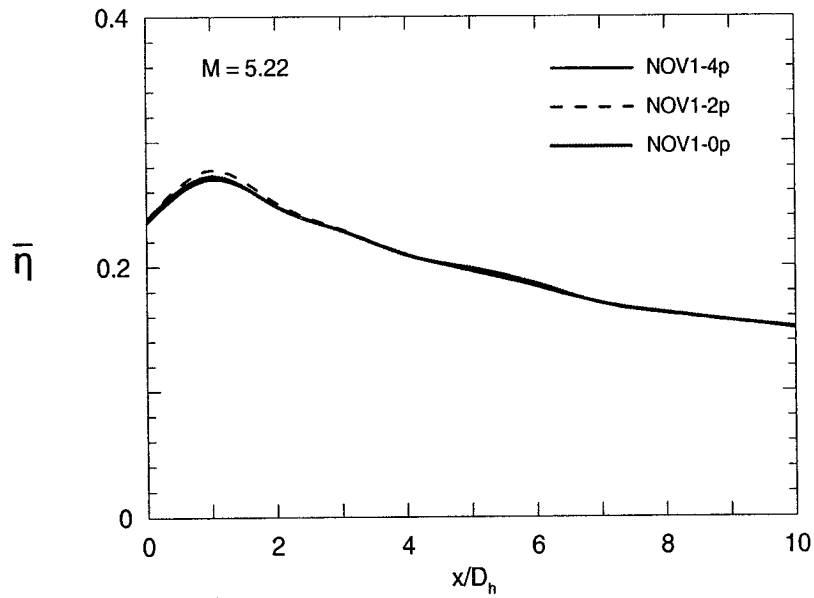

(b) $M_i = 5.22$

Figure 4-16. Spanwise averaged adiabatic film cooling effectiveness for three pedestal configurations: (a) $M_i = 0.87$, (b) $M_i = 5.22$ (Ti = 3%, realizable k-ε turbulence model).

material has not been investigated. The slot inlet geometry was tested at all blowing rates, namely, 0.87, 1.74, 3.48, and 5.22. The centerline adiabatic film cooling effectiveness obtained for each blowing rate is presented in Figure 4-17. The trends in centerline effectiveness observed with this geometry are similar to those observed for the NOV1-4p geometry. In fact, analysis of Figure 4-18 shows that there is no noteworthy difference in the downstream centerline effectiveness obtained with for the two geometries, at either $M_i = 0.87$ or $M_i = 5.22$.

Figure 4-19 presents the spanwise distribution of effectiveness at $x/D_h = 1$, 4, 7, and 10, for $M_i = 5.22$ for the NOV1-4p and NOV2-4p hole geometries. According to this figure, the downstream effectiveness distribution is dissimilar only at $x/D_h = 1$, suggesting that the nozzle geometry affects the flow solely in the near hole region around the centerline. In addition, Figure 4-20 reveals that the streamwise velocity field in the near-hole region depends on the nozzle geometry only at high blowing rates. This figure shows profiles of normalized streamwise velocity at the centerline at $x/D_h = 1$ for all blowing rates. As the blowing rate increases from 3.48 to 5.22, the NOV1-4p geometry shows greater velocities than for the NOV2-4p geometry. At $M_i = 0.87$ and $M_i = 1.74$, the difference in the profiles is minute. The influence of the nozzle geometry is small enough that the changes it imposed on the flow structure level out as the jet energy is dissipated.

In order to understand the difference in cooling mechanisms of the two geometries, the structure of the flow is analyzed. A look at the normalized streamwise and vertical velocity contours at $x/D_h = 1$ for the NOV1-4p and NOV2-4p geometries provides a

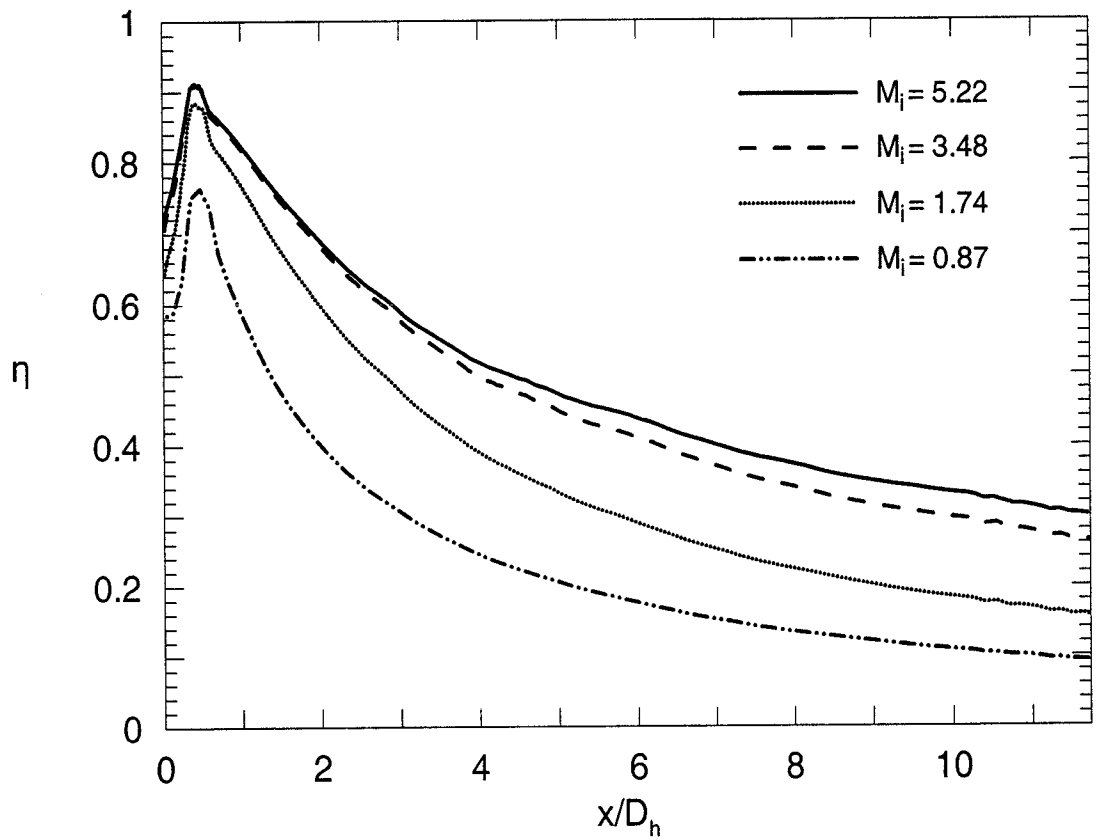

Figure 4-17. Centerline adiabatic film cooling effectiveness for the NOV2-4p geometry at various M_i (Ti = 3%, realizable k-ε turbulence model).

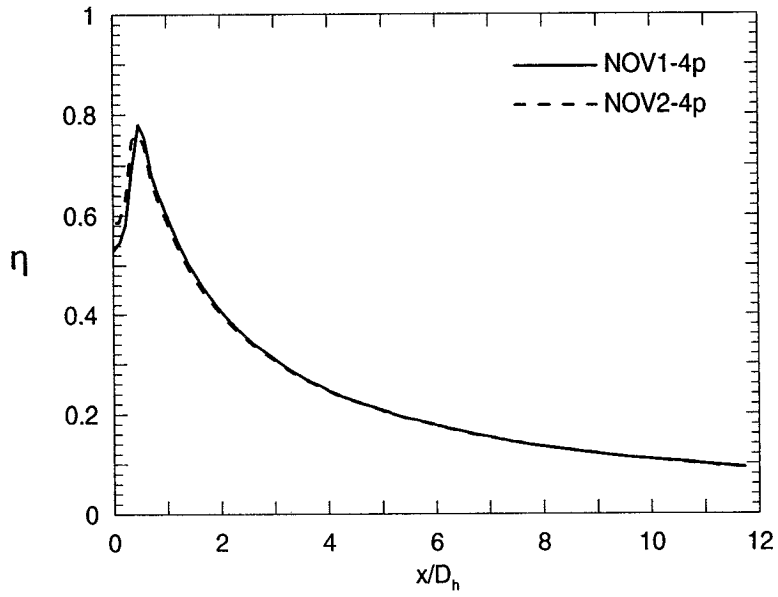

(a) $M_i = 0.87$

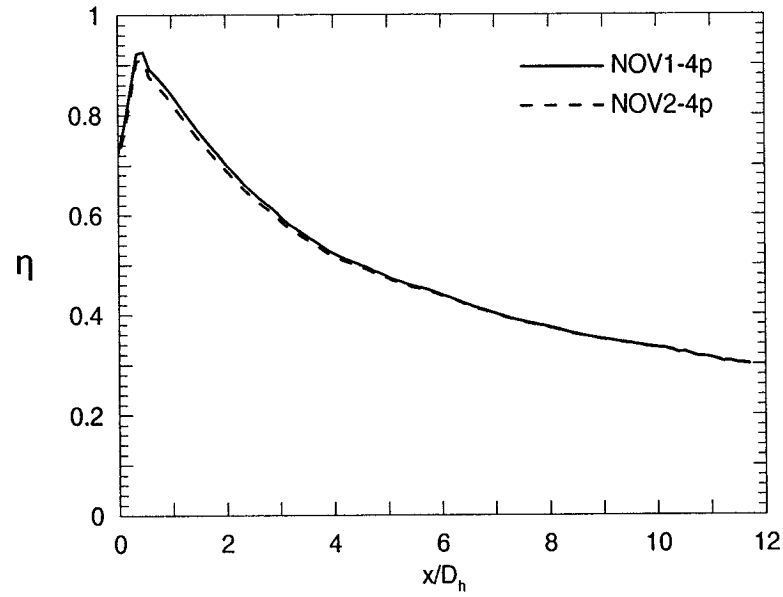

(b) $M_i = 5.22$

Figure 4-18. Centerline adiabatic film cooling effectiveness for two hole inlet geometries: (a) $M_i = 0.87$, (b) $M_i = 5.22$ (Ti = 3%, realizable k-ε turbulence model).

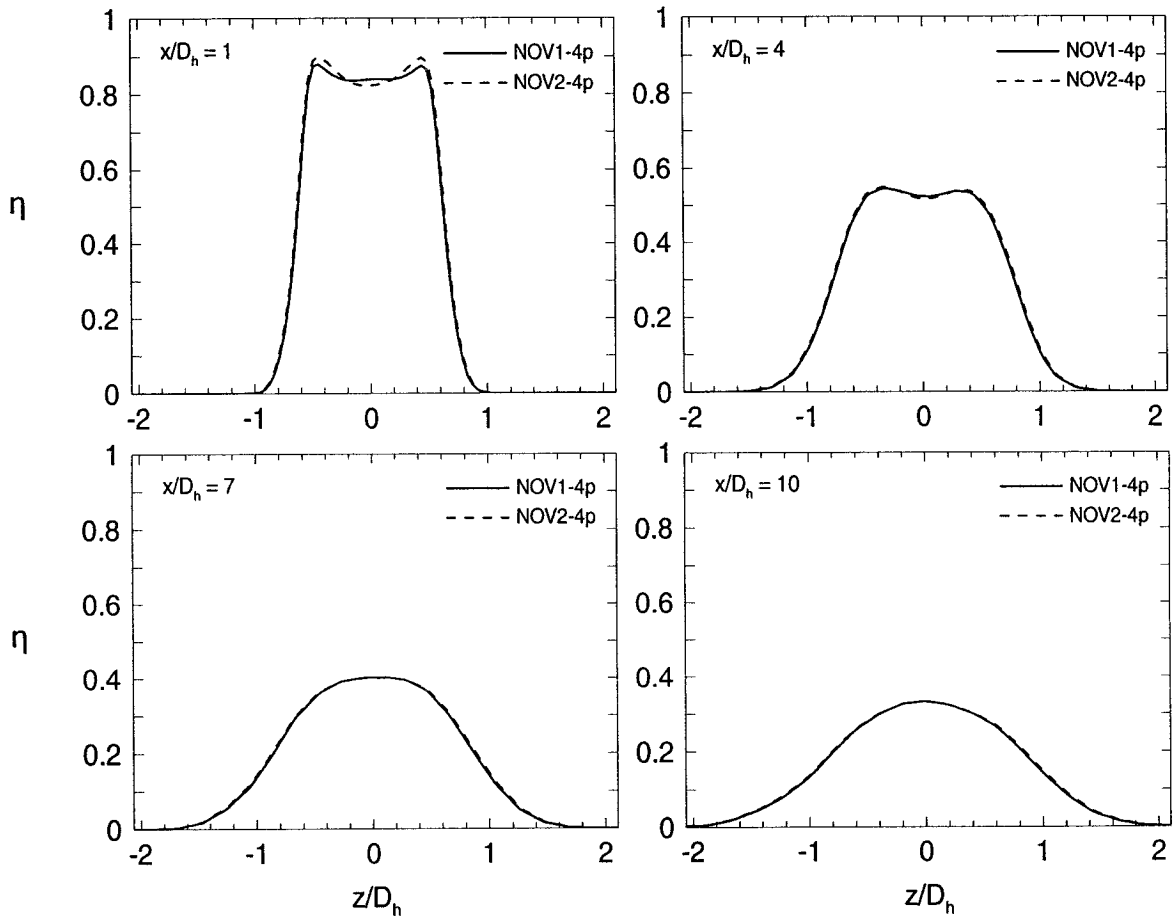

Figure 4-19. Spanwise distribution of adiabatic film cooling effectiveness at various downstream positions for the NOV1 and NOV2 geometries (M_i = 5.22, Ti = 3% realizable k-ε model).

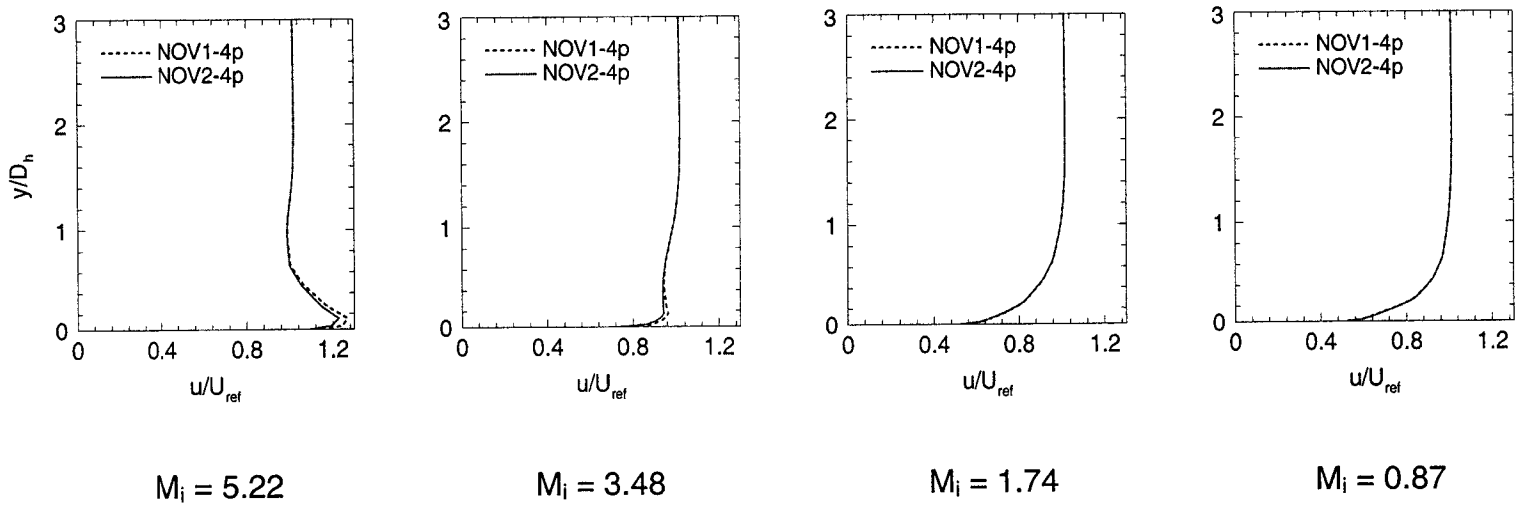

Figure 4-20. Centerline profiles of normalized streamwise velocity for two hole geometries at $x/D_h = 1$ for various blowing rates (Ti = 3%, realizable k-ε turbulence model).

better understanding of the structure of the coolant jet just downstream of injection. These contours are displayed in Figure 4-21. Figure 4-21(a) shows higher streamwise velocity concentrated in a smaller area for the NOV1-4p geometry. This denotes an overall narrower and faster jet core for this geometry than that for the NOV2-4p geometry. The vertical velocity contours in Figure 4-21(b) extend approximately 13% higher for the NOV2-4p than those for the NOV1-4p geometry, indicating that the jet height remains closer to the surface for the latter case. This suggests that the three discrete impingement nozzles act like flow separators which "pre-spread" the coolant laterally inside the hole without losing momentum, so that it tends to remain closer to the wall and is faster once it exits into the mainstream. With a slot nozzle, the coolant exits though only one opening and loses momentum as it tries to fill the hole interior. As the flow further expands laterally towards the hole sides, the jet is depleted in the centerline, thus explaining the slower and larger jet just downstream of injection.

This explains the increased lateral coverage of the jet for the NOV2-4p geometry, as conveyed by the spanwise distribution of effectiveness at $x/D_h = 1$ in Figure 4-19. The effectiveness distribution in this figure also confirms that the jet protection is less effective in the centerline for the NOV2-4p geometry. These results lead to the conclusion that the jet coverage is more uniform for the NOV1-4p geometry than for the NOV2-4p geometry. Figure 4-22 enables to visualize the increased streamwise velocity in the centerline as generated by the NOV1-4p geometry. The normalized streamwise velocity contours presented in Figure 4-22(a) extend approximately 25% farther

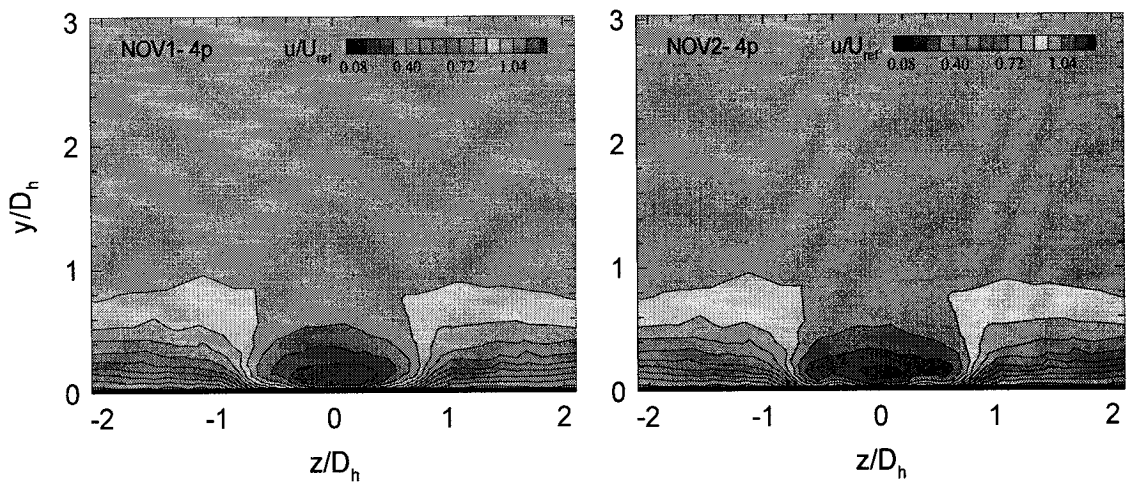

(a) Streamwise Normalized Velocity

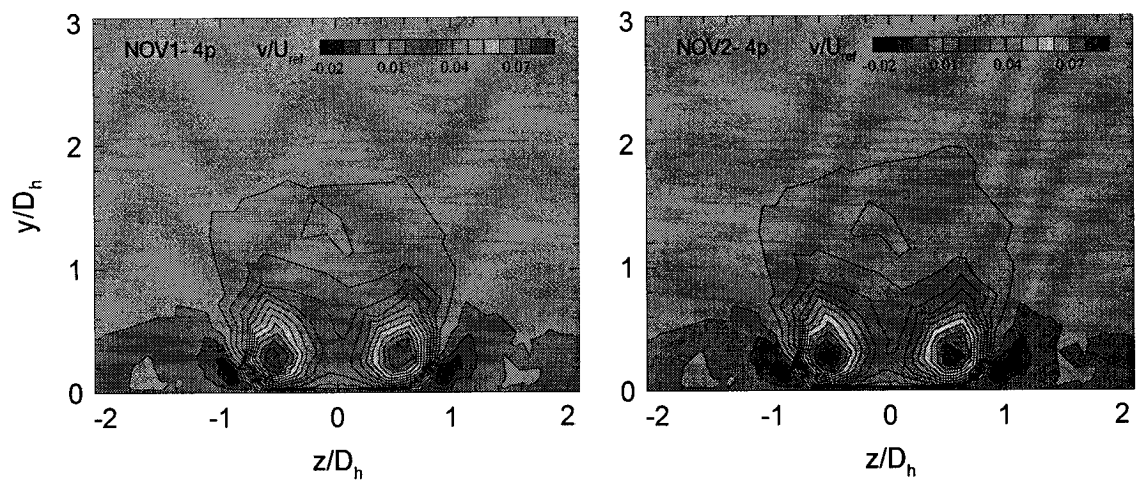

(b) Vertical Normalized Velocity

Figure 4-21. Contours of velocity components at $x/D_h = 1$, for two hole inlet geometries: (a) streamwise normalized velocity, (b) vertical normalized velocity ($M_i = 5.22$, Ti = 3%, realizable k-ε turbulence model).

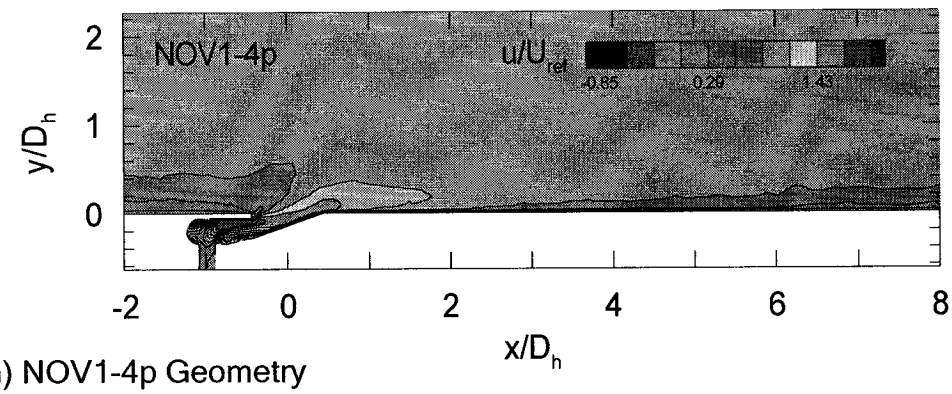

(a) NOV1-4p Geometry

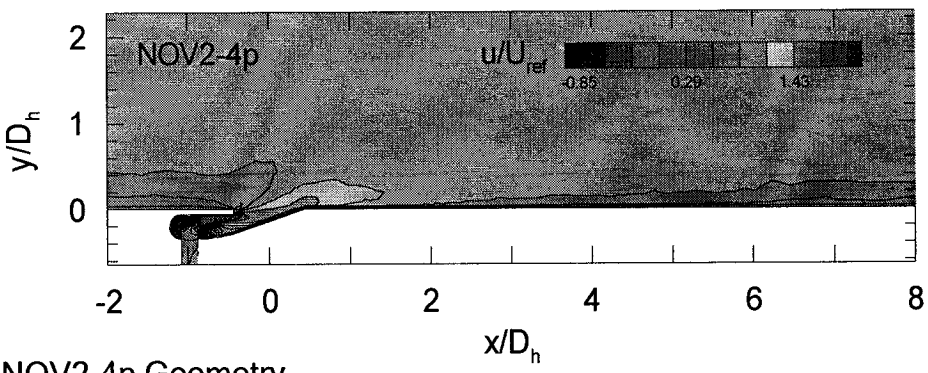

(b) NOV2-4p Geometry

Figure 4-22. Contours of the normalized streamwise component of velocity in the centerline plane for two hole inlet geometries: (a) NOV1-4p, (b) NOV2-4p (M_i = 5.22, Ti = 3%, realizable k-ε turbulence model).

downstream than those in Figure 4-22(b). This indicates a greater downstream coverage for the NOV1-4p geometry.

4.4 Effect of Turbulence Models

Tests were performed to determine the effect the different turbulence models had on the solution. Three turbulence models were utilized, namely the realizable, RNG and standard k-ε models, each with enhanced wall treatment. These were chosen because they were found to give accurate results when used in a validation study (results compared to those of Walters and Leylek (2000), and Sinha et al. (1991)). In the present study, it was concluded that the choice of turbulence models does not significantly affect the prediction of the downstream distribution of effectiveness.

Figure 4-23 displays the downstream centerline effectiveness for the NOV1-4p geometry at $M_i = 0.87$ and $M_i = 5.22$, obtained using the three turbulence models mentioned above. For either blowing rate, the difference in centerline effectiveness was found to be lower than approximately 9%. In general, the RNG k-ε turbulence model yields the lowest prediction of centerline effectiveness of all three models for both blowing rates. The results obtained with the realizable and standard k-ε turbulence models are essentially the same at $M_i = 5.22$. However at low blowing ratio, the realizable k-ε turbulence model gives a slightly higher prediction than the standard one for $x/D_h \leq 4$.

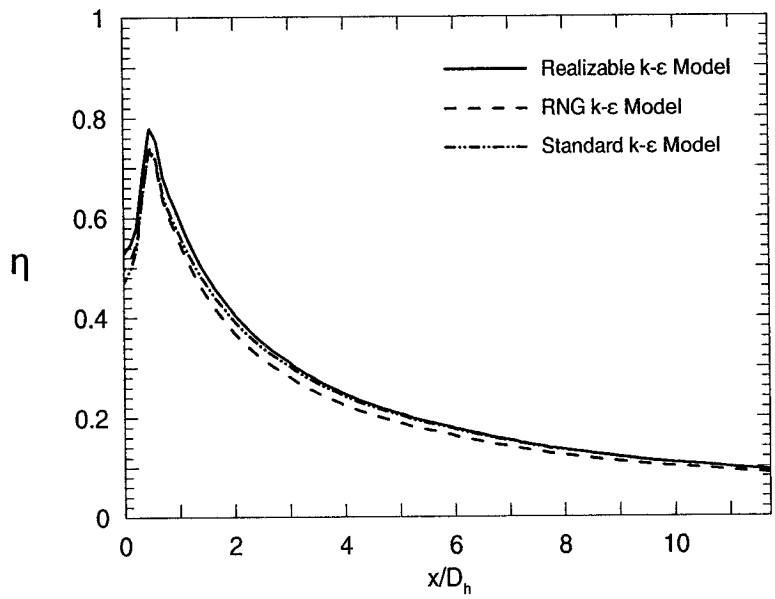

(a) $M_i = 0.87$

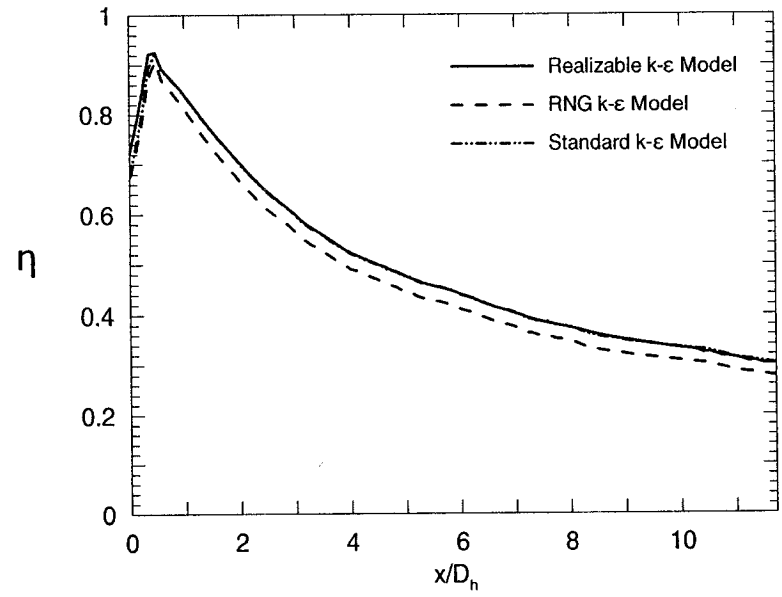

(b) $M_i = 5.22$

Figure 4-23. Centerline adiabatic film cooling effectiveness for the NOV1-4p geometry, computed with various turbulence models for a mainstream turbulence intensity of 3%: (a) $M_i = 0.87$, (b) $M_i = 5.22$.

Figure 4-24 displays the contours of normalized streamwise velocity in the centerline plane obtained with the three turbulence models at $M_i = 5.22$. These contours reveal that there are slight discrepancies in the results between each of the three cases. Figure 4-25 shows the contours of normalized vertical velocity in the centerline plane as well, for the same turbulence models, again at $M_i = 5.22$. The similar contour plots show there are no major discrepancies in the behavior of the flow. Overall, the three turbulence models yield rather similar predictions of the velocity flowfield for the NOV1-4p geometry at high blowing rate.

Figure 4-26 presents contours of turbulent kinetic energy in the centerline plane obtained for the NOV1-4p geometry, with the three turbulence models. The contour plots show the high turbulent kinetic energy levels generated inside the hole from the impingement process. Turbulent kinetic energy levels are also high near the injection locus, and are generated by a shearing process between the mainstream and the coolant. The turbulent kinetic energy is transported with the coolant as it is convected downstream, and dissipates through frictional losses incurred by the mainstream/coolant interactions. The contours of turbulent kinetic energy for the RNG case extend farther above the surface than for the other cases. This denotes that the RNG model overpredicts the turbulence levels in the coolant compared to the other models. This turbulence contributes to enhance the degree of mixing between the mainstream and the coolant, and also accelerates the dissipation of energy within the flow. This explains why the centerline effectiveness is almost always lower when using the RNG model than with the other models tested.

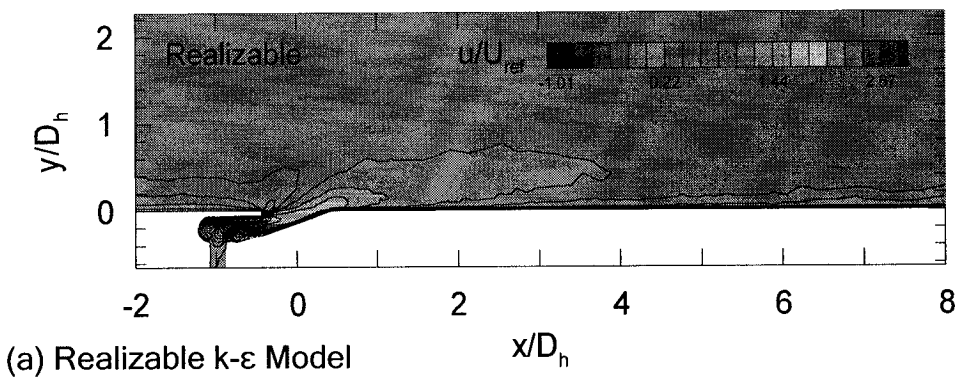

(a) Realizable k-ε Model

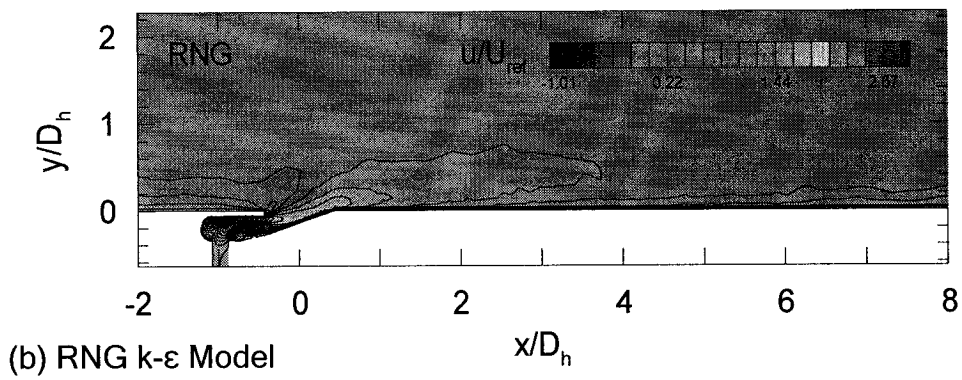

(b) RNG k-ε Model

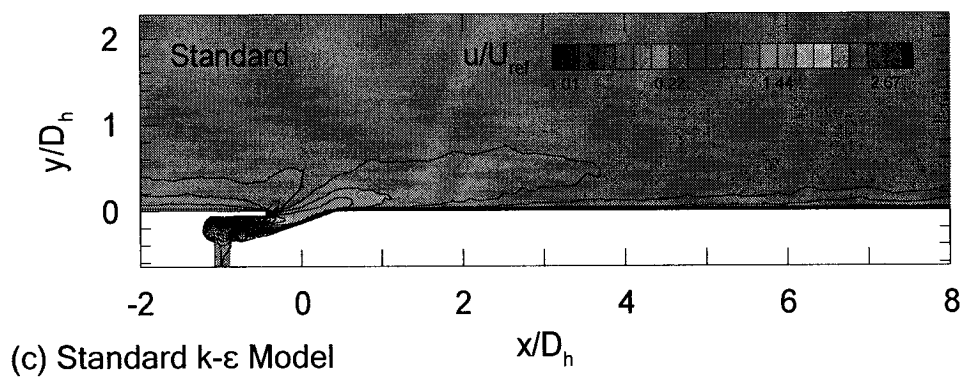

(c) Standard k-ε Model

Figure 4-24. Contours of the normalized streamwise component of velocity in the centerline plane computed with three turbulence models with enhanced wall treatment: a) RKE Model, b) RNG Model, c) SKE Model (NOV1-4p, $M_i = 5.22$, Ti = 3%).

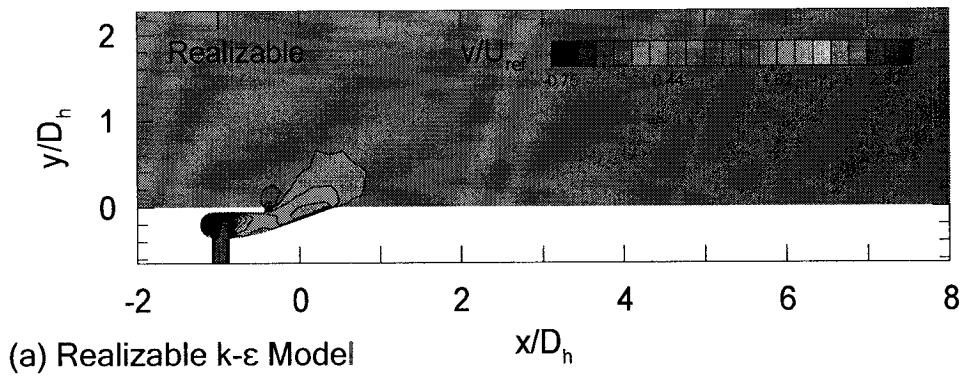

(a) Realizable k-ε Model

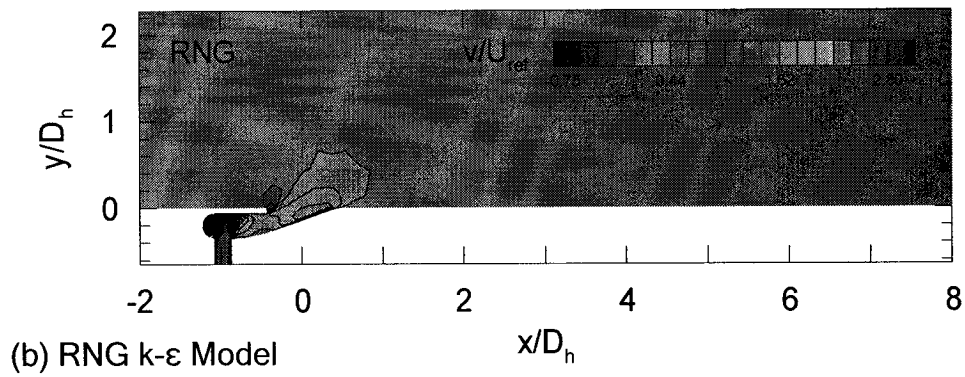

(b) RNG k-ε Model

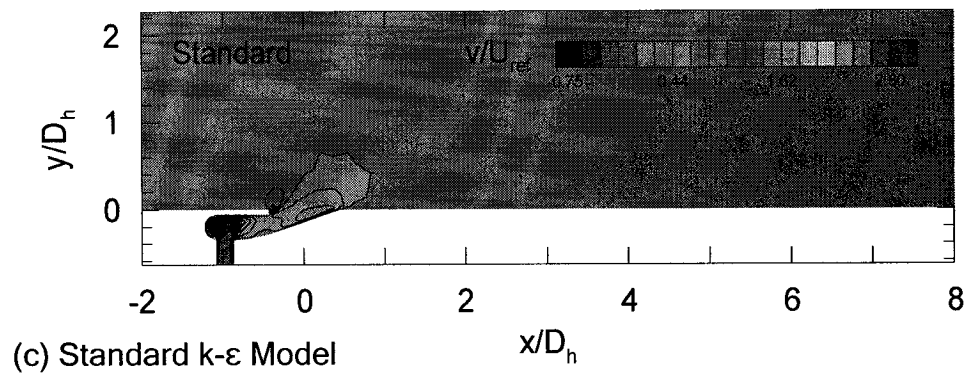

(c) Standard k-ε Model

Figure 4-25. Contours of the normalized vertical velocity component in the centerline plane computed with three turbulence models with enhanced wall treatment: a) realizable k-ε model, b) RNG k-ε model, c) standard k-ε model (NOV1-4p, $M_i = 5.22$, Ti = 3%).

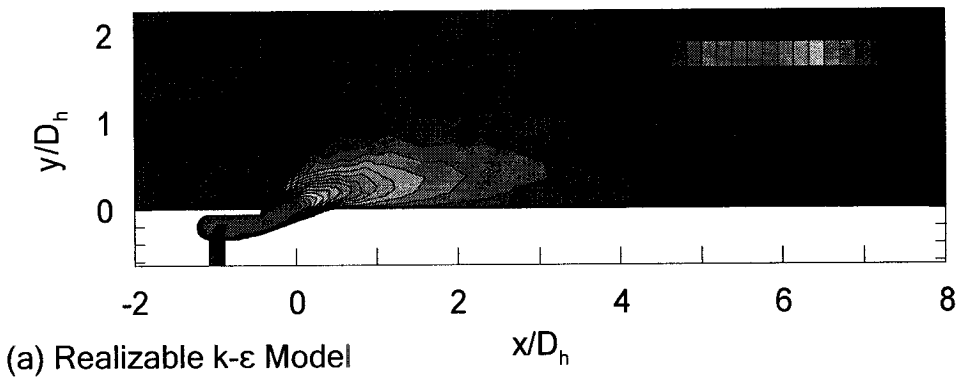

(a) Realizable k-ε Model

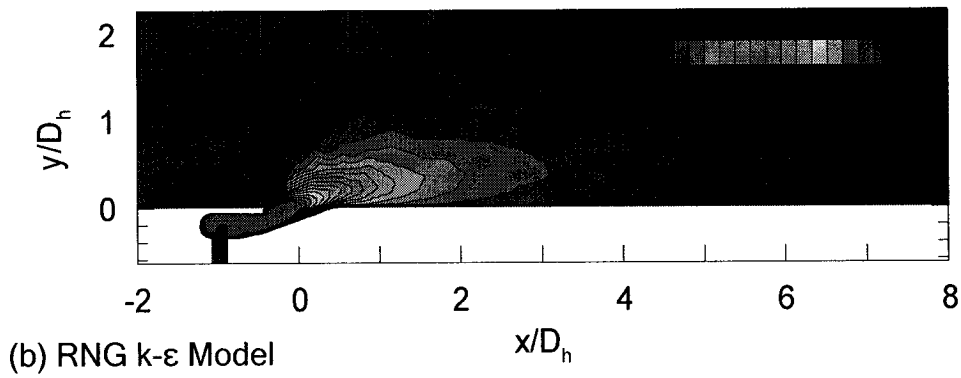

(b) RNG k-ε Model

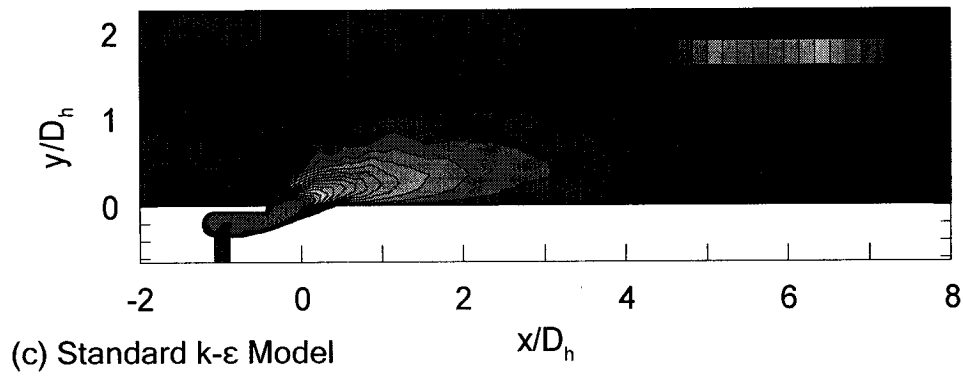

(c) Standard k-ε Model

Figure 4-26. Contours of the turbulent kinetic energy in the centerline plane computed with three turbulence models with enhanced wall treatment: a) RKE Model, b) RNG Model, c) SKE Model (NOV1-4p, M_i = 5.22, Ti = 3%).

Figure 4-27 present the profiles of turbulent kinetic energy in the centerline at various downstream positions, as computed by the realizable and RNG k-ε turbulence models, and for two mainstream turbulence intensities. The profiles illustrate the dissipation of energy as the jet moves downstream. The disagreement between the two predictions is more prominent at locations closer to the locus of injection. This is where it is hardest to predict the behavior of the fluid, due to the enhanced mainstream/coolant interactions. The turbulence kinetic energy levels in the RNG case are almost always superior to those found in the RKE case, except close to the wall ($y/D_h \leq 0.5$). This Figure also shows that the turbulence kinetic energy profiles are essentially the same for mainstream turbulence intensities of 3% and 10%. This suggests that the mainstream turbulence intensity bears no effect on the prediction capability of either model.

Figure 4-28 presents the downstream spanwise average adiabatic film cooling effectiveness obtained with the three turbulence models for the NOV1-4p geometry at $M_i = 5.22$. Results show that the realizable and standard k-ε turbulence models produce very similar predictions. The RNG k-ε turbulence model consistently predicts lower values of spanwise averaged effectiveness downstream of injection than the other models. This is caused by the overprediction of the turbulent kinetic energy field in the entire domain, which reduces the overall cooling performance of the jet.

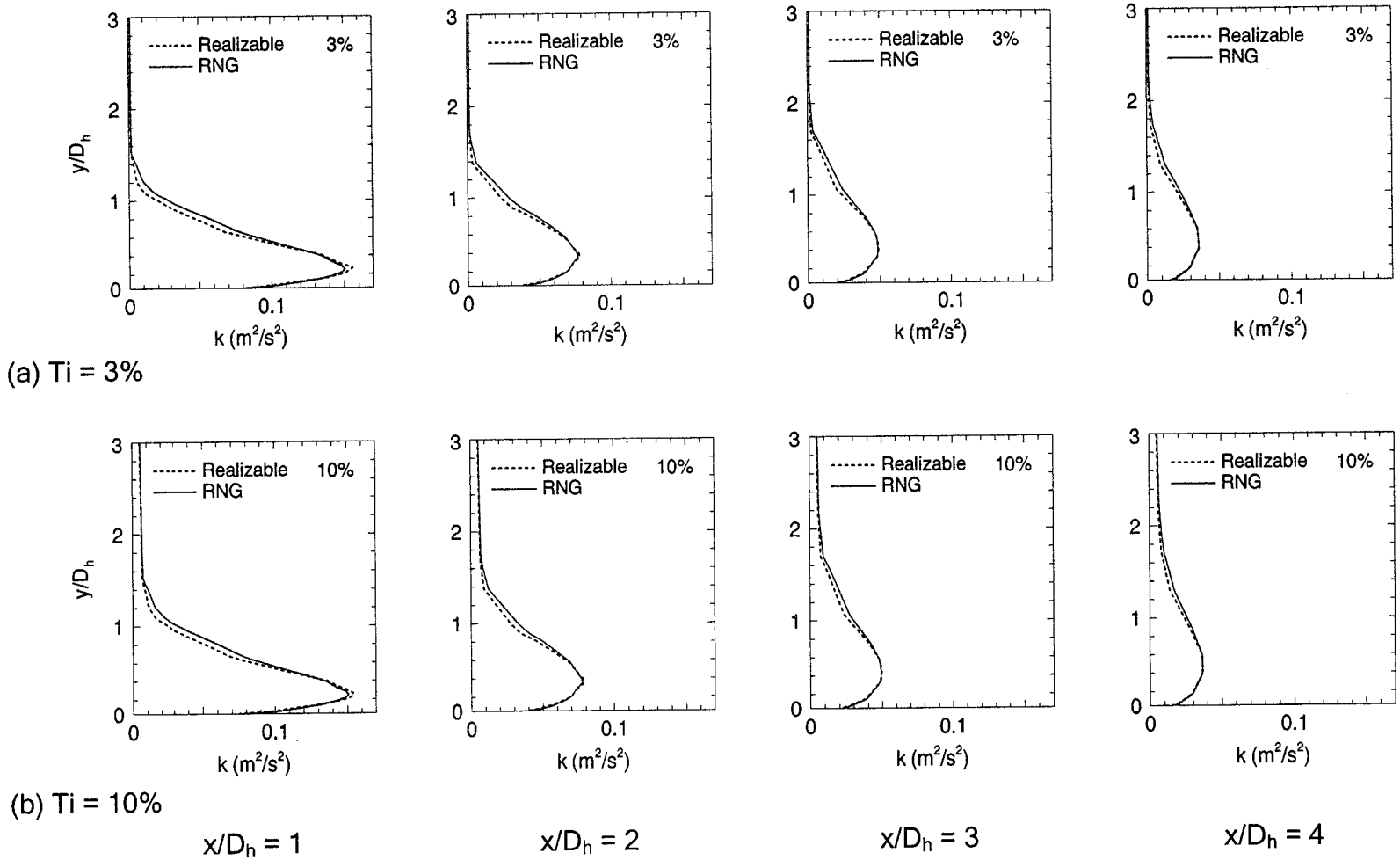

Figure 4-27. Centerline profiles of turbulent kinetic energy obtained for the realizable and RNG k-ε turbulence models at zarious downstream positions: a) at Ti = 3%, b) Ti = 10% (NOV1-4p, M_i = 5.22).

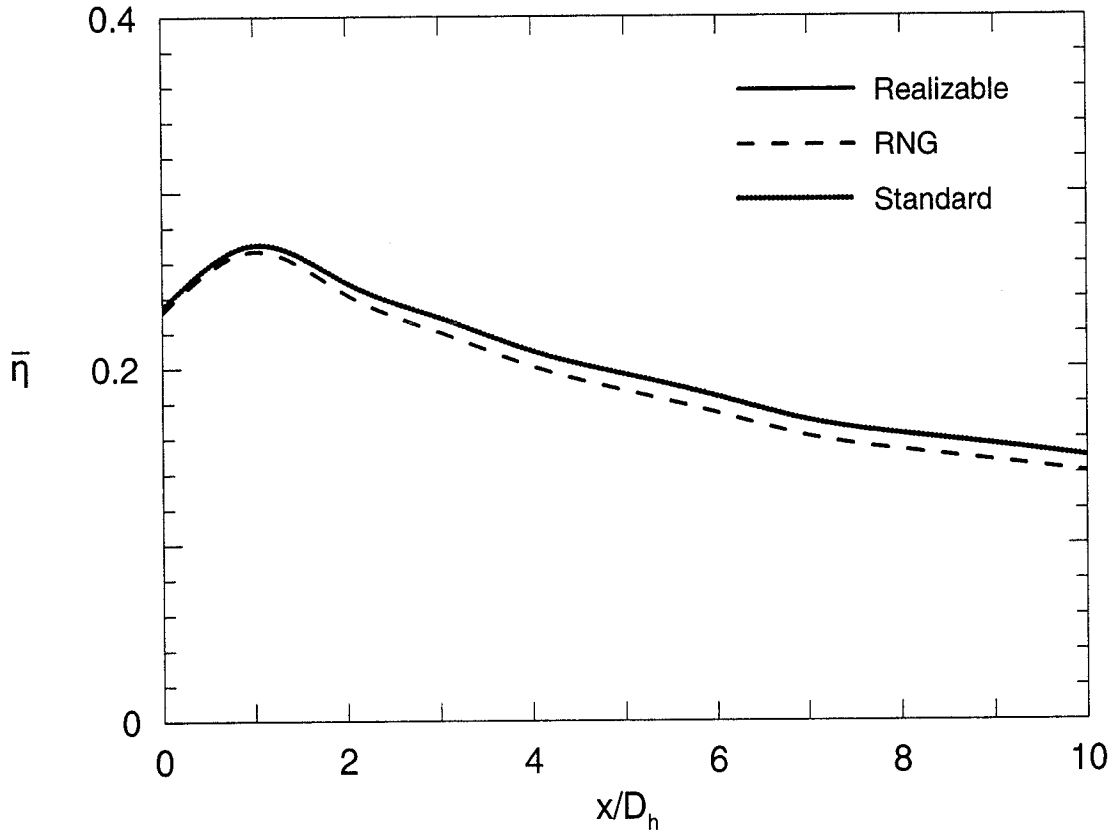

Figure 4-28. Spanwise averaged adiabatic film cooling effectiveness for the NOV1-4p geometry computed with three turbulence models (M_i = 5.22, Ti = 3%).

4.5 Effect of Turbulence Intensity

Figure 4-29 displays the downstream centerline adiabatic film cooling effectiveness as a function of blowing rate and mainstream turbulence intensity. This figure shows that the turbulence intensity has a negligible effect on the centerline effectiveness downstream of injection, whether computed at $M_i = 5.22$ or $M_i = 0.87$.

Figure 4-30 shows the profiles of normalized streamwise velocity at the centerline, at various downstream positions, obtained for $M_i = 0.87$ and $M_i = 5.22$, with mainstream turbulence intensities of 3% and 10%. These profiles show no major difference in streamwise velocity in the flowfield near the wall for Ti = 3% and 10%. This signifies that the mainstream turbulence intensity does not significantly affect the structure of the flow, at either high or low blowing rates. Figure 4-31 shows lateral distributions of effectiveness at $x/D_h = 1$ and $x/D_h = 5$ for high and low blowing rates, obtained with 3% and 10% mainstream turbulence intensities. For both values of Ti, the distributions of effectiveness are essentially the same, confirming that the mainstream turbulence bears no effect on the film performance at these two downstream positions.

Figure 4-32 presents the downstream spanwise averaged film cooling effectiveness obtained for Ti = 3% and 10%. This plot shows that the predicted spanwise averaged effectiveness is effectively the same for the two mainstream turbulence intensities implemented. This provides additional confirmation that the performance, in terms of effectiveness distribution for the present cooling scheme, is not affected by the

mainstream turbulence intensity, for turbulence intensities equal to or lower than 10%. Many previous studies using standard circular holes have shown that the mainstream turbulence intensity increases the degree of mixing between the coolant and the mainstream, thus degrading the downstream effectiveness. It seems the hole geometry plays a fundamental role in reducing the interactions between the mainstream and the coolant jet. The diffused hole, flared both in the lateral and forward directions, reduces the coolant momentum compared to a standard circular hole. The gradual slope ensures a low-disturbance coolant delivery, so that the jet is not prone to mixing with the mainstream even if its turbulence levels are high.

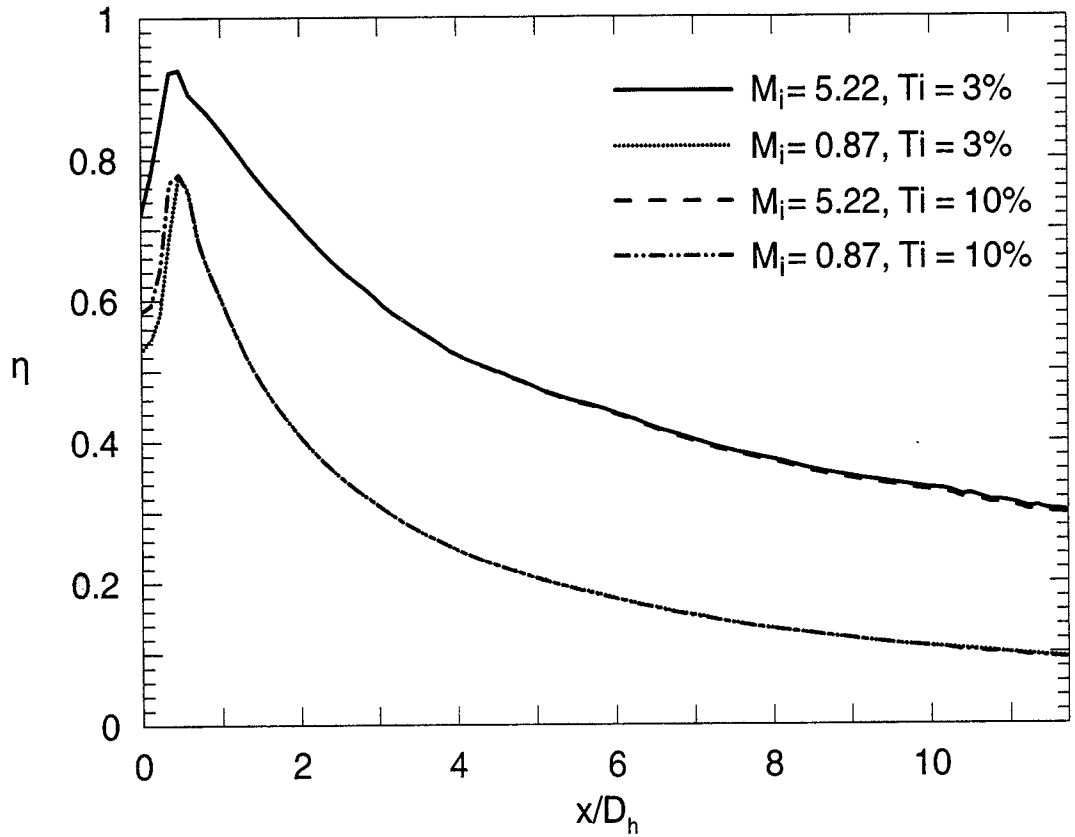

Figure 4-29. Centerline adiabatic film cooling effectiveness for the NOV1-4p, at various mainstream turbulence intensities, at high and low blowing rates (realizable k-ε turbulence model).

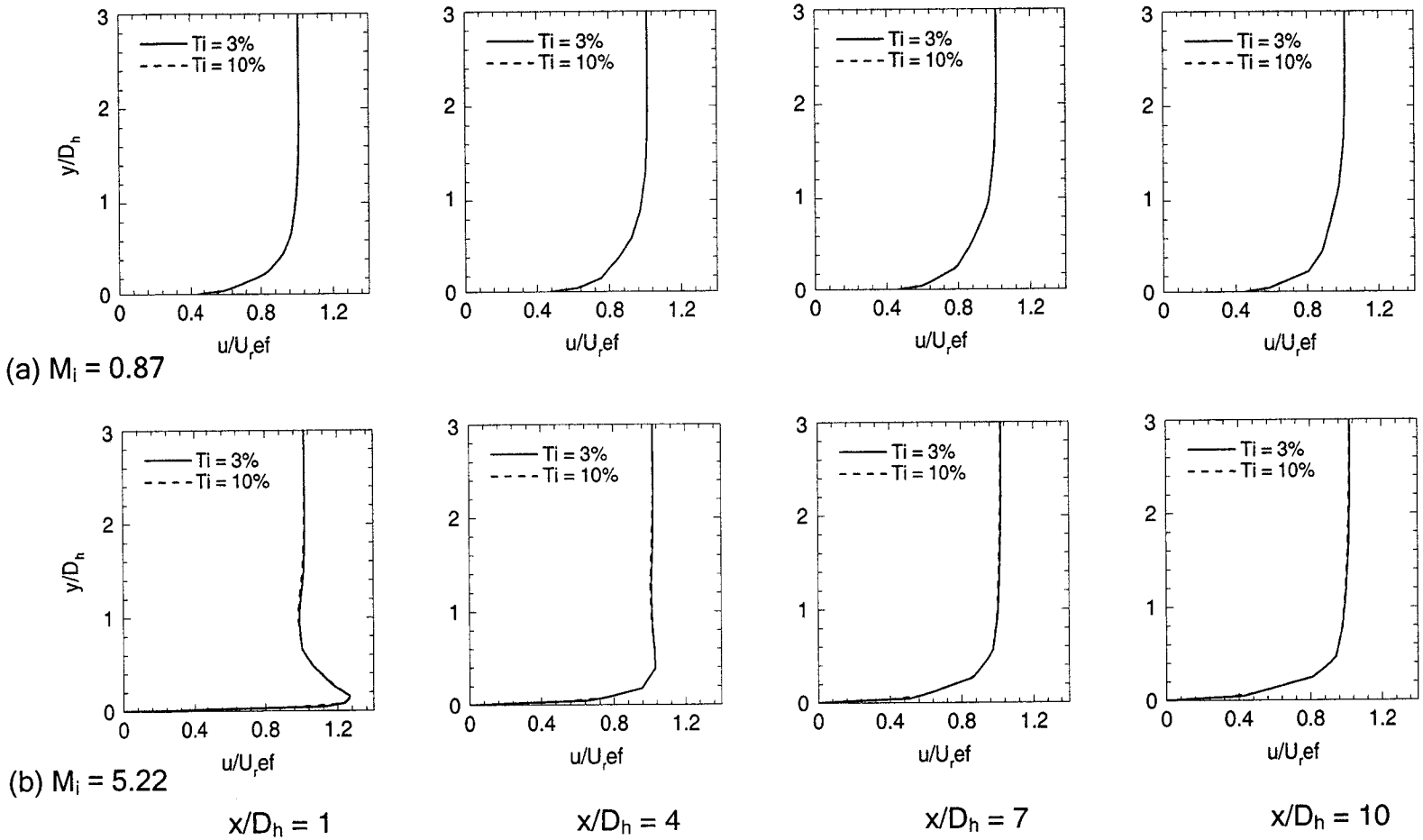

Figure 4-30. Centerline profiles of normalized streamwise velocity at various downstream positions for mainstream turbulence intensities of 3% and 10%: (a) $M_i = 0.87$, (b) $M_i = 5.22$ (NOV1-4p, realizable k-ε turbulence model).

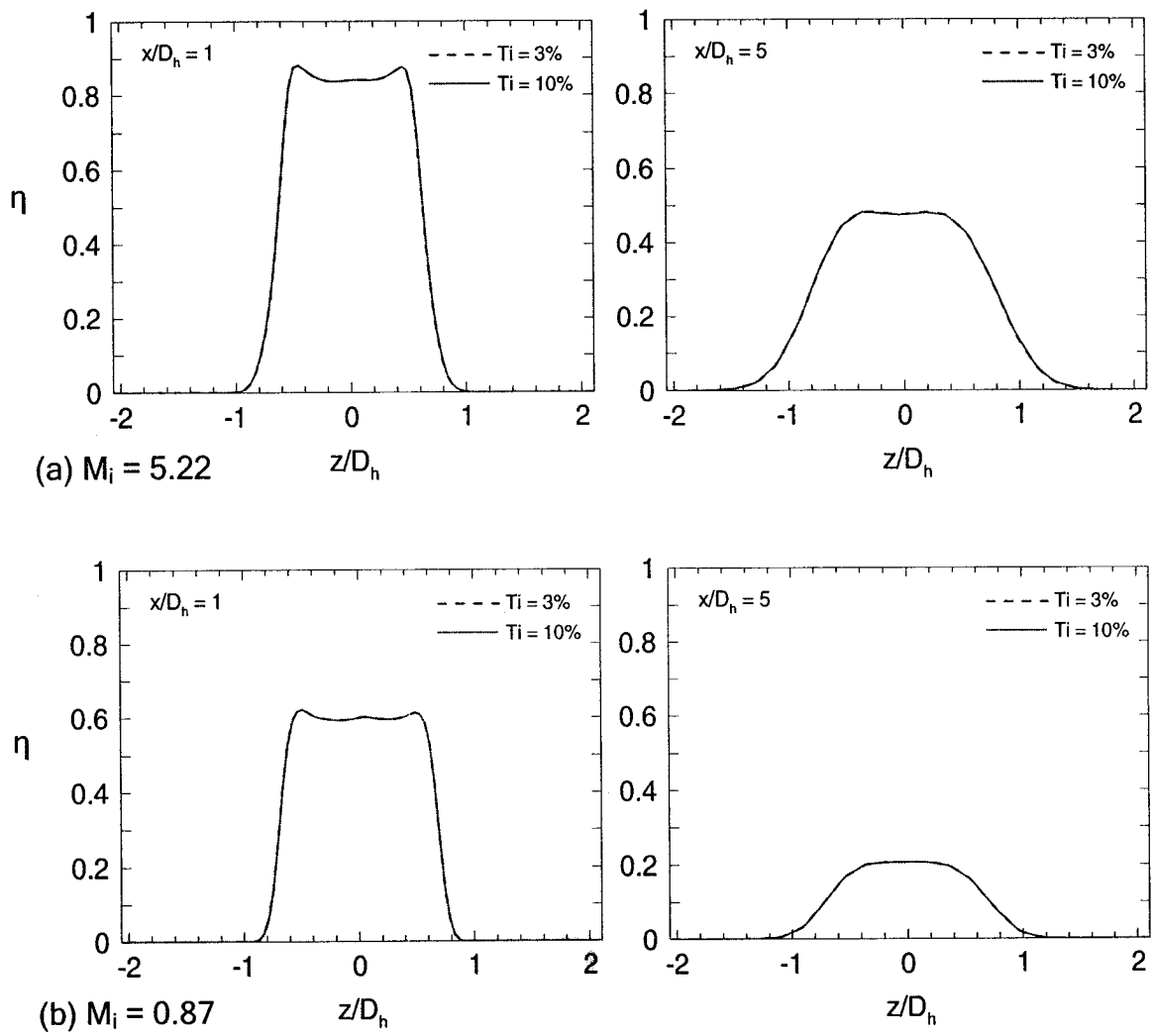

Figure 4-31. Spanwise distribution of adiabatic film cooling effectiveness at $x/D_h = 1$ and $x/D_h = 5$, for Ti = 3% and 10%: (a) $M_i = 5.22$, (b) $M_i = 0.87$ (NOV1-4p, realizable k-ε turbulence model).

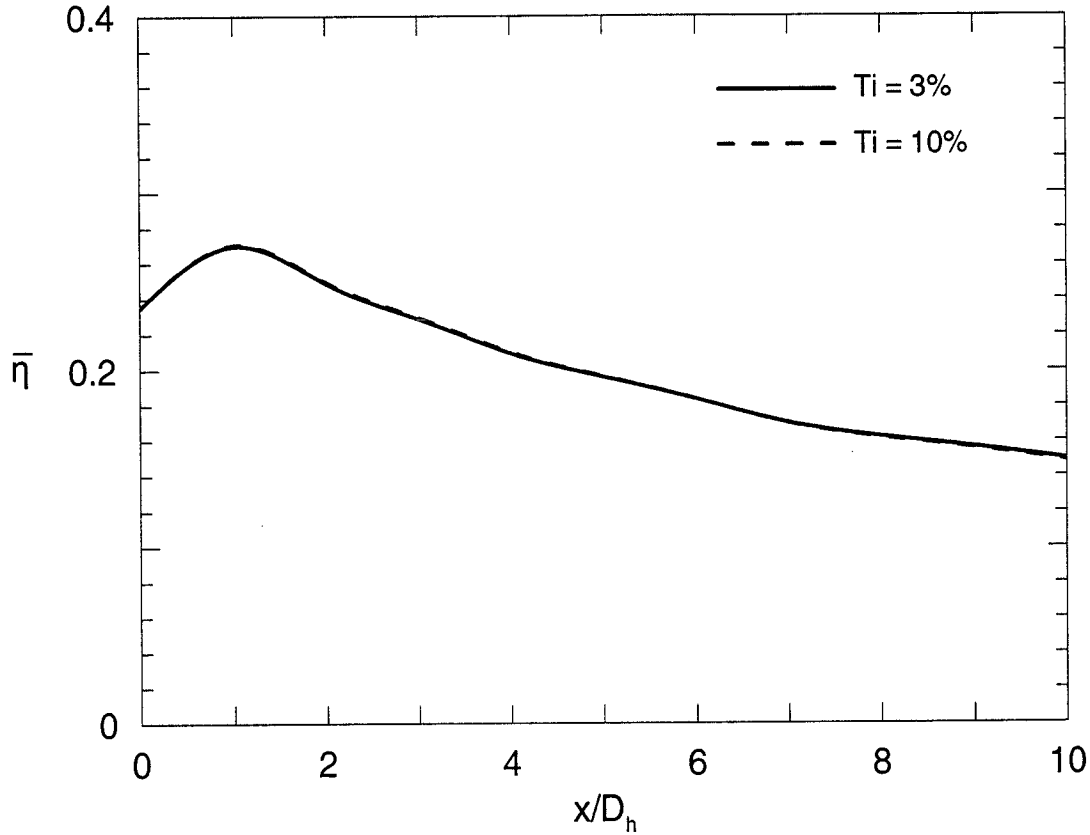

Figure 4-32. Spanwise averaged adiabatic film cooling effectiveness for the NOV1-4p geometry with mainstream turbulence intensities of 3% and 10% (M_i = 5.22, realizable k-ε turbulence model).

Chapter V

Conclusions and Future Directions

5.1 Conclusions

A new film cooling scheme was designed and tested at various flow conditions by means of computational simulations. This innovative scheme combines in-hole impingement cooling and flow turbulators with traditional downstream film-cooling for improved cooling capabilities. This study focused solely on the downstream cooling effectiveness aspect of performance with no investigation on heat transfer characteristics of the flow. The temperature, turbulence kinetic energy and flow fields were analyzed in centerline and spanwise planes in order to get a fundamental understanding of the cooling mechanisms. This is the first study in the open literature to investigate such a cooling scheme, and therefore no experimental data was available for comparison purposes.

Tests involved four versions of the cooling hole, where the impingement nozzle geometry (slot or three inlet tubes) and pedestal configurations were varied. The temperature ratio was selected in the practical range for high temperature gas-turbine engines, with the coolant temperature set to 750K and the mainstream temperature set to 1300K. The coolant inlet velocity was fixed at 3 m/s, while the mainstream inlet velocity was varied between 1 m/s and 6 m/s, corresponding to blowing rates M_i of 0.87 to 5.22 (or corresponding to blowing rates M_e of 0.44 to 1.77 based on the hole exit conditions).

Cases were run using the commercial CFD package FLUENT 6.1, where turbulence was modeled using either the realizable, RNG or standard k-ε turbulence models. Tests were conducted to evaluate the effect of the blowing rate, mainstream turbulence intensity (set in turn to 3% and 10%), hole geometry, and choice of turbulence model, have on the film cooling effectiveness.

It was determined that this new hole geometry can prevent coolant lift-off much better than standard round holes. While the hole was tested for a large range of blowing rates (0.87 to 5.22 based on hole inlet conditions, or 0.44 to 1.77 based on hole exit conditions), the centerline effectiveness obtained for each case, presented as a function of downstream position, increased or remained constant with increasing M_i. The decrease in spanwise-averaged effectiveness downstream of injection from $M_i = 3.48$ to $M_i = 5.22$ in the near-hole region revealed that the coolant coverage does in fact lessen in that region due to the edges of the jet lifting off from the surface. At $M_i = 5.22$, the jet momentum is highest compared to the mainstream momentum, and this yields the greatest overall wall protection of all cases. However, the jetting observed at $M_i = 5.22$ also causes the coolant to exit the hole mainly in the centerline and leeward portion of the hole exit, allowing for increased hot gas ingestion in the windward portion of the hole exit when compared to the jet at $M_i = 0.87$.

Results show that pedestals have a small effect in the spanwise averaged film cooling effectiveness at high blowing rate ($M_i = 5.22$), and near the locus of injection ($x/D_h \leq 2$). The pedestals act as a comb inside the hole, redistributing the coolant, so that it spreads

more in the lateral direction and less in the vertical direction. The pedestals were found to help spread the coolant downstream of injection. While the four-pedestal configuration ensures a lower jet with more outwards momentum than for the other configurations, the two-pedestal configurations gives the best performance in terms of downstream effectiveness distributions, due to the lower levels of mixing it promotes within the mainstream.

It was observed that the nozzle geometry does not affect the centerline effectiveness much downstream of injection. However, it does affect the lateral distribution of effectiveness at $x/D_h = 1$. The NOV1-4p geometry ensures a more uniform distribution of effectiveness (i.e. a more uniform film coverage) than the NOV2-4p geometry at $x/D_h = 1$. While it yields the best effectiveness in the centerline compared to the NOV2-4p geometry, it also yields lower effectiveness on the edges of the coolant jet than the latter.

It was determined that whether the mainstream turbulence intensity was set at 3% or 10%, it has no significant effect on downstream distributions of effectiveness for the present flow parameters. The choice of turbulence model in the CFD computations proves to be of significance, since the RNG k-ε turbulence model generally predicts lower effectiveness than the other models implemented.

5.2 Future Directions

Evidently, more research must be done in order to understand the importance and effect of the various geometrical parameters on the cooling mechanisms. The results presented in this work provide important insights for future studies on this topic. The present study was only concerned with the downstream effectiveness aspect of performance. The performance related to the heat transfer coefficient is a prospective topic for future studies. In particular, the heat transfer characteristics of the impingement jet inside the hole have an effect on the temperature of the target wall, thus influencing the performance of this cooling scheme overall. Future studies need to investigate how these heat transfer characteristics are influenced by such parameters as the geometry of the nozzle. These findings will complement the results found in the present study and give a better overall understanding of the cooling performance of this scheme.

The hole geometry was tested for a range of blowing rates which did not show any jet detachment. It is recommended to test the cooling hole at higher blowing rates in order to better understand the jet detachment process in this particular hole geometry. Similarly, since only three pedestal configurations were investigated, it would be interesting to observe the behavior of the flow when other configurations of pedestals are involved. In particular, the effect of half-pedestals (pin fins) should be investigated, as these may provide the same advantages as full-length pedestals with less flow blockage. As observed from the literature, compound injection has some advantages over streamwise

injection. Simulations of the present hole with compound orientation would provide further information on the mainstream and coolant interaction.

Many simplifications have been made in the present study, which affect in some way the accuracy of the numerical solution. One simplification comes from representing the blade by a flat surface. Various studies have shown that the curvature does indeed have an effect on film cooling performance. The extent to which this affects the results is not yet known, and future studies could aim at evaluating it. Another simplification arises from the fact that the plenum was not modeled. In reality the coolant travels through intricate channels inside the blade before exiting through the cooling hole and does not arrive at the hole inlet in a uniform velocity distribution as was assumed in this study. Based on previous work in the literature, it is expected that modeling the plenum will give more realistic results.

Experimental research is an essential complement to computational research. Turbulence modeling is one example of the limitations of numerical simulations. Experimental studies pertaining to the present hole geometry would provide valuable corroboration of the results. Since experimental research is in general more expensive and time consuming than its numerical counterpart, a "rapid prototyping" approach is recommended, where both numerical and experimental research is combined, resulting in a higher turnover rate. This study represents the preliminary step in developing a novel gas turbine film cooling scheme. The promising results presented in this study provide the motivation to

continue developing this scheme so that it becomes feasible for modern gas turbine applications.

References

Ahn, J., I. S. Jung, J. S. Lee, "Film Cooling from Two Rows of Holes with Opposite Orientation Angles: Heat Transfer", JSME International Journal, Series B, Vol. 43, pp. 706-711, 2000.

Ajersch, P., J. M. Zhou, S. Ketler, M. Salcudean, I. S. Gartshore, "Multiple Jets in a Crossflow: Detailed Measurements and Numerical Simulations", ASME Paper 95-GT-9, 1995.

Amer, A. A., B. A. Jubran, M. A. Hamdan, "Comparison of Different Two-equation Turbulence Models for Prediction of Film Cooling from Two Rows of Holes", Numerical Heat Transfer, Part A, Vol. 21, pp. 143-162, 1992.

Ammari, H. D., N. Hay, D. Lampard, "The Effect of Density Ratio on the Heat Transfer Coefficient From a Film-Cooled Flat Plate", Journal of Turbomachinery, Vol. 112, pp. 444-450, 1990.

Bergeles, G., A. D. Gosman, B. E. Launder, "Near-Field Character of a Jet Discharged through a Wall at 30 Degrees to a Mainstream", AIAA Journal, Vol. 15, No. 4, pp. 499-504, 1977.

Berger, P. A., J. A. Liburdy, "A Near-Field Investigation into the Effects of Geometry and Compound Angle on the Flowfield of Film Cooling Holes", ASME Paper No. 98-GT-278, 1998.

Berhe, M. K., S. V. Patankar, "A Numerical Study of Discrete-Hole Film Cooling", ASME Paper No. 96-WA/HT-8, 1996.

Berhe, M. K., "A Numerical Study of Discrete-Hole Film Cooling", Ph.D. dissertation, University of Minnesota, 1997.

Brittingham, R. A., J. H. Leylek, "A Detailed Analysis of Film Cooling Physics: Part IV - Compound - Angle Injection With Shaped Holes", Journal of Turbomachinery, Vol. 122, pp. 133-145, 2000.

Burd, S. W., T. W. Simon, "The Influence of Coolant Supply Geometry on Film Coolant Exit Flow and Surface Adiabatic Effectiveness", ASME Paper 97-GT-25, 1997.

Cho, H. H., D. H. Rhee, B. G. Kim, "Enhancement of Film Cooling Performance Using a Shaped Film Cooling Hole with Compound Angle Injection", JSME International Journal, Series B, Vol. 44, No. 1, pp. 99-110, 2001.

Cohen, H., G. F. C. Rogers, H. I. H. Saravanamutto, "Gas Turbine Theory", Fourth Edition, Addison Wesley Longman, 1996.

Demirdzic, I., Z. Lilek, M. Peric, "Fluid Flow and Heat Transfer Test Problems for Non-Orthogonal Grids: Bench-mark Solutions", International Journal for Numerical Methods in Fluids, Vol. 15, pp. 329-354, 1992.

Drost, U., A. Bölcs, A. Hoffs, "Utilization of the Transient Liquid Crystal Technique for Film Cooling Effectiveness and Heat Transfer Investigations on a Flat Plate and a Turbine Airfoil", ASME Paper 97-GT-26 , 1997.

Drost, U., A. Bölcs, "Investigation of Detailed Film Cooling Effectiveness and Heat Transfer Distributions on a Gas Turbine Airfoil", ASME Paper 98-GT-20, 1998.

Ekkad, S. V., D. Zapata, J. C. Han, "Heat Transfer Coefficients Over a Flat Surface with Air and CO2 Injection Through Compound Angle Holes Using a Transient Liquid Crystal Image Method", Journal of Turbomachinery, Vol. 119, pp. 580-586, 1997.

Ekkad, S. V., J. C. Han, "A Transient Liquid Crystal Thermography Technique for Gas Turbine Heat Transfer Measurements", Measurement Science and Technology, Vol. 11, No. 7, pp. 957-968, 2000.

Ekkad, S. V., J. C. Han, H. Du, "Detailed Film Cooling Measurements on a Cylindrical Leading Edge Model: Effect of Free-Stream Turbulence and Coolant Density", Journal of Turbomachinery, Vol. 120, pp. 799-807, 1998.

Eriksen, V. L., R. J. Goldstein, "Heat Transfer and Film Cooling Following Injection Through Inclined Circular Tubes", Journal of Heat Transfer, Series C, Vol. 96, No. 2, pp. 239-245, 1974.

Ferguson, J. D., D. K. Walters, J. H. Leylek, "Performance of Turbulence Models and Near-Wall Treatments in Discrete Jet Film Cooling Simulations", ASME Paper 98-GT-438, 1998.

FLUENT 6.1 Documentation, Fluent Inc., 2003.

Forth, C. J. P., T. V. Jones, "Scaling Parameters in Film-Cooling", Proceedings 8th International Heat Transfer Conference, Vol. 3, pp. 1271-1276, 1988.

Forth, C. J. P., P. J. Loftus, T. V. Jones, "The Effect of Density Ratio on the Film-Cooling of A Flat Plate", AGARD Conference Proceedings 390, 1985.

Foster, N. W., D. Lampard, "The Flow and Film Cooling Effectiveness Following Injection through a Row of Holes", Journal of Engineering for Power, Vol. 102, pp. 584-588, 1980.

Garg, V. K., R. E. Gaugler, "Effect of Velocity and Temperature Distribution at the Hole Exit on Film Cooling of Turbine Blades", ASME 95-GT-2, 1995.

Garg, V. K., R. E. Gaugler, "Effect of Coolant Temperature And Mass Flow on Film Cooling of Turbine Blades", International Journal of Heat Mass Transfer, Vol. 40, No. 2, pp. 435-445, 1997.

Gartshore, I., M. Salcudean, I. Hassan, "Film Cooling Injection Hole Geometry: Hole Shape Comparison for Compound Cooling Orientation", AIAA Journal, Vol. 39, No. 8, pp. 1493-1499, 2001.

Gillespie, D. R. H., Z. Wang, P. T. Ireland, S. T. Kohler, "Full Surface Local Heat Transfer Coefficient Measurements in a Model of an Integrally Cast Impingement Cooling Geometry", ASME Paper 96-GT-200, 1996.

Goldstein, R. J., E. R. G. Eckert, F. Burggraf, "Effects of Hole Geometry and Density on Three-Dimensional Film Cooling", International Journal of Heat Mass Transfer, Vol. 17, pp. 595-607, 1974.

Goldstein, R. J., E. R. G. Eckert, J. W. Ramsey, "Film Cooling with Injection through Holes: Adiabatic Wall Temperatures Downstream of a Circular Hole", Journal of Engineering for Power, Series A, Vol. 90, pp. 384-395, 1968.

Goldstein, R. J., E. R. G. Eckert, V. L. Eriksen, J. W. Ramsey, "Film Cooling Following Injection through Inclined Circular Tubes", Israel Journal of Technology, Vol. 8, No. 1-2, pp. 145-154, 1970.

Goldstein, R. J., P. Jin, "Film Cooling Downstream of a Row of Discrete Holes With Compound Angle", Journal of Turbomachinery, Vol. 123, pp. 222-230, 2001.

Gritsch, M., A. Schulz, S. Wittig, "Adiabatic Wall Effectiveness Measurements of Film-Cooling Holes With Expanded Exits", Journal of Turbomachinery, Vol. 120, pp. 549-556, 1998a.

Gritsch, M., A. Schulz, S. Wittig, "Heat Transfer Coefficient Measurements of Film Cooling Holes with Expanded Exits" ASME Paper No. 98-GT-28, 1998b.

Hale, C. A., "An Experimental and Numerical Study of the Hydrodynamics and Surface Heat Transfer Associated With Short Film Cooling Holes Fed by a Narrow Plenum", Ph.D. dissertation, Purdue University, 1999.

Hale, C. A., M. W. Plesniak, S. Ramadhyani, "Film Cooling Effectiveness for Short Film Cooling Holes Fed by a Narrow Plenum", Journal of Turbomachinery, Vol. 122, pp. 553-557, 2000.

Hale, C. A., S. Ramadhyani, M. W. Plesniak, "Film Cooling Effectiveness Predictions for Short Holes Fed by a Narrow Plenum", ASME Paper No. 99-GT-162, 1999.

Han, J.-C., S. Dutta, S. Ekkad, "Gas Turbine Heat Transfer and Cooling Technology", Taylro and Francis, 2000.

Haven, B. A., M. Kurosaka, "Kidney and Anti-kidney Vortices in Crossflow Jets", Journal of Fluid Mechanics, Vol. 352, pp. 27-64, 1997.

Holman, J. P., "Heat Transfer", Eight Edition, McGraw-Hill, 1997.

Hyams, D. G., K. T. McGovern, J. H. Leylek, "Effects of Geometry on Slot-Jet Film Cooling Performance" ASME Paper No. 96-GT-187, 1996.

Hyams, D. G., J. H. Leylek, "A Detailed Analysis of Film Cooling Physics: Part III - Streamwise Injection With Shaped Holes", Journal of Turbomachinery, Vol. 122, pp. 122-132, 2000.

Jumper, G. W., W. C. Elrod, R. B. Rivir, "Film Cooling Effectiveness in High-Turbulence Flow", Journal of Turbomachinery, Vol. 113, pp. 479-483, 1991.

Jung, I. S., J. S. Lee, "Effects of Orientation Angles on Film Cooling Over a Flat Plate: Boundary Layer Temperature Distributions and Adiabatic Film Cooling Effectiveness", Journal of Turbomachinery, Vol. 122, pp. 153-160, 2000.

Kim, S. W., T. J. Benson, "Calculation of a Circular Jet in Crossflow with a Multiple Time Scale Turbulence Model", Journal of Heat Transfer. Vol. 35, No. 10, pp. 2357-2365, 1992.

Kohli, A., D. G. Bogard, "Effects of Hole Shape on Film Cooling With Large Angle Injection", ASME Paper 99-GT-165, 1999.

Launder, B. E., D. B. Spalding, "The numerical computation of turbulent flows", Computer Methods in Applied Mechanics and Engineering, Vol. 3, pp. 269-289, 1974.

Lee, H.-W., J. J. Park, J. S. Lee, "Flow Visualization and Film Cooling Effectiveness Measurements around Shaped Holes with Compound Angle Orientations", International Journal of Heat and Mass Transfer, Vol. 45, pp. 145-156, 2002.

Le Ribault, C., M. Buffat, D. Jeandel, " Introduction of Turbulent Model in a Mixed Finite Volume/ Finite Element Method", International Journal for Numerical Methods in Fluids, Vol. 21, pp. 667-681, 1995.

Leylek, J. H., R. D. Zerkle, "Discrete-Jet Film Cooling: A Comparison of Computational Results with Experiment", ASME 93-GT-207, 1993.

Licu, D. N., M. J. Findlay, I. S. Gartshore, M. Salcudean, "Transient Heat Transfer Measurements Using a Single Wide-Band Liquid Crystal Test", Journal of Turbomachinery, Vol. 122, pp. 546- 552, 2000.

Ligrani, P. M., S. Ciriello, D. T. Bishop, "Heat Transfer, Adiabatic Effectiveness, and Injectant Distributions Downstream of a Single Row and Two Staggered Rows of Compound Angle Film-Cooling Holes", Journal of Turbomachinery, Vol. 114, pp. 687-700, 1992.

Lutum, E., B. V. Johnson, "Influence of the Hole Length-to-Diameter Ratio on Film Cooling With Cylindrical Holes", Journal of Turbomachinery, Vol. 121, pp. 209-216, 1999.

Makki, Y. H., G. S. Jakubowski, "An Experimental Study of Film Cooling from Diffused Trapezoidal Shaped Holes", AIAA paper AIAA-86-1326, 1986.

McGovern, K. T., J. H. Leylek, "A Detailed Analysis of Film Cooling Physics: Part II: Compound-Angle Injection With Cylindrical Holes", Journal of Turbomachinery, Vol. 122, pp. 113-121, 2000.

McGrath, E. L., J. H. Leylek, "Physics of Hot Crossflow Ingestion in Film Cooling", ASME Paper 98-GT-191, 1998.

Mehendale, A. B., J. C. Han, "Influence of High Mainstream Turbulence on Leading Edge Film Cooling Heat Transfer", Journal of Turbomachinery, Vol. 114, pp. 707-715, 1992.

Nirmalan, N.V., L. D. Hylton, " An Experimental Study of Turbine Vane Heat Transfer With Leading Edge and Downstream Film Cooling", Journal of Turbomachinery, Vol. 112, pp. 477-487, 1990.

Obot, N. T., A. S. Majumdar, W. J. M. Douglas, "The Effect of Nozzle Geometry on Impingement Heat Transfer under a Round Turbulent Jet", ASME Paper 79-WA/HT-53, 1979.

Papell, S. S., "Vortex Generating Coolant Flow Passage Design for Increased Film-Cooling Effectiveness and Surface Coverage", NASA Technical Paper 2388, 1984.

Patankar, S. V., "Numerical Heat Transfer and Fluid Flow", Taylor and Francis, 1980.

Pedersen, D. R., E. R. G. Eckert, R. J. Goldstein, "Film Cooling With Large Density Differences Between the Mainstream and the Secondary Fluid Measured by the Heat-Mass Transfer Analogy", Journal of Heat Transfer, Vol. 99, pp. 620-627, 1977.

Pietrzyk, J. R., D. G. Bogard, M. E. Crawford, "Hydrodynamic Measurements of Jets in Crossflow for Gas Turbine Film Cooling Applications", Journal of Turbomachinery, Vol. 111, pp. 139-145, 1989.

Salcudean, M., I. Gartshore, K. Zhang, Y. Barnea, "Leading Edge Film Cooling of a Turbine Blade Model Through Single and Double Row Injection: Effects of Coolant Density", ASME Paper 94-GT-2, 1994.

Sarkar, S., T. K. Bose, "Comparison of Different Turbulence Models for Prediction of Slot-film Cooling: Flow and Temperature Field", Numerical Heat Transfer, Vol. 28, No. 2, pp. 217-238, 1995.

Saumweber, C., A. Schulz, S. Wittig, "Free-Stream Turbulence Effects on Film Cooling with Shaped Holes", Journal of Turbomachinery, Vol. 125, pp. 65-72, 2003.

Schmidt, D. L., B. Sen, D. G. Bogard, "Film Cooling With Compound Angle Holes: Adiabatic Effectiveness", Journal of Turbomachinery, Vol. 118, pp. 807-813, 1996.

Schmidt, D.L., D. G. Bogard, "Effects of Free-Stream Turbulence and Surface Roughness on Film Cooling", ASME 96-GT-462, 1996.

Sen, B., D. L. Schmidt, D. G. Bogard, "Film Cooling With Compound Angle Holes: Heat Transfer", Journal of Turbomachinery, Vol. 118, pp. 800-806, 1996.

Shih, T.-H., W. W. Liou, A. Shabbir, Z. Yang, J. Zhu, "A New k-ε Eddy Viscosity Model for High Reynolds Number Turbulent Flows", Computers Fluids, Vol. 24, No. 3, pp. 227-238, 1995.

Sinha, A. K., D. G. Bogard, M. E. Crawford, "Film-Cooling Effectiveness Downstream of a Single Row of Holes With Variable Density Ratio", Journal of Turbomachinery, Vol. 113, pp. 442-449, 1991.

Teekaram, A. J. H., C. J. P. Forth, T. V. Jones, "The Use of Foreign Gas to Simulate the Effects of Density Ratios in Film Cooling", Journal of Turbomachinery, Vol. 111, pp. 57-62, 1989.

Thole, K., M. Gritsch, A. Schulz, S. Wittig, "Flowfield Measurements for Film-Cooling Holes With Expanded Exits", Journal of Turbomachinery, Vol. 120, pp. 327-336, 1998.

Vedula, R. J., D. E. Metzger, "A Method for the Simultaneous Determination of Local Effectiveness and Heat Transfer Distributions in Three-Temperature Convection Situations", ASME Paper 91-GT-345, 1991.

Walters, D. K., J. H. Leylek, "A Detailed Analysis of Film Cooling Physics: Part I: Streamwise Injection With Cylindrical Holes", Journal of Turbomachinery, Vol. 102, pp. 102-112, 2000.

Walters, D. K., K. T. McGovern, J. J. Butkiewicz, J. H. Leylek, "A Systematic Computational Methodology Applied to a Jet-In-Crossflow Part 2: Unstructured/Adaptive Grid Approach", ASME 95-WA/HT-2, 1995.

Wilfert, G., S. Wolff, "Influence of Internal Flow on Film Cooling Effectiveness", Journal of Turbomachinery, Vol. 122, pp. 327-333, 2000.

Yakhot, V., S. A. Orszag, "Renormalization Group Analysis of Turbulence. I. Basic Theory.", Journal of Scientific Computing, Vol. 1. No. 1, pp. 3-51, 1986.

Zhou, J.-M., M. Salcudean, I. S. Gartshore, "Prediction of Film Cooling by Discrete-Hole Injection", ASME Paper 93-GT-75, 1993.

Appendix

Benchmark Studies

Several benchmark studies were performed in order to validate results obtained with the CFD package FLUENT 6.1. Various problems were selected, for which experimental data was available in the literature. For each study, the simulated results were compared to the experimental data in order to determine the accuracy of the CFD software and validate the computational method. This section presents the benchmark results for some of the validation studies that were carried out.

Lid-Driven Cavity Flow

The lid-driven inclined cavity flow is a simple fluid flow problem often simulated to validate CFD codes when non-orthogonal grids are used. This simple two-dimensional problem is shown in Figure A-1. Viscous fluid inside a 45°-inclined cavity of length L is entrained by the lid which moves at a constant velocity U_L, thus resulting in a vortex motion inside the cavity. All wall boundaries of the cavity satisfy the no-slip condition. This motion was simulated using the CFD software FLUENT 6.1, and results were compared to those of Demirdzic et al. (1992).

Demirdzic et al. modeled a lid-driven cavity flow problem for which the Reynolds number, based on the lid velocity U_L and the cavity length L, is set to 1000. This Reynolds number is defined as:

$$Re = \frac{\rho U_L L}{\mu} \tag{A.1}$$

The authors conducted the simulations with six non-uniform structured grids using a multi-grid procedure. Each grid had a different density, from 10 x 10 nodes for the coarsest mesh to 320 x 320 nodes for the finest mesh and for each mesh nodes were concentrated near the walls of the cavity with an expansion ratio of 1.00096. They considered the solution to be converged when the solutions remained unchanging up to the six most significant digits. The under-relaxation factors were set to 0.7-0.8 for the velocities and 0.3-0.4 for the pressure. The authors found that the two finest grids, containing 160 x 160 and 320 x 320 elements, yield solutions which are essentially the same, hence denoting grid-independent results.

In the present study, the cavity flow was modeled using FLUENT 6.1 by solving the Navier-Stokes equations with the SIMPLE pressure-velocity coupling algorithm, with convergence criteria of 10^{-4} for the continuity and momentum equations. The equations were discretized using the second order upwind scheme, with under-relaxation factors of 0.3 and 0.4 for the pressure and momentum equations, respectively. A non-orthogonal structured quadrilateral grid approach was used, with 220 x 220 elements. A sample grid is shown in Figure A-2. Figure A-3 shows the predicted streamlines inside the cavity, and

Figures A-4 and A-5 present the distribution of velocities u and v along Centerline 1 and Centerline 2 for Re = 1000, respectively. These figures show that the present results are in good agreement with those of Demirdzic et al.

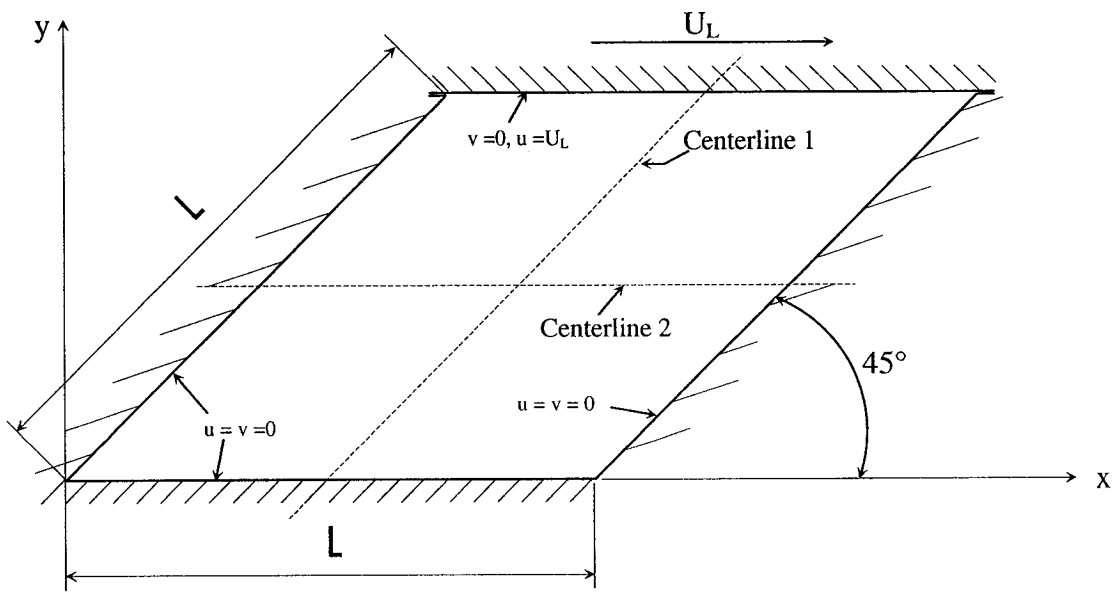

Figure A-1. Geometry and boundary conditions for the lid-driven cavity flow problem.

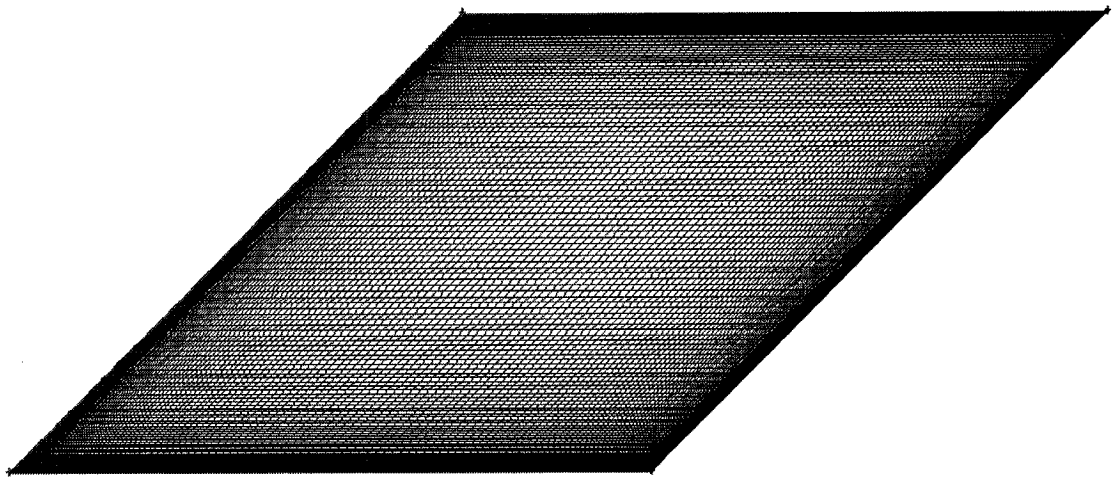

Figure A-2. Computational mesh for lid-driven cavity flow problem.

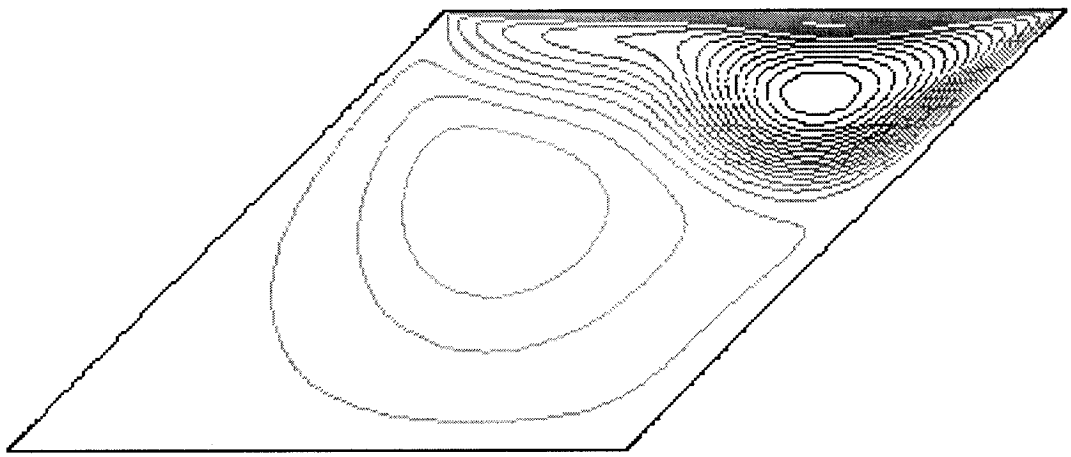

Figure A-3. Qualitative streamlines for Re = 1000.

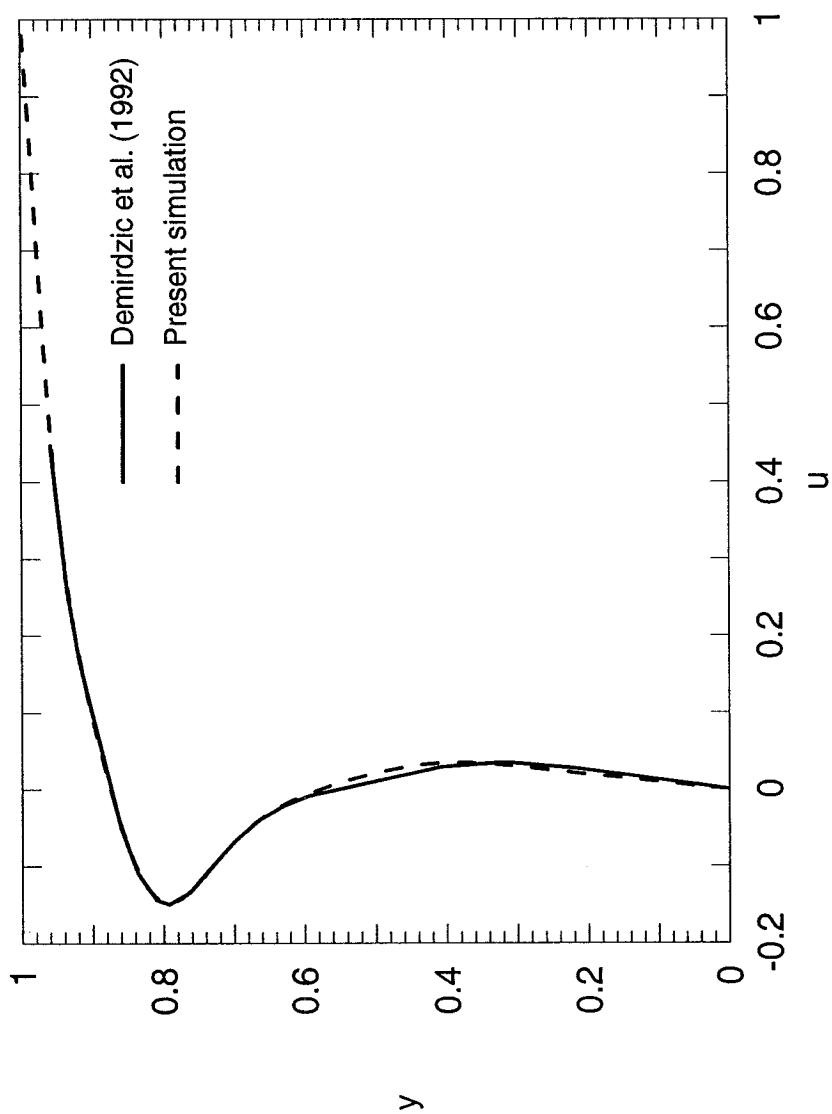

Figure A-4. U-velocity on Centerline 1.

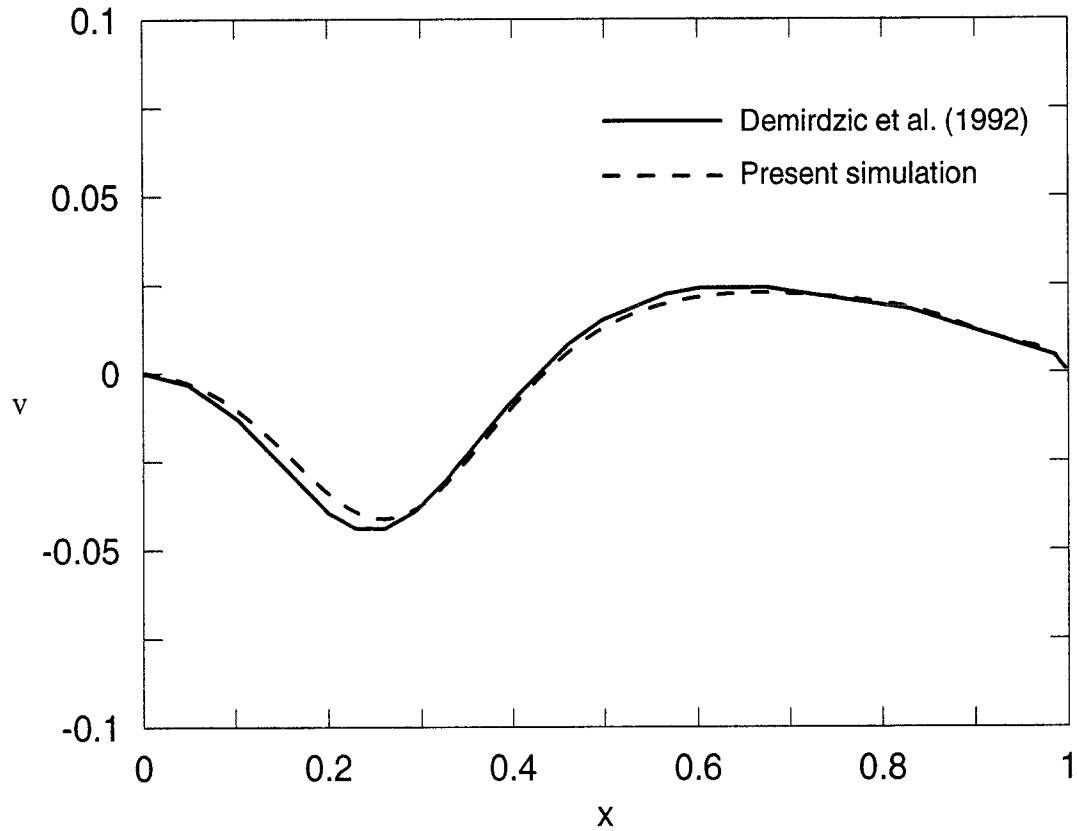

Figure A-5. V-velocity on Centerline 2.

Flow over a Backward Facing Step

Simulation of fluid flow over a two-dimensional backward facing step is a classical benchmark problem. This is a problem where the flow is considered incompressible, steady, and turbulent, so that it is a good validation case to check the accuracy of turbulence modeling. The domain and boundary conditions are shown in Figure A-6. Flow enters a channel with uniform velocity U_0. The sudden increase in channel height causes the flow to detach and form a recirculation bubble behind the step. The flow then reattaches further downstream. This problem was simulated using the CFD software FLUENT 6.1, and results were compared to those obtained numerically by Le Ribault et al. (1995).

In the concerned case, Le Ribault et al. set the inlet velocity to 18 m/s so that the Reynolds was equal to 44580. This Reynolds number is written as:

$$Re = \frac{\rho U_0 h}{\mu} \tag{A.2}$$

where h is the step height. In order to make the flow incompressible, they conducted the simulations with a Mach number of 0.1. Turbulence closure was achieved by using the standard k-ε model, and wall functions were used to model the near-wall region, therefore requiring a wall $y^+ \geq 11.6$. An unstructured triangular mesh approach was implemented,

and elements were concentrated around the step and near the expected region of flow reattachment, for a total of 2101 nodes.

In the present study, an unstructured mesh approach was also used, where the mesh contains 15375 nodes. Elements were concentrated in the step region and in the reattachment region. The mesh was heavily adapted in order to ensure grid-independent solutions. The average y^+ in the domain is equal to 24.8. A sample mesh is shown in Figure A-7. Simulations were done with the CFD software FULENT 6.1 with the SIMPLE pressure-velocity coupling algorithm. Equations were discretized using the second-order upwind scheme, with under-relaxation factors of 0.3, 0.7, 0.6, 0.6, and 0.5 for the pressure, momentum, turbulent kinetic energy, turbulent dissipation rate, and turbulent viscosity equations, respectively. The convergence criterion was set to 10^{-6} for the continuity, momentum and turbulence equations. Le Ribault et al. found that their simulation predicted a reattachment length L of about 5 times the height of the step ($L \approx 5h$), and they state that experimentally this length is found to be $L \approx 7h$. In the present study the predicted reattachment length is found to be $L \approx 6.4h$. The axial velocity profile is obtained at $x = 10.7h$, and it is compared to that found by Le Ribault et al. in Figure A-8. This Figure shows the present results are in good agreement with those of Le Ribault.

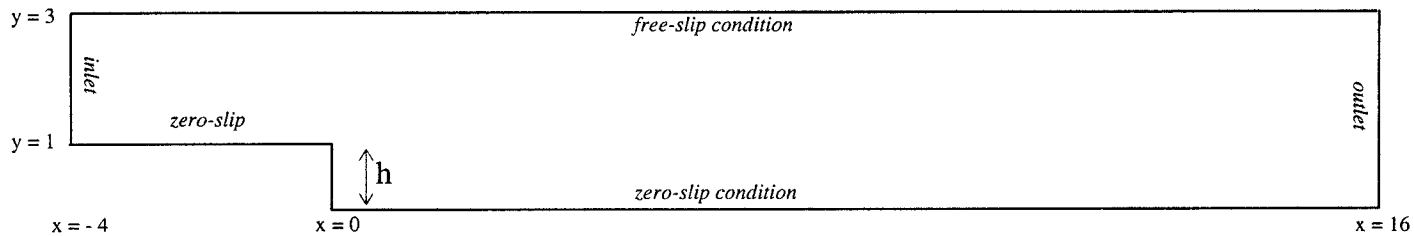

Figure A-6. Computational domain and boundary conditions for the backward facing step problem.

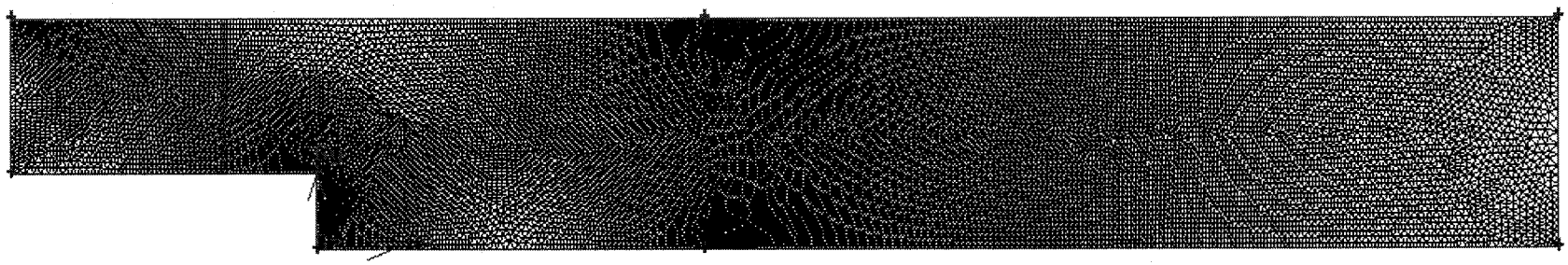

Figure A-7. Sample mesh for the backward facing step problem.

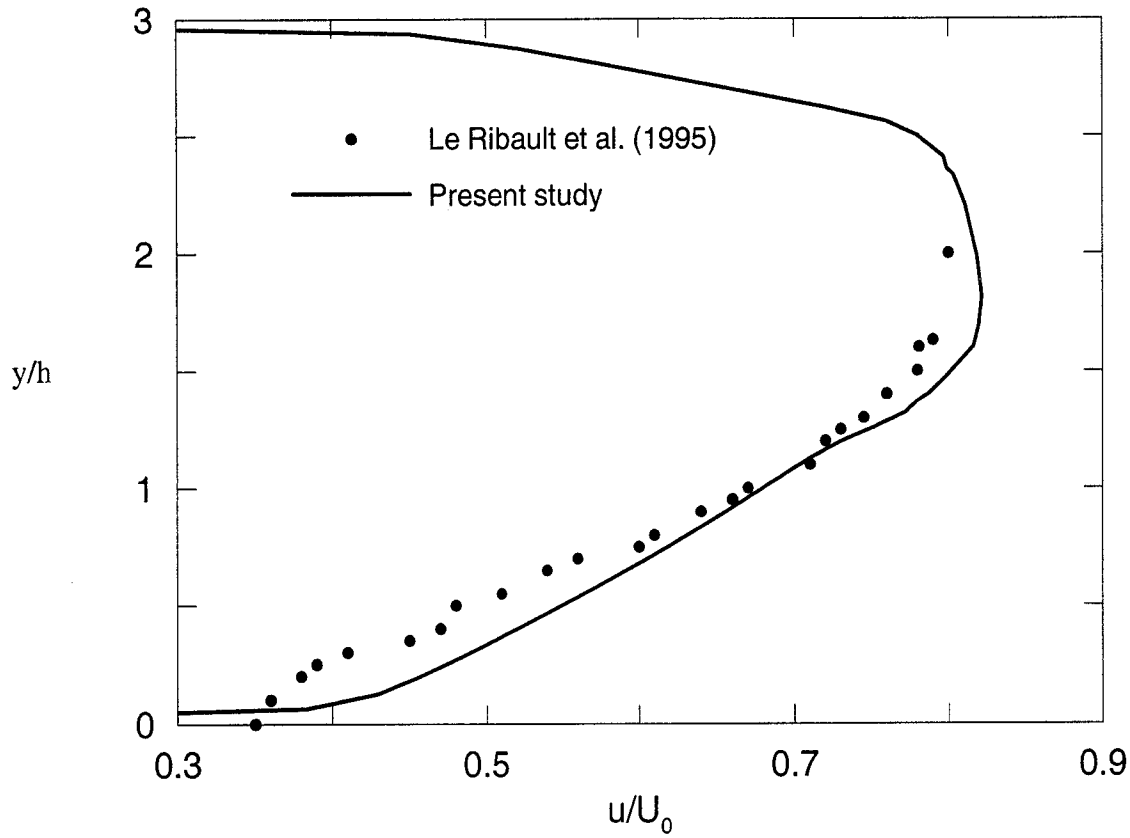

Figure A-8. Axial velocity profile at x/h = 10.7 for the backward facing step problem.

Inclined Circular Film Cooling Hole

The steady-state three-dimensional problem of inclined circular film cooling holes with incompressible flow has been investigated time and again, both in experimental and computational studies. Sinha et al. (1991) studied experimentally a row of 35-degree inclined circular film cooling holes of length L/D = 1.75 in a flat plate. The hole had a diameter of 1.27 cm. They obtained the effectiveness distribution downstream of injection for various blowing rates and density ratios. The freestream velocity was set to 20 m/s with a turbulence intensity of 0.2%, and a temperature of 300 K. Coolant was supplied through a plenum with varying velocities and temperatures. Walters and Leylek (2000) investigated numerically the same cooling arrangement for a blowing rate of 1.0 with a density ratio of 2.0, corresponding to crossflow and coolant temperature of 302 K and 150 K, respectively. All the other flow conditions were the same as for Sinha et al. The authors neglected end-wall effects so that they were able to simulate a single cooling hole due to the periodic nature of the flow. Their computational domain extended 19D upstream, 30D downstream and 10D above the locus of injection. They also included a plenum of length and height equal to 8D and 4D, respectively. A three-dimensional tetrahedral mesh approach with 250000 elements was used for the computations. The standard k-ε turbulence model with wall-functions was used to achieve turbulence closure. The turbulence length scale was taken as 1/10 of both the mainstream and coolant inlet extents. All walls were considered adiabatic. The Navier-Stokes equations were solved using a commercial software by Fluent Inc. The equations were discretized using the second-order upwind scheme and convergence was assumed when the

normalized residuals were reduced by three orders of magnitude and no flow variables were seen to change significantly from one iteration to the next.

In the present study, the circular hole injection with M = 1.0 and DR = 2.0 as studied by Sinha et al. was modeled using the same computational domain as Walters and Leylek. The results were obtained computationally by FLUENT 6.1. The computational domain and boundary conditions are shown in Figure A-9. A tetrahedral/hybrid grid approach was implemented, and grids of 618048 elements were found to yield grid-independent solutions. A sample grid is shown in Figure A-10. Three different discretization schemes were used in the solution (first-order upwind, second-order upwind and power law scheme), and under-relaxation factors were set to 0.3, 0.7, 0.5, 0.5, 0.5, and 0.8 for the pressure, momentum, turbulent kinetic energy, turbulent dissipation rate, turbulent viscosity equations, and energy respectively. The turbulence was modeled using three different models, i.e. the standard k-ε, realizable k-ε and RNG k-ε turbulence models, with enhanced wall treatment. This called for very fine mesh near the walls of the domain and a wall $y^+ \approx 1$. A grid-independence study was conducted in order to determine the amount of elements needed in the grid to obtain grid-independent solutions. Figure A-11 presents the downstream centerline adiabatic film cooling effectiveness for three grids containing 466158, 618048 and 751488 elements each. The discrepancies in the solution are found to be small for the three grids, so the 618048-element grid was considered to yield grid-independent results, and was used for all the simulations. Figure A-12 presents the downstream centerline adiabatic film cooling effectiveness obtained with three turbulence models, compared to experimental data by Sinha et al. and computational data

by Walters and Leylek. Results are in good agreement with those of Sinha et al. especially in the near-hole region ($x/D \leq 4$). The predictions there are much more accurate than those of Walters and Leylek. Farther downstream, the predictions become less accurate than those of Walters and Leylek. The three turbulenve models yield similar results, with the realizable k-ε turbulence model giving the most accurate prediction overall, followed by the RNG k-ε turbulence model. Figure A-13 presents the downstream centerline adiabatic film cooling effectiveness obtained for the three discretization schemes mentioned above, and compared to the centerline effectiveness found experimentally by Sinha et al. Results show that all three schemes yield very similar results, except in the near-hole region where the first-order upwind scheme gives the worst prediction. The second-order discretization scheme was selected for all the novel cooling hole simulations because according to this benchmark case, it is a good compromise between accuracy of the solution and computational time.

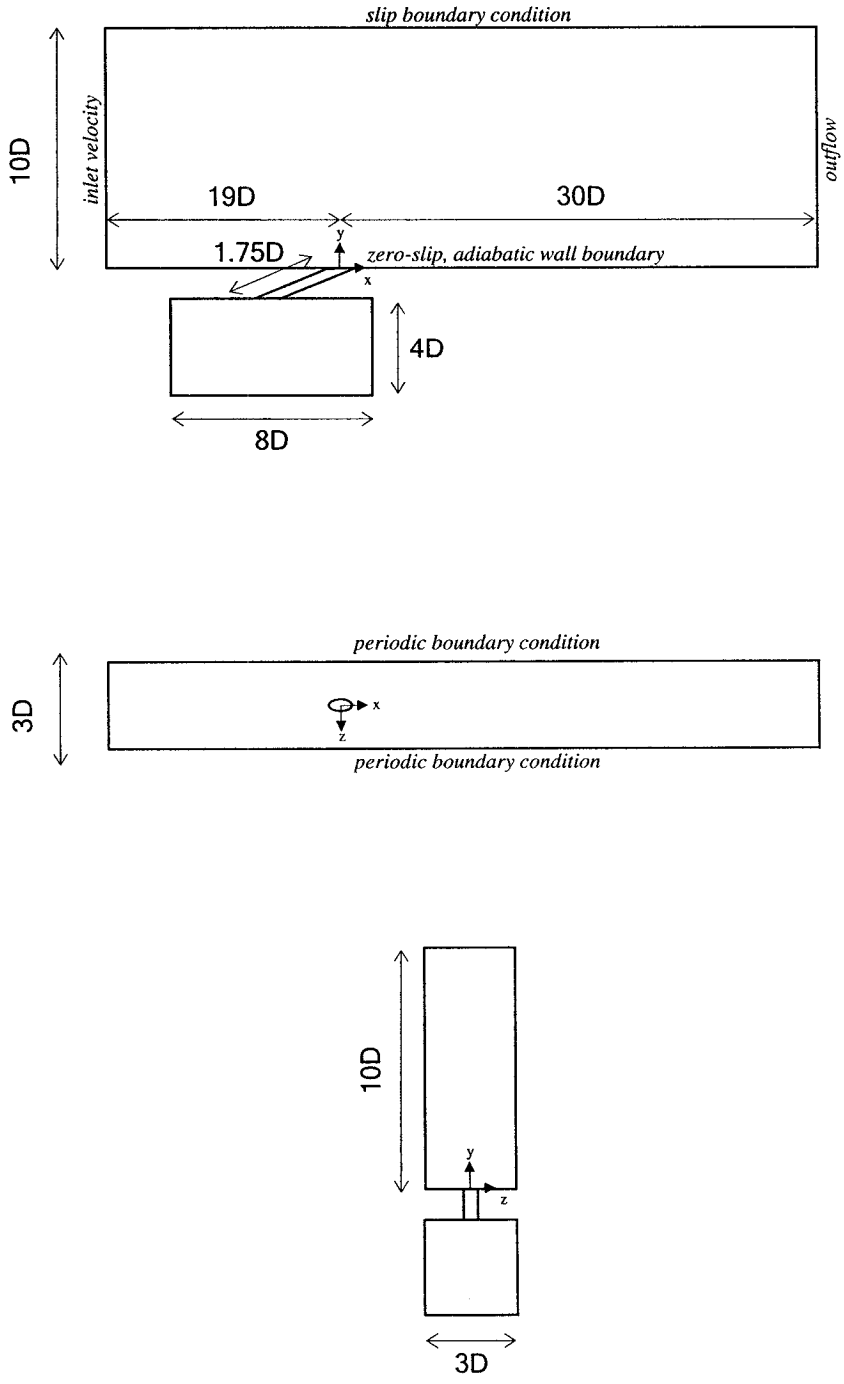

Figure A-9. Computational domain and boundary conditions for the inclined circular film cooling hole problem.

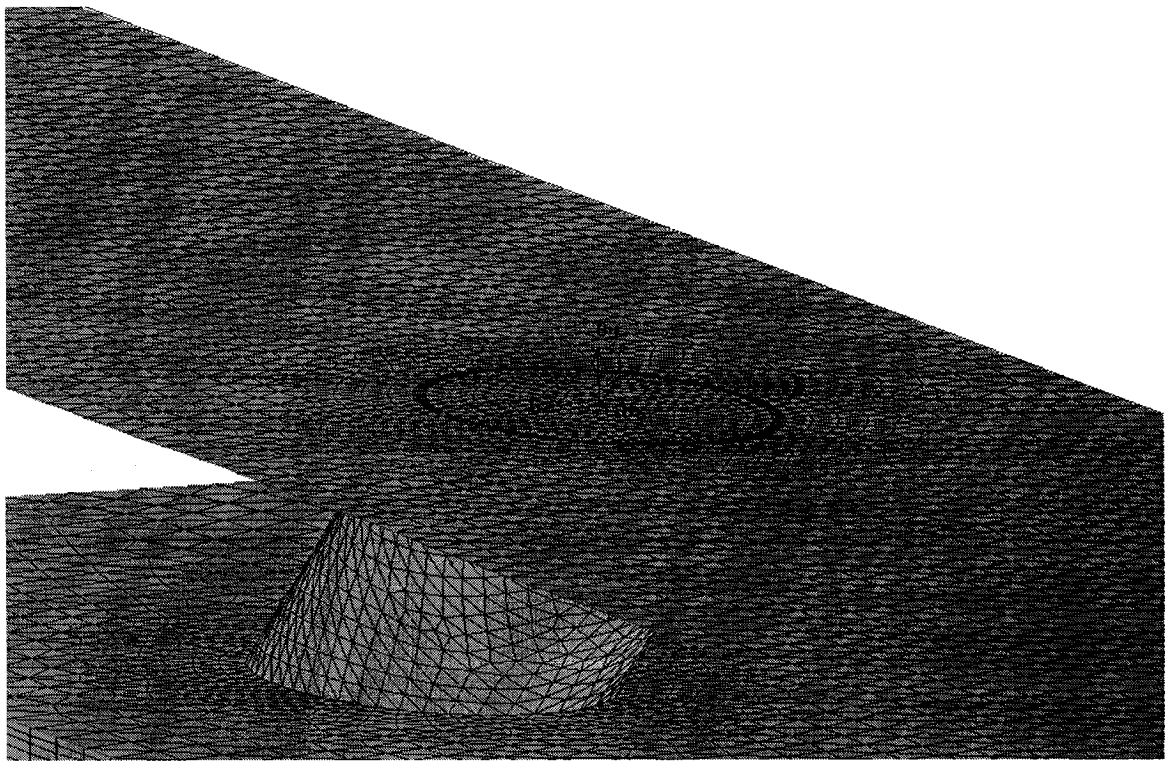

Figure A-10. Computational grid in the near-hole region for the inclined circular film cooling hole problem.

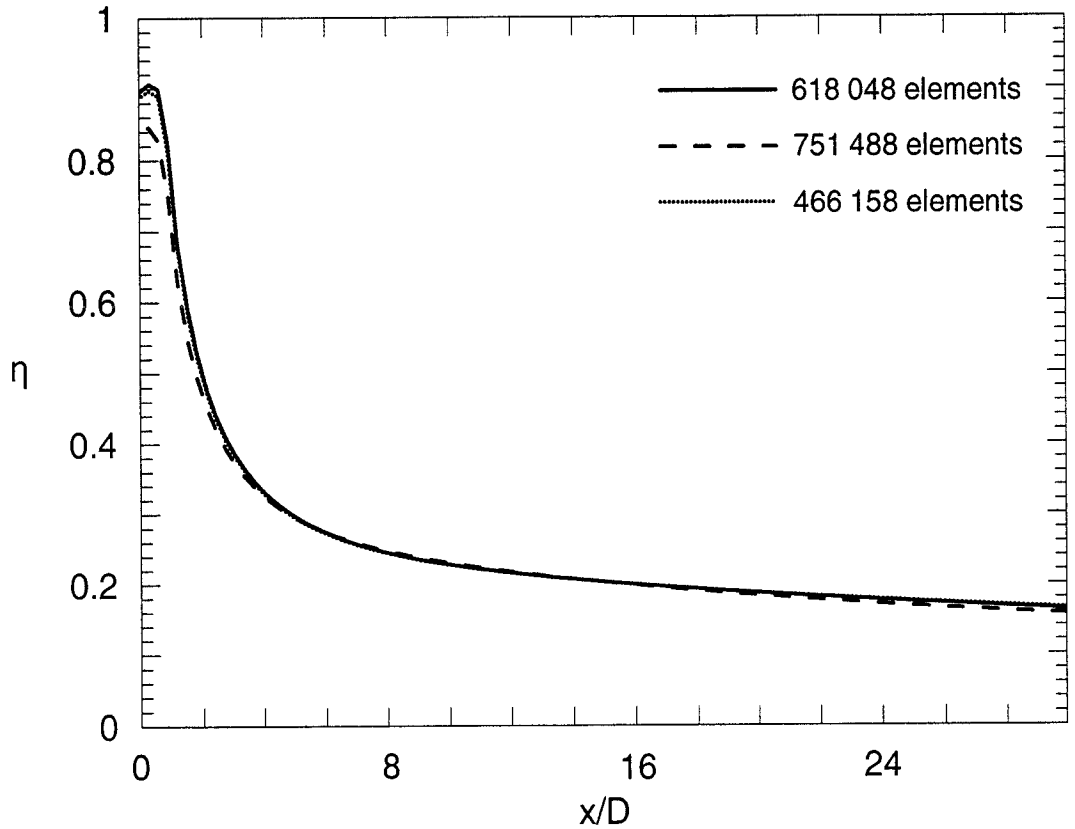

Figure A-11. Centerline adiabatic film cooling effectiveness for various grid densities at M = 1.0 and DR = 2.0 (realizable k-ε turbulence model, second order discretization scheme).

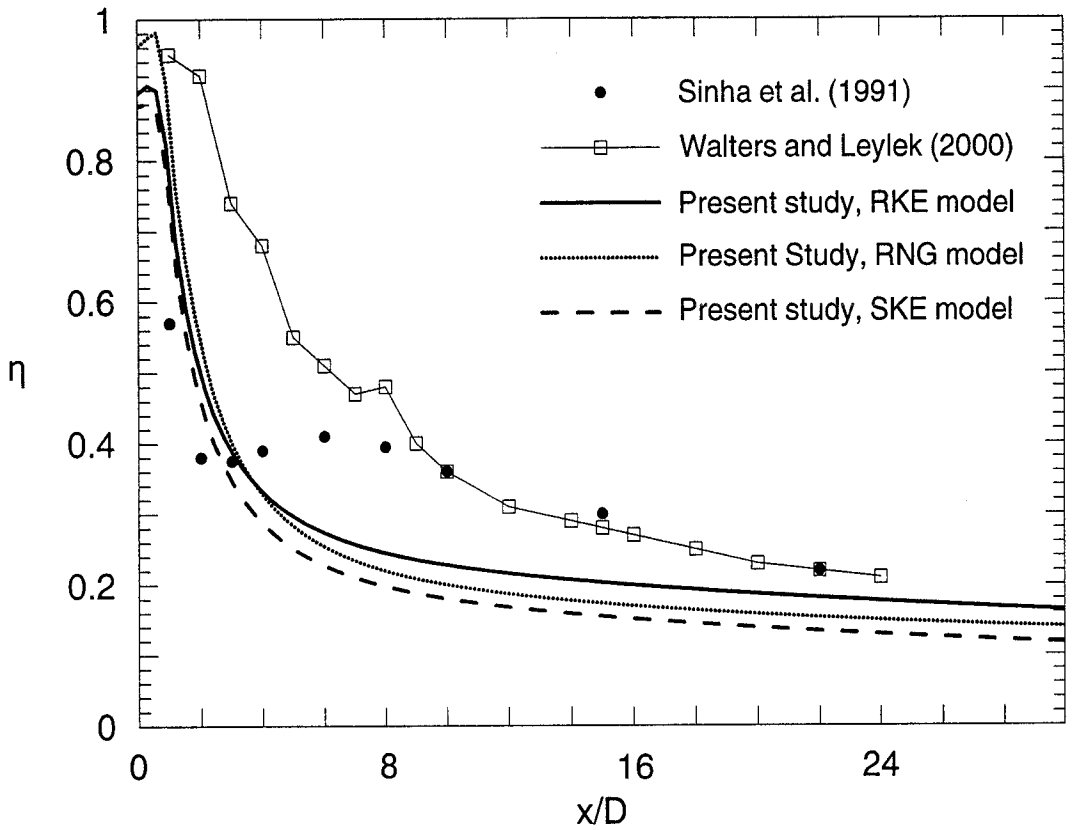

Figure A-12. Centerline adiabatic film cooling effectiveness for the inclined circular film cooling hole, obtained with various turbulence models, at M = 1.0.

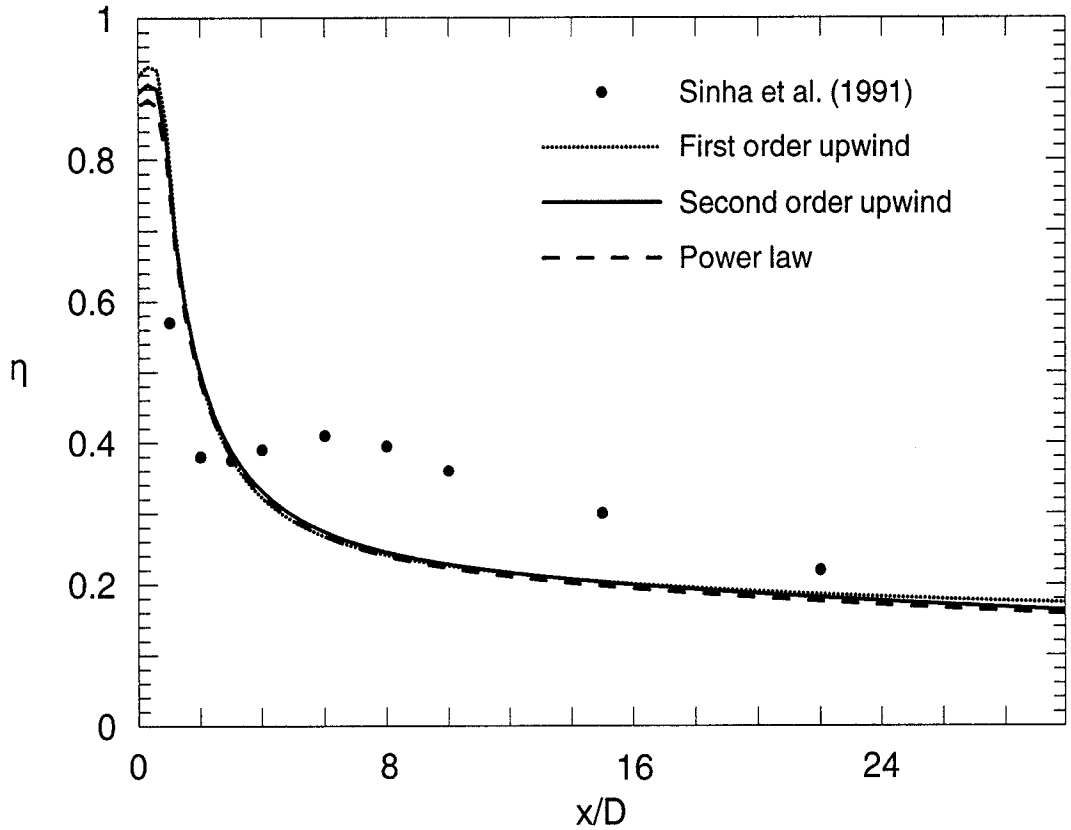

Figure A-13. Centerline adiabatic film cooling effectiveness for the inclined circular film cooling hole, obtained with three discretization schemes, at M = 1.0.